Springer Theses
Recognizing Outstanding Ph.D. Research

Monica Frega

Neuronal Network Dynamics in 2D and 3D in vitro Neuroengineered Systems

Springer

Springer Theses

Recognizing Outstanding Ph.D. Research

Aims and Scope

The series "Springer Theses" brings together a selection of the very best Ph.D. theses from around the world and across the physical sciences. Nominated and endorsed by two recognized specialists, each published volume has been selected for its scientific excellence and the high impact of its contents for the pertinent field of research. For greater accessibility to non-specialists, the published versions include an extended introduction, as well as a foreword by the student's supervisor explaining the special relevance of the work for the field. As a whole, the series will provide a valuable resource both for newcomers to the research fields described, and for other scientists seeking detailed background information on special questions. Finally, it provides an accredited documentation of the valuable contributions made by today's younger generation of scientists.

Theses are accepted into the series by invited nomination only and must fulfill all of the following criteria

- They must be written in good English.
- The topic should fall within the confines of Chemistry, Physics, Earth Sciences, Engineering and related interdisciplinary fields such as Materials, Nanoscience, Chemical Engineering, Complex Systems and Biophysics.
- The work reported in the thesis must represent a significant scientific advance.
- If the thesis includes previously published material, permission to reproduce this must be gained from the respective copyright holder.
- They must have been examined and passed during the 12 months prior to nomination.
- Each thesis should include a foreword by the supervisor outlining the significance of its content.
- The theses should have a clearly defined structure including an introduction accessible to scientists not expert in that particular field.

More information about this series at http://www.springer.com/series/8790

Monica Frega

Neuronal Network Dynamics in 2D and 3D in vitro Neuroengineered Systems

Doctoral Thesis accepted by
the University of Genoa, Italy

Springer

Author
Monica Frega
Department of Informatics, Bioengineering, Robotics and System Engineering
University of Genoa
Genoa
Italy

Supervisor
Prof. Sergio Martinoia
Department of Informatics, Bioengineering, Robotics and System Engineering
University of Genoa
Genoa
Italy

ISSN 2190-5053 ISSN 2190-5061 (electronic)
Springer Theses
ISBN 978-3-319-30236-2 ISBN 978-3-319-30237-9 (eBook)
DOI 10.1007/978-3-319-30237-9

Library of Congress Control Number: 2016932514

Printed on acid-free paper

This Springer imprint is published by Springer Nature
The registered company is Springer International Publishing AG Switzerland

Part of this thesis have been published in the following articles:

Peer-reviewed International Journals

[J.1] Tedesco, M., Frega, M., Martinoia, s., Pesce, M., Massobrio, P. (2015). Interfacing 3D engineered neuronal cultures to Micro-Electrode Arrays: an innovative in vitro experimental model. Journal of Visualized Experiments (104), e53080, doi: 10.3791/53080.

[J.2] Frega, M., Tedesco, M., Massobrio, P., Pesce, M., Martinoia, S. (2014). Enhanced network dynamics in 3D engineered neuronal cultures: a new experimental model for network electrophysiology. Scientific Reports, 4, 5489.

[J.3] Colombi, I., Mahajani, S., Frega, M., Gasparini, L., Chiappalone, M. (2013). Effects of antiepileptic drugs on hippocampal neurons coupled to micro-electrode arrays. Frontiers in Neuroengineering, 6, 10.

[J.4] Frega, M., Pasquale, V., Tedesco, M., Marcoli, M., Contestabile, A., Nanni, M., Bonzano, L., Maura, G., Chiappalone, M. (2012). Cortical cultures coupled to Micro-Electrode Arrays: A novel approach to perform in vitro excitotoxicity testing. Neurotoxicology and teratology, 34(1), 116-127.

Peer-reviewed conference proceedings

[C.1] Tedesco, M., Frega, M., Pastorino, L. Massobrio, M., Martinoia, S. 3D engineered neural networks coupled to Micro-Electrode based devices: a new experimental model for neurophysiological applications. AISEM Annual Conference, 2015 XVIII, 3rd–5th February 2015, Trento, Italy.

[C.2] Frega, M., Tedesco, M., Massobrio, P., Pesce, M., Martinoia, S. 3D neural networks coupled to planar microtransducer arrays: an innovative in-vitro experimental model for investigating network dynamics. 9th International Meeting on Substrate-Integrated Mircoelectrode Arrays, 1st–4th July 2014, Reutlingen, Germany.

[C.3] Frega, M., Tedesco, M., Massobrio, P., Martinoia, S. 3D neural networks coupled to Micro Electrode Arrays: a new experimental model for neuro-electronic interfaces. 4th congress - National Group of Bioengineering (GNB), 25th–27th June 2014, Pavia (Italy).

[C.4] Frega, M., Tedesco, M., Massobrio, P., Pesce, M., Williamson, A., Schober, A., Martinoia, S. 3D Engineered Neural Networks Coupled to Micro-Electrode Arrays: Development of an Innovative In-Vitro Experimental Model for Neurophysiological Studies. 6th International IEEE/EMBS Conference on Neural Engineering (NER), 5th–8th November 2013, San Diego (USA).

[C.5] Frega, M., Tedesco, M., Massobrio, P., Pesce, M., Martinoia, S. 3D neuronal networks coupled to Micro-Electrode Arrays: an innovative in vitro experimental model to study network dynamics. 8th International Meeting on Substrate-Integrated Microelectrode Arrays (SIMEA 2010), 10th–13th July 2012, Reutlingen (Germany).

Abstract to National and International conferences

[A.1] Tedesco, M., Frega, M., Massobrio, P., Pesce, M., Martinoia, S. 3D neuronal cultures coupled to multi-electrode arrays: a new experimental model for in-vitro electrophysiology. 9th Forum of European Neuroscience (FENS 2014), 5th–9th July 2014, Milan (Italy).

[A.2] Frega, M., Tedesco, M., Massobrio, P., Martinoia, S. Comparison between the electrophysiological activity of 2D and 3D hippocampal neural networks coupled to micro-electrode arrays. 9th Forum of European Neuroscience (FENS 2014), 5th–9th July 2014, Milan (Italy).

[A.3] Frega, M., Tedesco, M., Massobrio, P., Pesce, M., Martinoia, S. Comparison between electrophysiological activity of 2D and 3D cultured hippocampal networks coupled to micro-electrode arrays. Neuroscience, 9th–13th November 2013, San Diego (USA).

[A.4] Martinoia, S., Tedesco, M., Frega, M., Massobrio, P., Wiliamson, A., Schober, A. 3-D neuronal cultures coupled to 3-D multi-electrode arrays: a new biohybrid investigational platform for network neurophysiology. Neuroscience, 9th–13th November 2013, San Diego (USA).

[A.5] Martinoia, S., Frega, M., Tedesco, M., Pesce, M., Massobrio, P. 3D neuronal networks coupled to Micro-Electrode Arrays: development of an in vitro experimental model to study network dynamics. 8th Forum of European Neuroscience (FENS 2012), 14th–18th July 2012, Barcelona (Spain).

Supervisor's Foreword

It is a great pleasure to introduce Dr. Monica Frega's thesis work accepted for publication within Springer Theses and awarded with a prize for outstanding original work. Monica Frega performed her Master thesis under my supervision and then joined my research group on Neuroengineering and Bionanotechnologies (Department of Informatics, Bioengineering, Robotics and Systems Engineering) for her Ph.D. program on Bioengineering at the University of Genova. She started in January 2011 and completed her studies with a successful thesis defense on April 4, 2014.

The thesis reports an innovative study in the design and implementation of new-engineered three-dimensional (3D) neuronal cultures coupled to micro electrode arrays (MEAs). Part of the presented results have been awarded by the National Bioengineering Group with the "Award for young scientists" in 2014 and most of them have been published in Scientific Report (Nature Publishing Group) on June 30, 2014.

The use of in vitro neuronal networks for neurophysiological investigation is a well-established technique since decades. It is widely used for molecular, cellular, and networks studies, mainly for its possibility of manipulation, observation, control, and long-term culturing. The coupling of such in vitro models, derived from primary cultures of rodents (embryo or neonatal), to MEAs technology goes back to the '70s. These model networks are routinely grown onto planar substrate; attempts in improving this approach are concentrated on developing new technologies for recording and stimulating the electrophysiological activity of such experimental preparations. In the past decade, there was increasing attention to the development of 3D cultured networks simply by recognizing the advantages, from the physiological point of view, of such in vitro preparations capable of better mimicking and recapitulating the in vivo situation. Notwithstanding the increased momentum in 3D networks, all the electrophysiological studies at the network level are still based on two-dimensional (2D) in vitro models (i.e., networks grown onto a planar substrate).

In her thesis work, Monica Frega greatly contributed to the development of a new experimental paradigm constituted by 3D neural networks coupled to micro electrode arrays (MEAs). These 3D networks were systematically characterized from an experimental point of view, and the network dynamics deeply investigated, analyzed, and compared with standard 2D networks. Her work included experimental design, data collection, and specific data processing. For the first time, Monica Frega demonstrated the possibility of coupling 3D cultured networks to planar MEAs, and verified the capability of such 3D networks of showing a different electrophysiological activity (with respect to 2D sister-cultures) with specific features and with much more similarities to the in vivo situation.

This new approach opens new avenues in the network electrophysiology field, allowing studying in vitro neuronal systems in a more physiological condition, approaching and mimicking natural in vivo assemblies. Moreover, it constitutes a step forward in the field of neuroengineering, with specific relevance for the development of new cellular, tissue-like in vitro experimental model systems with future far-reaching implications in the field of in vivo neural interface and neural grafting.

Genoa
November 2015

Prof. Sergio Martinoia

Acknowledgments

During my Ph.D. I had the occasion to go deeper into my interest for research and at the end of these years my passion gradually grew. This personal growth would not have been possible without competent and professional people who were really passionate in their work and humanly interesting. I would like to thank these people one by one. First of all, I express my sincere gratitude to my supervisor Sergio Martinoia. This work could not be performed without his valuable guidance and trust. I also thank Paolo Massobrio. Working with the two of you was great. I really enjoyed my research, and you strongly supported and encouraged my enthusiasm. I was sharing with both of you not only scientific ideas and results, but also my personal life. You were not only my supervisors, but great friends of mine. Without such a good relationship, I am sure that the outcome of my Ph.D. would not have been the same, both in terms of "results" and in terms of my personal growth. I thank MariaTeresa Tedesco: you provided me a lot of support and help and you conveyed to me the passion for your work. I also thank Michela Chiappalone: you always supported me and you were important for my scientific and personal growth.

I thank Virginia, Andrea, and Daniele: with you I shared most of the time during my Ph.D. We did not share only scientific ideas, but also many nice moments and interesting talks together.

These three years of Ph.D. were a long journey: I could not have completed this journey without the support of my friends and family. I thank all of you!

In particular, I thank the friends with whom I have shared almost everything: Albertone, Giulia, Davide, Andrea, Luca, Ignazio, Chiusky, Marialaura, Anna, and Susanna. You were great and helpful company: I shared my life and the important steps of my personal development with you. It is incredible how our friendship grew with time. I have no words to express my gratitude.

And of course, a big thank you to Mattia. You always provide me support, help, and encouragement. You are a gift to me: you really changed my life in this year. I am impressed by how we were able to face difficulties and how the distance made us closer and made our relationship stronger. I am really grateful to have you at my side. And the best is yet to come!

I would like to conclude with thanks to my family, especially my brothers Andrea and Simone, my parents Marina and Mauro, and my super grandmother Maria! Here I also to thank Cinzia. You have always been a presence, a support, an encouragement. You always supported me. I am impressed to have such a great family; if I am who I am and I could face all these challenges, it is mostly thanks to you, the education that you gave me, and all the great people and beautiful things that you have always shown me.

Genoa Monica Frega
April 2014

Contents

About the Author

Monica Frega was born on the 2nd of April 1985 in Genova, Italy. After finishing her secondary education, in 2004 she started in the Bachelor program of Biomedical Engineering at the University of Genova, Italy. Directly after the graduation, she started the Master program in Bioengineering at the University of Genova with specialization in Neuroengineering. In 2010, the master program was successfully finished and Monica graduates cum laude with the thesis "Electrical stimulation and synaptic plasticity protocols on cultured hippocampal networks", supervised by Prof. Sergio Martinoia. After graduating, she worked as a researcher collaborator at the Italian Institute of Technology, Genova, Italy, under the supervision of Michela Chiappalone.

In 2011, she started a Ph.D. project at the University of Genova titled "Neuronal network dynamics in 2D and 3D in vitro neuro-engineered systems". The thesis work has been judged excellent by the commission of the Ph.D. in Bioengineering: the results of this thesis are presented in this book.

Starting from September 2014, she is working as a post-doc researcher at the Donders Institute for Brain, Cognition and Behaviour, Radboud University medical center in Nijmegen, the Netherlands, under the supervision of Nael Nadif Kasri. In particular, she is currently working on neurons derived from human Pluripotent Stem Cells in the context of cognitive disorders.

Chapter 1
Introduction

Bi-dimensional networks of dissociated neurons developing in vitro and coupled to Micro-Electrode Arrays devices (MEAs) represent a valid experimental model for studying the universal mechanisms governing the formation and conservation of neuronal cell assemblies (Marom and Shahaf 2002). 2D neuronal networks are used as an experimental model for studying the neuronal dynamics and for understanding some fundamental principles of brain coding (Rieke et al. 1997), learning (Marom and Eytan 2005) and memory (Marom and Shahaf 2002). In this kind of preparation, neurons self-organize during development creating networks which exhibit complex spatio-temporal patterns of activity (van Pelt et al. 2004; Wagenaar et al. 2005; Rolston et al. 2007). Moreover, such recurring activation patterns have been demonstrated to remain stable over long-term recordings of spontaneous activity (Beggs and Plenz 2004) and, at the same time, to change in response to the application of appropriate stimulations. The use of MEAs coupled to neuronal cultures offers the unique opportunity of recording and stimulating, simultaneously and non-invasively, the electrophysiological activity at many sites, allowing detailed investigations on the dynamics of the neuronal system.

Up to now, all the studies performed on cultured cells are based on bi-dimensional (2D) neuronal networks. As recently pointed out (Eytan and Marom 2006; Gal et al. 2010; Cullen et al. 2011; Dranias et al. 2013), besides clear advantages related to controllability and observability, such 2D neuronal model systems have major limitations as they might be inherently unable to exhibit characteristics of in vivo systems. For instance, soma and growth cones in 2D are unrealistically flattened and the axons-dendrites outgrowth cannot occur in all directions (Cullen et al. 2011). With particular reference to the electrophysiological activity, a long-lasting debate has taken place over the years and various criticisms have been introduced on the validity of such 2D experimental reduced models to investigate mechanisms of coding and information transmission (Gal et al. 2010), network plasticity and functional connectivity (Shahaf and Marom 2001; Eytan and Marom 2006), and memory (Dranias et al. 2013). Although these model systems are somehow widely accepted,

M. Frega, *Neuronal Network Dynamics in 2D and 3D in vitro Neuroengineered Systems*, Springer Theses, DOI 10.1007/978-3-319-30237-9_1

one of the major issues raised has often been related to the poor dynamics exhibited by such networks, often dominated by bursting activity encompassing most of the neurons in the network (Wagenaar et al. 2005). This particular behavior has been partly justified with the absence of afferent inputs (Hasselmo 1995; Timofeev et al. 2000a, b) as compared to the wide repertoire of electrical activity patterns found in in vivo studies (Timofeev et al. 2000a, b).

Under this prospective, it is clear that a bi-dimensional model for studying the characteristic of the in vivo system is too reduced: it is needed to scale up to 3D neuronal network systems.

In recent years, scientists have used tissue engineering in attempts to create 3D neuronal cultures that emulate the high cell density and connectivity seen in vivo (Pautot et al. 2008; Cullen et al. 2011). Cells cultured in a 3D environment have been shown to better represent in vivo cellular behavior than cells cultured in a monolayer in several cell types (Smalley et al. 2006). A growing body of evidence suggests that cells grown in planar cultures do not have the same morphology (Cukierman et al. 2001), proliferation rates (Hindie et al. 2006; Willerth et al. 2006), migration (Friedl et al. 1998), gene expression (Birgersdotter et al. 2005; Liu et al. 2006), differentiation (Chun et al. 2006; Willerth et al. 2006), cellular signaling (Pedersen and Swartz 2005), or pathological susceptibility (Behravesh et al. 2005; Hindie et al. 2006; Smalley et al. 2006) as in 3D culture or in vivo.

Pautot and coworkers have recently designed a 3D in vitro system where cell density and network connectivity can be controlled to resemble in vivo conditions while enabling real-time imaging of the network (Pautot et al. 2008). This method is extremely simple and exploit the spontaneous assembly properties of monodispersed beads to form 3D layered hexagonal arrays containing distinct subsets of neurons in different layers with constrained connectivity among neurons on different beads.

Even if several studies have been devoted to the introduction of in vitro 3D neuronal systems (Pautot et al. 2008; Cullen et al. 2011), the use of such experimental models is still limited and no attempt has been presented in the literature related to functional multisite electrophysiological measurements on 3D neuronal networks. The design and implementation of 3D neuronal networks with embedded sensors and recording-stimulating electrodes, would certainly open new opportunities for investigation and new biomedical applications in the neuroscientific domain.

In this thesis I present a new experimental paradigm constituted by 3D hippocampal and cortical neuronal networks coupled to Micro-Electrode Arrays devices (MEAs). 3D neuronal constructs were developed and implemented by using glass micro-beads (Pautot et al. 2008) to design engineered in vitro systems where thickness of the preparation, cell density and network connectivity can be partly controlled to resemble brain tissue while enabling optical observation, environmental control and multisite electrical recording-stimulation. This model is very close to the real brain structure. In fact, there is a dense, layered, 3D interconnected network of neuronal cells, in which every neuron makes hundreds to thousands of specific connections with nearby and remote cognate partners.

By using this model, multi-site electrophysiological recordings of 3D neuronal preparations can be performed. In this work, I show for the first time spontaneous and electrically evoked electrophysiological activity in 3D neuronal cultures coupled to substrate embedded MEAs. I demonstrate how the recorded 3D network dynamics are enhanced with respect to the corresponding 2D model.

Given the intricate relationship between structure and function, the question of how patterns of anatomical connectivity constrain or determine dynamical patterns is of considerable theoretical importance. It is essential to understand how these patterns are generated and how they depend on the underlying anatomical substrate because of the clear correlation between dynamics and perception, cognition and action in the brain (Sporns and Tononi 2001). 3D neuronal networks coupled to MEAs represent an experimental model more realistic than the commonly experimental model used for studying how connectivity and expressed dynamics are related.

3D neuronal network coupled to MEAs is a new and powerful in vitro model capable of better emulating in vivo physiology. It is possible to construct patterned or hybrid (i.e. co-culture) neuronal networks that mimic the in vivo model. For example, it is possible to emulate the modular organization of the cortex constructing a column system in which strong vertical connections between neurons belonging to the same column and weak horizontal connections between neurons of different column are present.

Further development of such a 3D in vitro model with the addition of embedded functionalized scaffolds will open new perspectives for manipulating, stimulating and recording neuronal activity in the direction of elucidating neurophysiological mechanisms and for the future design of bio-hybrid microsystems.

The thesis is organized in four parts.

The first one is entirely dedicated to the scientific and technical background which my study relies on. Basic notions about in vitro electrophysiology of neuronal networks and a technical description of the experimental set-up used for recordings are reported in Chap. 2. Then, an overview of different types of 2D neuronal networks with advantages and limitations of these models are reported in Chap. 3. Finally, the state of the art about 3D neuronal network is reported in Chap. 4.

The second part of the thesis deals with the results coming from 3D networks coupled to MEAs (Chap. 5). Firstly, the method for constructing the 3D neuronal network is presented. Then, the 3D hippocampal neuronal network dynamics (both spontaneous, stimulus-evoked, and after chemical manipulation) are shown. Finally, the spontaneous activity of 3D cortical neuronal networks is reported.

The third part reports further MEA applications in which I was involved during these years. Results about neuro-pharmacological (Chap. 6) are reported.

The fourth part regards the discussion and conclusions of the thesis. Conclusion of the work and future perspectives are reported in Chap. 7.

References

Beggs JM, Plenz D (2004) Neuronal avalanches are diverse and precise activity patterns that are stable for many hours in cortical slice cultures. J Neurosci 24:5216–5229

Behravesh E, Emami K et al (2005) Comparison of genotoxic damage in monolayer cell cultures and three-dimensional tissue-like cell assemblies. Adv Space Res 35(2):260–267

Birgersdotter A, Sandberg R et al (2005) Gene expression perturbation in vitro–a growing case for three-dimensional (3D) culture systems. Semin Cancer Biol 15(5):405–412

Chun TH, Hotary KB et al (2006) A pericellular collagenase directs the 3-dimensional development of white adipose tissue. Cell 125(3):577–591

Cukierman E, Pankov R et al (2001) Taking cell-matrix adhesions to the third dimension. Science 294(5547):1708–1712

Cullen DK, Wolf JA et al (2011) Neural tissue engineering and biohybridized microsystems for neurobiological investigation in vitro (part 1). Crit Rev Biomed Eng 39(3):201–240

Dranias MR, Ju H et al (2013) Short-term memory in networks of dissociated cortical neurons. J Neurosci Off J Soc Neurosci 33(5):1940–1953

Eytan D, Marom S (2006) Dynamics and effective topology underlying synchronization in networks of cortical neurons. J Neurosci 26(33):8465–8476

Friedl P, Zanker KS et al (1998) Cell migration strategies in 3-D extracellular matrix: differences in morphology, cell matrix interactions, and integrin function. Microsc Res Tech 43(5):369–378

Gal A, Eytan D et al (2010) Dynamics of excitability over extended timescales in cultured cortical neurons. J Neurosci 30(48):16332–16342

Hasselmo ME (1995) Neuromodulation and cortical function: modeling the physiological basis of behavior. Behav Brain Res 67(1):1–27

Hindie M, Vayssade M et al (2006) Interactions of B16F10 melanoma cells aggregated on a cellulose substrate. J Cell Biochem 99(1):96–104

Liu H, Lin J et al (2006) Effect of 3D scaffold and dynamic culture condition on the global gene expression profile of mouse embryonic stem cells. Biomaterials 27(36):5978–5989

Marom S, Eytan D (2005) Learning in ex-vivo developing networks of cortical neurons. Prog Brain Res 147:189–199

Marom S, Shahaf G (2002) Development, learning and memory in large random networks of cortical neurons: lessons beyond anatomy. Q Rev Biophys 35(1):63–87

Pautot S, Wyart C et al (2008) Colloid-guided assembly of oriented 3D neuronal networks. Nat Methods 5(8):735–740

Pedersen JA, Swartz MA (2005) Mechanobiology in the third dimension. Ann Biomed Eng 33(11):1469–1490

Rieke F, Warland D et al (1997) Spikes: exploring the neural code. The MIT Press, Cambridge, Massachusetts

Rolston JD, Wagenaar DA et al (2007) Precisely timed spatiotemporal patterns of neural activity in dissociated cortical cultures. Neuroscience 148(1):294–303

Shahaf G, Marom S (2001) Learning in networks of cortical neurons. J Neurosci 21(22):8782–8788

Smalley KS, Lioni M et al (2006) Life isn't flat: taking cancer biology to the next dimension. In Vitro Cell Dev Biol Anim 42(8–9):242–247

Sporns O, Tononi G (2001) Classes of network connectivity and dynamics. Complexity 7(1):28–38

Timofeev I, Grenier F et al (2000a) Origin of slow cortical oscillations in deafferented cortical slabs. Cereb Cortex (New York, NY: 1991) 10(12):1185–1199

Timofeev I, Grenier F et al (2000b) Impact of intrinsic properties and synaptic factors on the activity of neocortical networks in vivo. J Physiol, Paris 94(5–6):343–355

van Pelt J, Wolters PS et al (2004) Long-term characterization of firing dynamics of spontaneous bursts in cultured neural networks. IEEE Trans Biomed Eng 51(11):2051–2062

Wagenaar DA, Madhavan R et al (2005) Controlling bursting in cortical cultures with closed-loop multi-electrode stimulation. J Neurosci 25(3):680–688
Willerth SM, Arendas KJ et al (2006) Optimization of fibrin scaffolds for differentiation of murine embryonic stem cells into neural lineage cells. Biomaterials 27(36):5990–6003

Part I
Scientific and Technical Background

Chapter 2
Dissociated Neuronal Networks Coupled to Micro-Electrode Arrays Devices

In this chapter, I will outline some basics about neurons and how they can communicate with each other (see Sect. 2.1). In the following section, I will report some brief notes about different kinds of in vitro neuronal preparations (see Sect. 2.2). Then I will present an overview about the state-of-the-art of electrophysiological techniques focusing on in vitro applications (see Sect. 2.3). Then I will dedicate three paragraphs to the description of Micro-Electrode Arrays (MEA) technique (see Sects. 2.4–2.6), which is the main tool exploited in the context of this thesis. Finally I will use an entire section for an overview of MEA applications (see Sect. 2.7).

2.1 Neurons and Synapses

Although the human brain contains a thousand different types of neurons, they all share the same basic architecture (Fig. 2.1). The complexity of human behavior depends less on the specialization of individual nerve cells and more on the fact that a great number of these cells define precise anatomical circuits. Hence, the capability of the nervous system to produce different actions in response to complex sensory stimuli derives from the way neurons are connected with each other and with sensory receptors and muscles, rather than single-cell specialization (Kandel et al. 2000).

A neuron has four morphologically defined regions: soma, dendrites, axon and presynaptic terminals. The soma is the metabolic centre of the cell, it contains the nucleus and the endoplasmic reticulum. The dendrites branch out from the soma and are the main apparatus for receiving incoming signals from other nerve cells. The axon extends away from the cell body and it is the main conducting unit for carrying signals to other neurons. A single neuron can communicate with another one thanks to synapses. The synapse is the point at which two neurons communicate and involves a presynaptic cell, which transmits a signal (i.e. axon), and a postsynaptic cell, receiving the signal (i.e. dendrites). The presynaptic terminal is a specialized

M. Frega, *Neuronal Network Dynamics in 2D and 3D in vitro Neuroengineered Systems*, Springer Theses, DOI 10.1007/978-3-319-30237-9_2

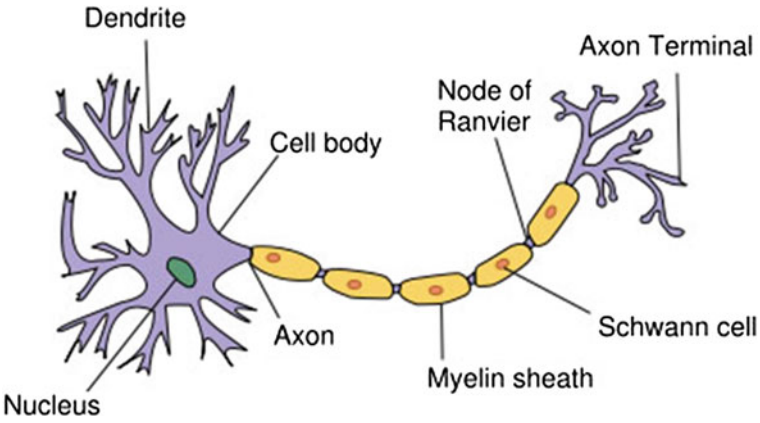

Fig. 2.1 Simplified sketch of a neuron

cell compartment in which the electrical signals (i.e. action potentials) traveling through the axon are transduced in a chemical signal (i.e. neuro-transmitter release) captured by the postsynaptic receptors present in the dendrites. This chemical signal is again translated in an electrical one, affecting the postsynaptic neuron's membrane potential, and thus accomplishing the synaptic transmission.

At rest, all nerve cells maintain a difference in the electrical potential (V) on either side of the plasma membrane: this is called the resting membrane potential (Fig. 2.2) and in a typical neuron it is about −65 mV (V = Vintracellular − Vextracellular). The difference in electrical potential when the cell is at rest results from two factors: the unequal distribution of electrically charged ions, in particular the positively charged Na^+ and K^+ ions and the negatively charged aminoacids and proteins on

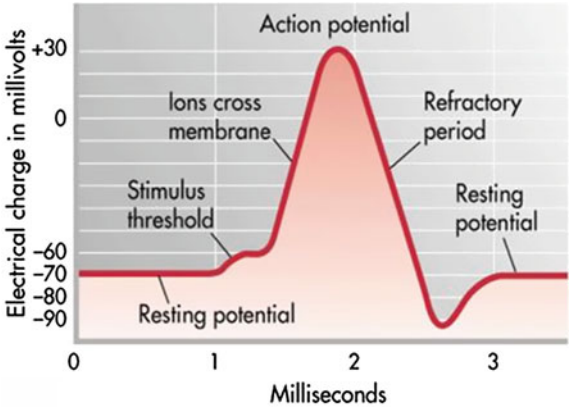

Fig. 2.2 Scheme of action potential generation

either side of the cell membrane, and the selective permeability of the membrane to just one of these ions, K^+.

In order to send a signal, in the presynaptic cell an action potential has to be generated. The action potential is composed of a rising phase (depolarization), followed by a falling phase bringing the membrane potential V down to a hyperpolarization phase. This shape is due to the activity of voltage-controlled channels of the membrane that modify the Na^+ and K^+ ion permeability as a function of the membrane potential. The phases of the action potential are reported in Fig. 2.2.

Briefly, when the presynaptic neuron receives an input (synaptic or sensory, mediated by receptors) an influx of Na^+ or Ca^{2+} ions depolarizes the membrane: when the depolarization exceeds a critical threshold, the voltage-gated Na^+—permeable ion channels are open and V rapidly increases towards positive values. When V reaches its peak, the voltage-gated Na^+ channels close and, at the same time, the voltage-gated K^+ channels open, leading to a strong outflux of K^+ ions that re-establishes a negative membrane potential. The action potential is an all-or-none

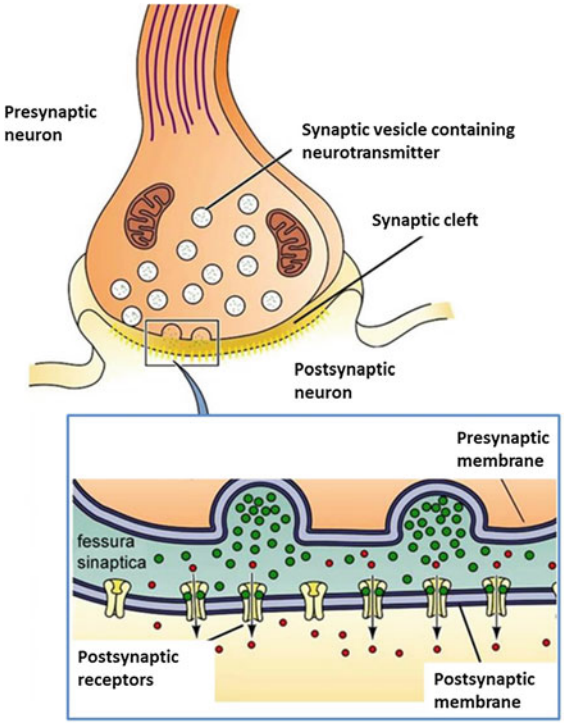

Fig. 2.3 Model of a synapse. Released of the neurotransmitters from the vesicles in the presynaptic neuron; neurotransmitters diffusion across the tight space that separates the presynaptic and postsynaptic terminals (i.e. synaptic cleft); neurotransmitters binding with the corresponding receptors in the membrane of the postsynaptic neuron

signal: this means that while stimuli below the threshold will not produce a signal, all stimuli above the threshold produce the same signal.

When an action potential reaches a pre-synaptic neuron's terminal, it stimulates the release of a chemical transmitter from the cell, as the neuron's output signal. The transmitters are held in vesicles, as it is shown in the sketch of Fig. 2.3. In the Central Nervous System (CNS) the major excitatory transmitter is L-glutamate, while the major inhibitory transmitter is γ-aminobutyric acid (GABA) (Kandel et al. 2000). After the transmitter is released from the presynaptic neuron, it diffuses across the tight space that separates the presynaptic and postsynaptic terminals (i.e. synaptic cleft) and it binds the corresponding receptors in the membrane of the postsynaptic neuron (Fig. 2.3). The binding of transmitter to receptors causes the postsynaptic cell to generate a synaptic potential. Whether the synaptic potential has an excitatory (i.e. depolarizing) or inhibitory (i.e. hyperpolarizing) effect will depend on the type of receptors in the postsynaptic cell, not on the particular neurotransmitter (Kandel et al. 2000).

2.2 In Vitro Preparations

In the early 1900s, the first studies in neurobiology employing tissue cultures were performed by Harrison (1907, 1912): he examined the outgrowth of fibers from fragments of frog and chick neural tube cultured in drops of clotted lymph or plasma and demonstrated for the first time that nerve fibers arise as outgrowths from individual nerve cell bodies (Banker and Goslin 1998). These studies paved the way to the use of tissue cultures' techniques to address biological problems (Carrell and Burroughs 1910). In the following decades, in vitro culturing began to gain a more prominent and important position in neurobiology. Today, tissue culture is an integral part of modern neurobiology.

Two main methodologies of in vitro preparations are usually used: slice cultures and dissociated neuronal networks. Even if dissociated neuronal networks are the preparation used in all the experiments presented in this work, however, a brief description of the slice cultures preparation will be provided.

2.2.1 Slice Preparations

Brain slices are thin hundreds micrometers slices (200–500 μm) of brain regions containing about 10^3 neurons.

Brain slices are freshly cut from in vivo developed animal brains. These kinds of cultures are called acute slices. Organotypic cultures are explanted from relatively young animals (e.g. rats, 1–3 weeks old) and allowed to attach to an appropriate substrate and cultured in a rich medium. These cells continue to differentiate and

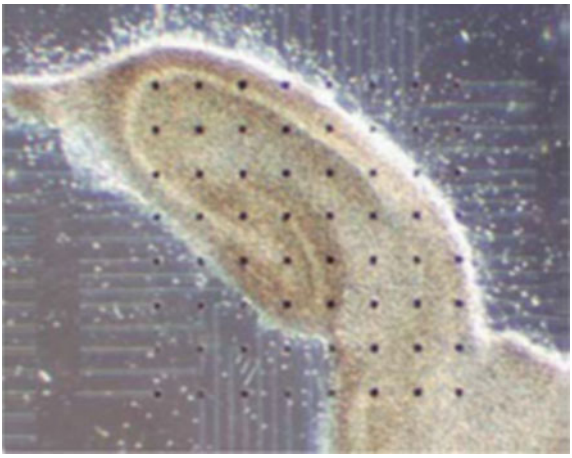

Fig. 2.4 Hippocampal slice from an 11-day-old rat, cultured and maintained on MED64 probes (Alpha Med Scientific Inc., Japan)

develop in culture, extending processes and forming new synapses and they can be maintained for months, in appropriate controlled conditions.

The main peculiarity and advantage of using this preparation consists in the partial preservation of the morphological and functional original structure of the intact brain. Brain slices allow recording from semi-intact neural circuits, with the advantages of mechanical stability and control over the extracellular environment. These preparations are used for a wide variety of studies, like synaptic plasticity and development, network oscillations, intrinsic and synaptic properties of defined neuronal populations (Kettenmann and Grantyn 1992). Many neuroscientists use brain slices coupled to Micro-Electrode Arrays devices (MEAs) instead of dissociated cultured neurons (Eytan and Marom 2006; Chialvo 2007) since they maintain the topology of the original tissue. An example of a brain slice coupled to MEA devices is reported in Fig. 2.4.

2.2.2 Cultured Neuronal Networks

At the beginning of the 20th century, the demonstration that the tissues could survive and grow outside the body and that complex aspects of neuronal maturation, such as synaptogenesis and myelination, could occur not only in vivo but also in vitro (Peterson and Murray 1955; Murray et al. 1977) opened new possibilities to study the nervous system creating a widespread interest from the scientific community and capturing the attention of many neuroscientists.

Since cultured neurons remain healthy for long periods (months), they represent an ideal substrate for investigating brain properties at the network and circuit, i.e.

parts of network, level. Thanks to the continuous technological improvements and with increasing experience, it has become possible preparing dissociated cell cultures from virtually every region of the nervous system and from many different animal species.

Generally, neurons in dissociated cultures appear to retain their individual identities and their morphological and physiological properties correspond closely to the characteristics of the cell populations in the original tissue (Kriegstein and Dichter 1983). Although synaptic interconnections grow randomly in culturing conditions and the morphology of the neuronal networks is not maintained with respect to in vivo condition, dissociated cultures represent a reasonable, simplified model of the brain. In fact, cultured neurons replicate in vivo synaptic events, at different scale levels, ranging from single synapses to complex circuitry. At the level of single synapse, both excitatory and inhibitory transmissions were observed and the kinetics of receptors, ion channels and neurotransmitters release were similar to the ones measured in in vivo conditions. At single-cell scale level, these analogies include action potentials and different types of modulatory currents. Finally, complex mechanisms, like long-term potentiation (LTP) which is interesting because it is considered the synaptic analogy of learning, have been observed and characterized in neuronal micro-cultures.

2.2.2.1 Preparation and Growth

In this thesis I made use of primary cultures of dissociated neurons (hippocampal and cortical) from rat embryos. In what follows, I briefly describe the procedure used to obtain and maintain the cultures.

Hippocampal and cortical neurons were dissociated from E18 Sprague Dawley rats (Charles River Laboratories, Milano). The procedure was approved by the European Animal Care Legislation and by the guidelines of the University of Genova. The day before the plating, MEAs (Multi Channel System MCS GmbH) are sterilized at 120 °C in the oven. The sterilized material is therefore exposed to the coating treatment with adhesion protein Laminin (L-2020 Sigma) and Poli-Lysin (P-6407 Sigma) at 0.05 µg/ml overnight in incubator at 37 °C. The adhesion factors are removed and the treated glass surfaces are washed with sterile water. MEAs are left to dry inside the laminar hood.

From each embryo, hippocampi and cortices were removed and placed into ice cold Hank's balanced salt solution. The tissue was then dissociated in 0.125 % of Trypsin/Hank's solution containing 0.05 % of DNAse (D-5025 Sigma-Aldrich) for 15–18 min at 37 °C. The supernatant solution was removed and the enzymatic digestion was stopped by adding 10 % fetal bovine serum (FBS) in Neurobasal medium for 5 min. Medium with FBS was removed and replaced with Neurobasal medium supplemented with B27, 1 % Glutamax, gentamicin 10 µg/ml (Gibco Invitrogen). Cells were then plated directly onto the area of MEA electrodes at the final concentration of about 1200 cells/µl. The obtained 2D cultures were maintained in a humidified CO_2 atmosphere at 37 °C for 3–4 weeks. Half of the media was replaced

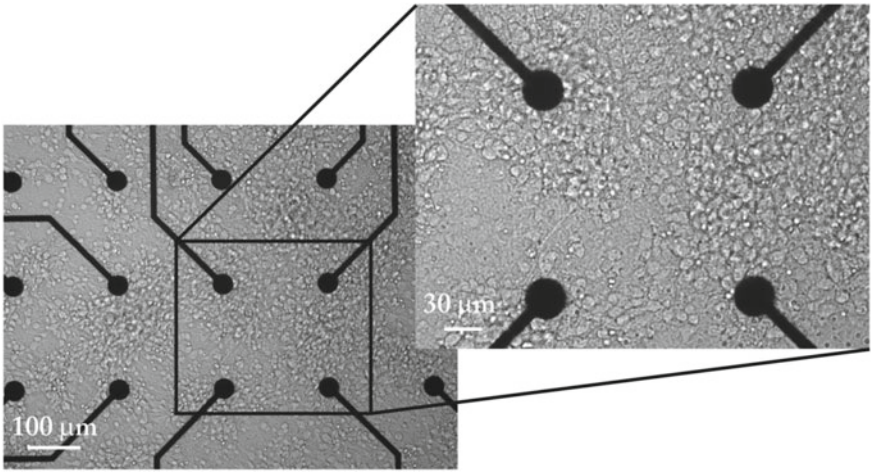

Fig. 2.5 Image of a neuronal network cultured over an MEA for 24 days in vitro at two magnifications (10× and 20×, calibration bars: 100 and 30 μm)

once a week. No antimitotic drug was added to prevent glia proliferation, since glial cells are essential elements for a healthy development of neuronal networks. The cultures can be kept in healthy conditions for several weeks and after 3–4 weeks in vitro they reach a mature developmental stage, characterized by quasi synchronous array-wide bursts, mixed with isolated random spike. In Fig. 2.5 an image of a dissociated neuronal network coupled to MEA is shown.

2.3 Electrophysiology Techniques

Different techniques exist for measuring and evoking the electrophysiological activity of in vitro neuronal networks: a first distinction can be made between intracellular and extracellular techniques.

The intracellular technique allows the direct measurement of the potential difference across the membrane. The action potential has been described considering the ionic flows across the cellular membrane. This kind of electrophysiological measurement needs two measuring points, one in the cell and the second outside and requires the breaking of the membrane.

Alternatively, utilizing an extracellular technique, one can place the first measuring point outside the cell, but very close to the membrane, and the second one, the reference, far away from the cell. When an action potential occurs, the intracellular and extracellular ionic concentrations are both modified by the membrane transport properties: the extracellular changes are localized near the membrane and currents entering or leaving a neuron generate voltage signals at the electrode nearby. This

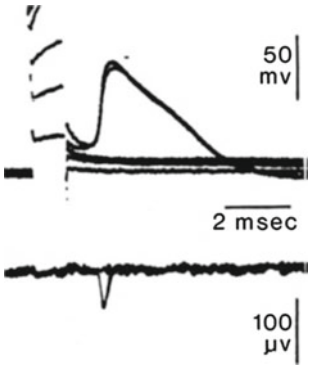

Fig. 2.6 Intracellular oscilloscope traces are at the top. Action potential signals are seen for the largest two. Below are extracellular recordings made simultaneously with the intracellular ones. The two below baseline are from the action potentials, and are too similar to resolve. From Pine (1980)

results from a resistive drop in the medium between the reference electrode and the recording electrode.

Intracellularly and extracellularly recorded signals are very different. Not only the amplitude of extracellular signals is lower than that of intracellular ones (20–200 μVpp for a typical action potential of 100 mVpp measured intracellularly), but also the shape is different (Fig. 2.6).

A neuron can be excited intracellularly by injecting a current directly into it, but also an extracellular stimulation can be realized by applying a voltage or a current pulse to the extracellular electrode. In both cases, however, membrane polarization of the target neurons is primarily affected by the voltage gradient generated by the local current density and tissue resistance in the vicinity of the cells (Fejtl et al. 2006).

In vitro electrophysiology has seen the majority of its development using glass pipette electrodes. Neurophysiologists have studied single-cell properties, ion channels, drugs' effects and synaptic signaling with these electrodes (Kettenmann and Grantyn 1992). The electrodes are made by pulling a glass tube into a fine capillary at one end (less than 1 μm in diameter) and filling it with a saline solution, whose composition matches with either the composition of the cytoplasm or of the bath solution, depending on the chosen configuration. Finally an electrode, typically platinum or Ag/AgCl, electrically contacts the solution to the measuring circuit. Glass pipettes are used in different configurations: intracellular, extracellular or patch-clamp.

Conventional methods (i.e. patch clamp) allow to record neuronal signals from only few cells at time in an invasive way. MEAs, on the contrary, allow recording extracellular neurons signals simultaneously from hundred electrodes at the time in a non-invasive way.

2.4 MEA for Network Electrophysiology

Thomas et al. described the first Micro-Electrode Arrays in 1972. It consisted of platinized gold microelectrodes (two rows of 15 electrodes each, spaced 100 μm apart) embedded onto a glass substrate and passivated by photoresist. This device allowed to record field potentials from spontaneous contracting sheets of cultured chick cardiomyocytes, but it was not able to record activity from each single cell.

Five years later, Guenter Gross and his collaborators proposed the idea of a MEA, without knowledge of the previous work (Gross et al. 1977). They showed recordings from an isolated snail ganglion laid over the electrodes, with single action potentials having amplitudes up to 3 mV, depending upon the cell size.

The first successful recordings from single dissociated neurons using a MEA were reported by Pine in 1980 (Fig. 2.6): he succeeded in recording from a network of rat superior cervical ganglion neurons, cultured for up to three weeks over an MEA with 32 gold electrodes (two parallel lines of 16 electrodes each, 10 μm square and 250 μm apart), platinized and insulated with silicon dioxide (Pine 1980). He also used the same MEA for stimulating neurons with a voltage pulse of 0.5 V and duration of 1 ms.

These three works put a milestone for the upcoming work and marked the beginning of in vitro network electrophysiology using MEAs.

In the 1980s, many studies employing MEAs for different purposes followed. Some exploited these new tools to investigate either the network activity of cultures of dissociated neurons (Gross et al. 1982) or of hippocampal slice preparations (Wheeler and Novak 1986). Soon, it was clear that large invertebrate neurons were the most suitable to be plated on top of MEAs (Regehr et al. 1989). They can be easily identified thanks to their size and location in the ganglia, can be dissected out, and can be used with other identified neurons to form simple networks in culture that replicate some of their connections in vivo. MEAs can provide a means for long-term noninvasive communication with such networks for stimulation and recording, much superior to conventional electrodes (Pine 2006). Differently, at the end of the 1980s, Meister et al. coupled an explanted salamander retina to an MEA (and later on retinas from newborn ferrets and cats) and they could record spontaneous and evoked by light stimulation bursts of activity (Meister et al. 1994).

At the beginning of the 1990s, the combination of a MEA (for stimulation) and voltage sensitive dyes (for recording) was exploited to allow the detection and measurement of subthreshold synaptic potentials, otherwise impossible by recording extracellular electrical signals (Chien and Pine 1991). At the same time, Fromherz and his collaborators investigated the use of a field effect transistor (FET) to record action potentials from large Retzius cells of the leech (Fromherz et al. 1991), and this began a series of investigations in the Fromherz lab aimed at understanding the FET-neuron interface. As originally foreseen by Thomas and collaborators (Thomas et al. 1972), network development and plasticity are the most interesting questions that can be addressed by using MEAs.

Nowadays the MEA technique offers a useful experimental approach for in vitro electrophysiological investigations. MEA technology and culture methods, in parallel, have continuously improved during these years. To date, MEAs find several applications in many research fields, such as neuroscience, pharmacology, physiology, biophysics and cardiac electrophysiology.

2.5 MEA Technology

The current technology typically provides MEAs formed by 60–256 electrodes, 10–30 μm in diameter spaced at 100–500 μm. MEAs consist of microfabricated electrodes embedded in a biocompatible insulation substrate (e.g., polyamide or silicon nitride/oxide) which prevents short circuits with the electrolyte bath, forming a sort of wired Petri dish. The electrodes, typically made of Au, Indium-Tin Oxide (ITO), Titanium Nitride (TiN), or black platinum, must be biocompatible, long-term lasting, and preferably should have low impedance (less than 500 KΩ at 1 kHz) for low thermal noise. Cells adhesion on the MEA is promoted by covering them with

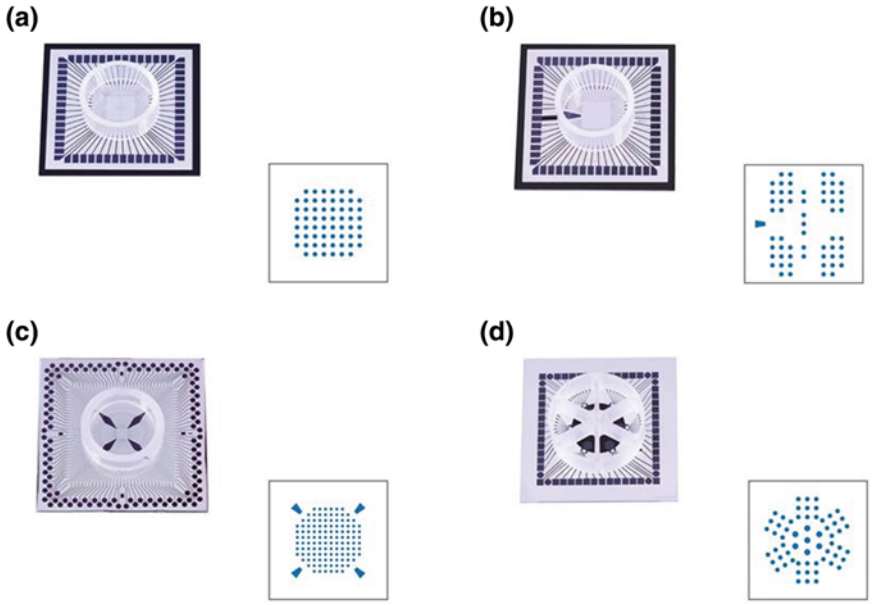

Fig. 2.7 MEA devices and electrodes layouts. **a** Standard 60MEA: 60 electrodes, electrode grid 8 × 8, electrode spacing 100 μm and electrode diameter 10 μm. **b** 60-4QMEA: 60 electrodes, electrode grid 4× (1 × 4 + 1 × 5 + 1 × 4) + center line 1 × 7, electrode spacing 200 μm inside the quadrants, 1000 μm between the quadrants, electrode diameter 30 μm. **c** 120MEA: 124 electrodes, electrode grid 12 × 12, electrode spacing 200 μm, electrode diameter 30 μm. **d** 60-6WellsMEA: 54 electrodes, electrode grid 3 × 3 in each area, electrode spacing 200 μm, electrode diameter 30 μm

laminin and poly-L-lysin or collagen (Robinson et al. 1993; Jimbo et al. 1999). In Fig. 2.7 four different types of MEA devices are presented.

Since neurons are directly cultured on the MEA, the distance between the cells (adhering to a surface containing the electrode) and the electrode typically ranges from 10 to 100 nm (www.multichannelsystems.com, Reutlingen, Germany). The electrode size is a compromise regarding both biological and electrical considerations. Indeed, the electrode should be as small and close as possible to the cells in order to obtain information from localized point. At the same time, the electrode should have a sufficient surface to detect electrical signals with an acceptable signal to noise ratio.

The fabrication of MEAs is based on the thin-film technology (Elshabini-Riad and Barlow 1998) and is realized in a clean-room. Photolithography, i.e., the process of transferring geometric shapes from a mask to the surface of a silicon wafer, is used to make MEAs.

The rapid success met by MEAs in the neuroscience research field moved some electronic companies to develop commercial systems to perform electrophysiological measurements using MEAs. At the present, there are on the market at least three complete acquisition systems based on MEAs: the MED System developed originally by Panasonic and now developed and manufactured by Alpha MED scientific (www.med64.com, Osaka, Japan), the MEA System by Multi Channel Systems (www.multichannelsystems.com, Reutlingen, Germany) and the 3-Brain system (www.3brain.com).

Other companies, such as Ayanda-Biosystems (www.ayanda-biosys.com, Lausanne, Switzerland), have only developed the microelectrode devices, for several different applications (cultures, slices, cardiomyocytes, retinal cells, pharmacological screening, etc.). Finally, Plexon (www.plexoninc.com, Dallas, USA) developed hardware and software tools to be used in conjunction with third parties microdevices.

All the experimental results involving standard commercial devices presented in this thesis were obtained from recordings performed on systems and MEAs manufactured by Multi Channel Systems. The following sections deal with the description of this experimental set-up.

2.5.1 Standard MEA

The experimental set-up used to perform the experiments analyzed in this thesis, was based on the MEA System (Multi Channel Systems, MCS, Reutlingen, Germany). They offer, together with the MEAs, complete workstations for electrophysiological investigation based on micro-electrode arrays.

The device utilized in this thesis consists of 60 round planar micro-electrodes made of TiN/SiN (see Fig. 2.8a), with a diameter of 30 μm and spaced at 200 μm. The electrodes are arranged in a 8×8 matrix configuration with the four electrodes at the corners disconnected (Fig. 2.8c). In order to record the extracellular signals,

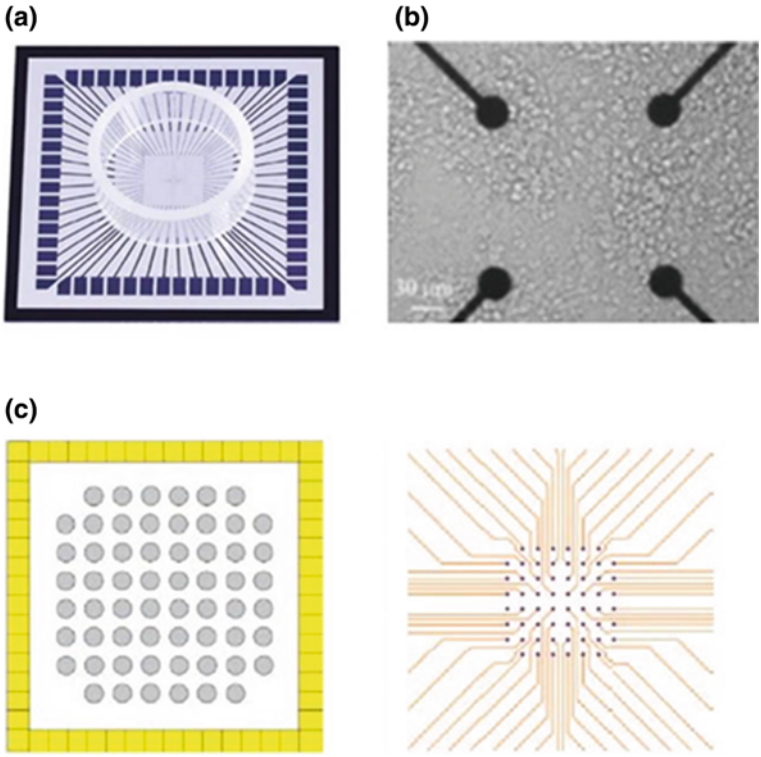

Fig. 2.8 Standard 60MEA. **a** Image of a typical MCS MEA. **b** Optical images of a neuronal network over an MEA at 14 days in vitro. **c** 8 × 8 layout of an MCS MEA (electrodes size of 30 µm and inter-electrode spacing of 200 µm)

MEAs need a reference electrode respect to which evaluating the voltage potential. Some arrays, presenting an internal reference electrode, do not need to hole the led protecting the culture (differently from what happens by using the external reference) which exposes neurons more easily to infections. For this reason, internal references are usually used during experiments on developmental studies in order to maintain the condition of the culture as much healthy as possible during the whole developmental stage.

A glass/plastic ring is placed at the center of the array, and it allows to contain the culture medium. In this way, when placed in an incubator, the culture can survive for several weeks (Fig. 2.8b).

2.5.2 Experimental Set-up

The Multi Channel Systems set-up is made up of the following components contained inside a Faraday cage in order to reduce electromagnetic interferences. During this thesis I utilized two different amplifiers. All the components are presented in Fig. 2.9.

- **MEA 2100 Amplifier**
  Extending the MultiChannel Systems MEA-product family, the MEA 2100-System follows the tradition of high-quality, low-noise amplifiers. It is the complete setup for extracellular recordings from MEAs. It includes data acquisition computer with software, interface board, MEA-headstage with integrated stimulation, MEAs. It is connected via only one MCS High Speed cable to the interface board, which offers various digital and analog in-/outputs for synchronization with other instruments. The main advantage of MEA-2100-System is the flexibility. Multichannel systems offers various contact units for the MEA headstage. It is possible to decide whether to work with one or two 32-electrodes MEA, one or two 60-electrodes MEA or one 120-electrodes MEA. The flexibility of the MEA-2100-System is also reflected in the possibility to connect two MEA-headstages to one interface board. This way, you can record from up to 240 channels. The MEA 2100 Amplifier is reported in Fig. 2.9a.
- **MEA 1060 Amplifier**
  An amplifier stage for multi-electrode recording has to meet two main requirements: eliminating the cables connecting the electrodes and coping with the interference (cross-talk phenomenon) among channels.
  The MEA1060 60-channel amplifier has a compact design ($165 \times 165 \times 19$ mm) and, due to the surface-mounted technology (SMD) of pre- and filter-amplifiers, the complete circuit and amplifier hardware was built into a single housing: this ensures optimal signal-to-noise ratio of the recording, because no further cables are necessary other than a single SCSI-type cable connecting the amplifier to the data acquisition card. This results in an overall low noise level of the complete amplifier chain ($\times 1200$, 12-bit resolution, 10 Hz to 3 kHz) of ± 3 μV, which is well within the ± 5 to 10 μV noise level of the MEA TiN electrode. Hence, the MEA sensor is placed directly inside the amplifier and settled so as to fit the standard microscopes. The MEA 60 Amplifier is reported in Fig. 2.9b.
- **PCI-based acquisition board**
  Standard PC technology is used as the backbone of high-speed multi-channel data acquisition. The data acquisition card is based on PCI-bus technology and allows the simultaneous sampling of up to 128 channels at a sampling rate of 50 kHz per channel. It is possible to set the input voltage range from ± 400 mV to ± 4 V in the data acquisition software and this allows to use the full 12-bit resolution bandwidth for signals of any amplitude. Three analog channels and a digital I/O port are accessible, allowing the simultaneous acquisition of analog data, such as current traces from a patch clamp amplifier or temperature together with the MEA electrode data.

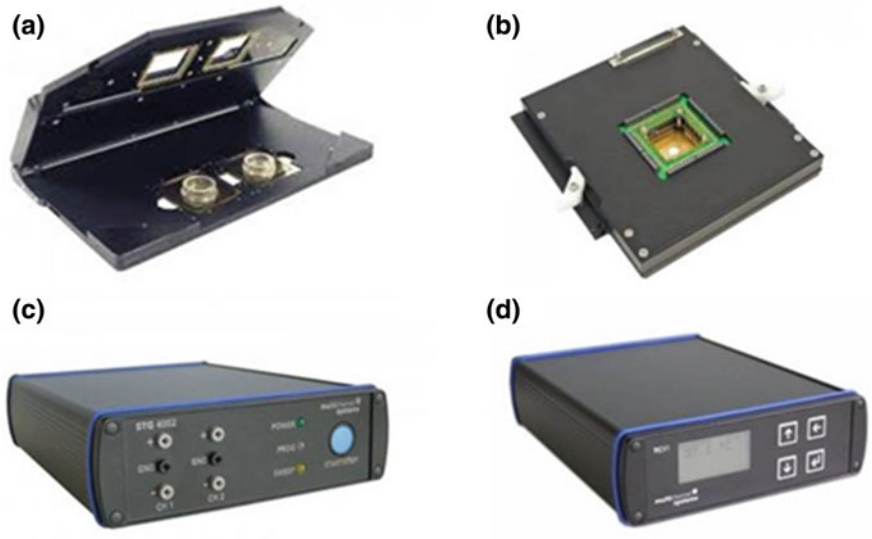

Fig. 2.9 Setup components. **a** MEA 2100 amplifier. **b** MEA 1060 amplifier. **c** Stimulus generator. **d** Temperature controller

- **MCS Stimulus Generator (STG1080)**
  The MCS stimulus generator is a general-purpose stimulator which generates pulses to be delivered to stimulating electrodes (2 for this model and up to 8 for upgraded models). Complex stimulus waveforms (both current and voltage) of arbitrary duration are designed by using the provided MCS stimulus software and then stored in the stimulus generator connected to the MEA. Stimuli are tailored by the user by specifying the desired pulse waveform defining parameters into a worksheet. The pulse PCI-based acquisition board waveform is then displayed and the stimulus protocol is downloaded to the stimulus generator via a serial communication port. The stimulus generator operates in both voltage and current mode, and it is equipped with separate voltage and current outputs for each channel. The STG stimulus generator is reported in Fig. 2.9c.
- **Acquisition software**
  The MC Rack software allows to record simultaneously the electrophysiological activity from the 60 electrodes of the MEA, and monitor the raw data in a real-time mode. Different parameters can be extracted from the data streams and the results can be plotted, saved, and exported to other programs for further analysis.
- **Temperature controller**
  The MCS Temperature Controller uses a Proportional Integrative Derivative (PID) based technology. The MEA temperature can vary in the range from room temperature to +50 °C. The set-point temperature is reached within a range of 30 s to 5 min, depending on the recording system configuration. The Temperature controller is reported in Fig. 2.9d.

2.6 Increasing Spatial Resolution with MEAs

Current MEAs provide typically 60–256 electrodes with 100–500 μm inter-electrode spacing. As the recorded signals originate from the cells in close proximity to the electrodes, and as the distribution of the cellular networks is random, the number of recording sites, i.e. the spatial resolution, is therefore limited. As an example, a culture of 50,000 neurons coupled to 50 electrodes presents an undersampling of the network activity by a factor of 10^3.

Although a typical spatial resolution (inter-electrode spacing) of 100 μm is adequate for studying the overall network activity, it is not enough to exploit the potential capability of MEAs: in particular, it does not provide electrophysiological data at a multi-level spatial resolution for correlating network, cellular and sub-cellular activities. It is necessary to plate cells at a relatively high density (about 2000 cells/mm^2) to get a good covering of the electrodes. These issues has led to the search for an array with a very high number of embedded microelectrodes, whose size (and distance) is comparable to that of a neuron (Imfeld et al. 2008). The availability of this feature is particularly suited for unraveling the fundamental properties of brain tissue, whose activity arises from signal integrations and propagations at synaptic, cellular and population levels.

Considering the technological advances of the modern electronic industry (i.e. ever increasing electronics miniaturization and machines' storage and computation capabilities), quite recently there has been a strong effort towards the production of high-density MEAs.

To achieve a high spatial resolution, Berdondini et al. (2009b) developed an high-density 60 microelectrode MEA (HD-MEA). Four different MEA layouts, (22 and 30 μm electrode diameters, 20 and 10 μm spaced) were designed. The layout of the array is divided into 4 clusters of 15 high-density microelectrodes each. The advantage of this configuration relies on the possibility of investigating interconnected neuron sub-population, both on a local network basis (i.e., considering the high-density clusters) and on a whole network basis (considering the four separated high-density clusters).

The previously described HD-MEAs offer the advantage to increase the spatial resolution with respect to the standard and commercial devices, but they are limited in terms of amount of electrodes. For studying signal propagation along neuronal networks it is essential to increase the recording sites of some order of magnitude. To achieve a high spatial resolution a CMOS technology-based solid state Active Pixel Sensor (APS) array, featuring 4096 pixels, has been developed (Fig. 2.10a) (Berdondini et al. 2005, 2009a; Imfeld et al. 2008). The APS-MEA core is a specific integrated circuit, which implements an array of 4096 electrodes (organized in a 64×64 grid) with corresponding amplification, addressing and multiplexing functions (Imfeld et al. 2008; Berdondini et al. 2009a).

The use of CMOS-based devices can overcome some limitations of passive MEAs, in particular for performing measurements at a high spatial and temporal resolution. The simultaneous recording from all electrodes requires the front-end

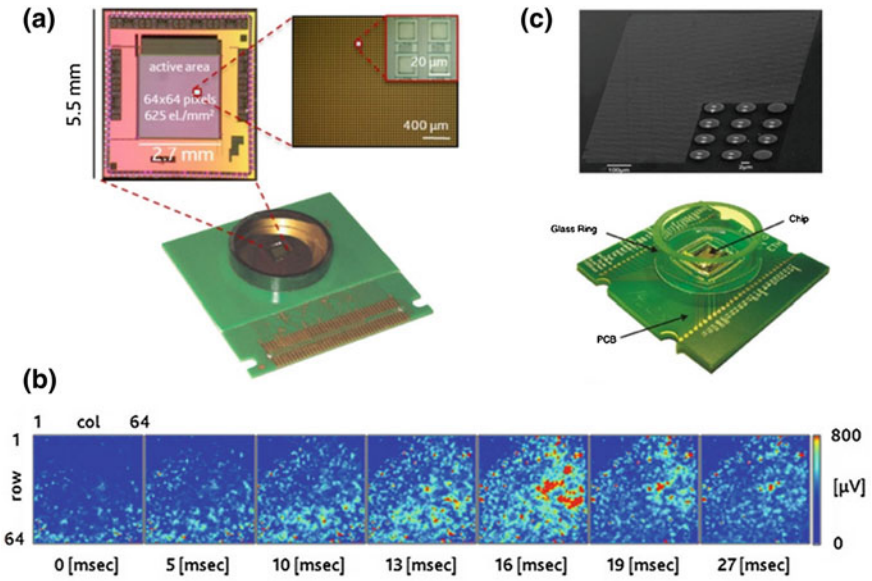

Fig. 2.10 High density devices. **a** CMOS technology-based solid state Active Pixel Sensor (APS) array (Berdondini et al. 2009a). **b** Activity recorded by 4096 electrodes of the APS device. **c** CMOS based device composed by 11,011 metal electrodes and 126 channels (Imfeld et al. 2008)

amplifiers being placed in each pixel (recording site), which, due to area constraints, entails rather high noise levels. Instead of scanning the entire electrode array, the approach presented by Frey and coworkers (Frey et al. 2007, 2009) provides a reconfigurable electrode/readout-channel routing to select an arbitrary subset of electrodes for recording and stimulation (Fig. 2.10b). The system is composed by 11,011 metal electrodes and 126 channels, each of which comprises recording and stimulation electronics. In another approach (Imfeld et al. 2008), an active MEA chip was described with a pitch of 42 µm of 4096 metal electrodes (subset of 126 channels for recording) on a CMOS chip with local filtering and amplification. In another work (Lambacher et al. 2010), Lambacher and co-workers reported a significant progress of neuronal recording by multi-transistor array (128 × 128 sensors) chips with EOMOS transistors.

2.7 MEA Applications

During these years I was also involved in neuro-pharmacological and synaptic plasticity studies. For this reason an overview of this type of MEA application are reported in the following paragraphs.

2.7.1 Neuro-Pharmacological Applications

In recent years the need of efficient neuropharmacological and neurotoxicological testing in vitro is increasing, as there are new directives to restrict animal use for laboratory tests (Johnstone et al. 2010). New experimental strategies based on alternative methods, in which the use of time, materials, and animals is reduced and refined or animal use is completely replaced, are required.

Thus, in vitro assessment of neurophysiological function could be used to screen chemicals for potential neuroactive or neurotoxic effects (Defranchi et al. 2011). To date, one of the most promising tools for neuropharmacological tests is the Micro-Electrode Array (MEA). MEA technology has been recognized as a standard experimental approach for in vitro long-term electrophysiological and neuropharmacological investigations (Gross et al. 1977; Gramowski et al. 2004). The pioneering works by Gross et al. (1977, 1992) demonstrated the possibility to use dissociated neuronal networks coupled to MEAs as a first prototype of cell-based biosensor. This system showed both high sensitivity to neuroactive and neurotoxic compounds and reproducible results (Gramowski et al. 2000). The biocompatibility of the used materials (i.e. titanium nitride for the electrodes and glass for the substrate) and the not invasive nature of the extracellular measurement, make this system a perfect candidate to routinely record and evaluate the dynamics of the network behavior, both in spontaneous condition and under chemical manipulation (Martinoia et al. 2005; Chiappalone et al. 2006), either on short or long time-scales. Cultured neuronal networks respond to neurotransmitters and their blockers in a similar way as the in vivo situation (Streit 1993; Gramowski et al. 2000; Martinoia et al. 2005), providing an excellent tool to study how pharmacological compounds can influence the electrophysiological behavior (Gross et al. 1977; Morefield et al. 2000; Keefer et al. 2001; Xia and Gross 2003; Parviz and Gross 2007). Moreover, by using MEA systems (i.e. MEA 2100 amplifier) and devices that allow activity

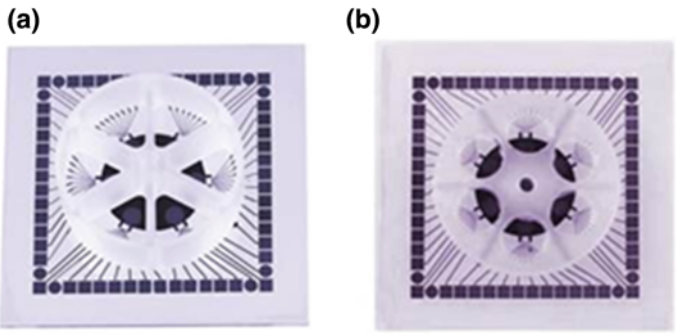

Fig. 2.11 MEA devices used for neuro-pharmacological investigations. 60-6Well MEA. MEA devices with 6 separated wells (9 recording channels plus 1 internal reference electrode for each compartment). **a** Six wells triangle chambers and **b** six wells round chambers

recordings from different cultures simultaneously (i.e. MEA devices with different wells reported in Fig. 2.11), high-throughput measurements are also possible.

In Chap. 6 a detailed report of two works I actively participated and in which MEA technology is used for neuro-pharmacological tests is reported. In the first paper (Frega et al. 2012) I evaluated the effect of ionotropic glutamate agonist (AMPA, NMDA) on the network activity. In the second paper (Colombi et al. 2013) I studied the effect of Antiepileptic drugs (CBZ and APV) on the spontaneous or induced-epileptic (i.e. after bicuculline treatment) network activity.

2.7.2 Plasticity Studies

Long Term Potentiation (LTP) and Long Term Depression (LTD) of synaptic strength are the most studied among the modifications that during processes, for instance, of learning and/or memory, synapses can undergo and that significantly depart from the background noise. Homosynaptic or Hebbian activity-dependent mechanisms are used primarily for learning and for short-term memory; on the other hand, heterosynaptic or modulatory input-dependent mechanisms are responsible for long-term memory and lead to transcription and to synaptic growth.

LTP and LTD were demonstrated in many experimental preparations in vitro and in vivo. Indeed, the great majority of the experimental works related to synaptic modifications concerns in vitro slices or dissociated cultures where defined synaptic pathways can be identified.

However, many studies on synaptic plasticity primarily focus attention on changes in the Excitatory Post Synaptic Potential (EPSP), rather than on changes in the firing behavior. In this respect, experimental investigations on the electrophysiological behavior shown by neuronal assemblies represent a fundamental step towards understanding the universal mechanisms of brain coding, learning and memory.

As reported in the literature, in order to understand such universal mechanisms, it is important to investigate how plasticity develops at network level. To address this issue, it is possible to use dissociated cortical cultures coupled to MEA devices, allowing to non-invasively stimulate the experimental preparations and to extracellularly record the output signals.

During these years of PhD I was involved in an Italian project (San Paolo Project) and I investigated neuronal events underlying the persistence of long-term memory, focusing on the role of structural changes at synaptic level. Experimental results showed differences in the electrophysiological activity of the cortical neuronal network after the application of a tetanic stimulation, denoting a potentiation, with respect to the level of ongoing activity initially shown by the cultured network (Chiappalone et al. 2008). It has been recently demonstrated how the effects induced by such protocols are long-lasting (i.e., hours), denoting a phenomenon of Long-Term Plasticity.

Following this line, I performed also experiments using dissociated hippocampal and cortical neuronal networks from a transgenic mouse model for Alzheimer disease. Compared to the control condition (wild-type mice), the results were ambiguous and up to now we could not draw any clear conclusion from that study. In some cases, we obtained no potentiation of the network activity after the application of a tetanic stimulation. In other cases, a network electrophysiological activity decrement is recorded 2 h after the tetanus delivery denoting a possible indication of late long term depression.

References

Banker G, Goslin K (1998) Culturing nerve cells. MIT Press, 2nd edn. p 9, 10

Berdondini L, van der Wal PD et al (2005) High-density electrode array for imaging in vitro electrophysiological activity. Biosens Bioelectron 21(1):167–174

Berdondini L, Imfeld K et al (2009a) Active pixel sensor array for high spatio-temporal resolution electrophysiological recordings from single cell to large scale neuronal networks. Lab Chip 9(18):2644–2651

Berdondini L, Massobrio P et al (2009b) Extracellular recordings from locally dense microelectrode arrays coupled to dissociated cortical cultures. J Neurosci Methods 177(2):386–396

Carrell A, Burroughs M (1910) Cultivation of adult tissues and organs outside of the body. JAMA 55:1379–1381

Chialvo DR (2007) The brain near the edge, in cooperative behavior in neural systems—Ninth Granada Lectures. Springer, Granada (Spain)

Chiappalone M, Bove M et al (2006) Dissociated cortical networks show spontaneously correlated activity patterns during in vitro development. Brain Res 1093(1):41–53

Chiappalone M, Massobrio P et al (2008) Network plasticity in cortical assemblies. Eur J Neurosci 28:221–237

Chien CB, Pine J (1991) Voltage-sensitive dye recording of action potentials and synaptic potentials from sympathetic microcultures. Biophys J 60(3):697–711

Colombi I, Mahajani S et al (2013) Effects of antiepileptic drugs on hippocampal neurons coupled to micro-electrode arrays. Front Neuroeng 6:10

Defranchi E, Novellino A et al (2011) Feasibility assessment of micro-electrode chip assay as a method of detecting neurotoxicity in vitro. Front Neuroeng 4:6

Elshabini-Riad A, Barlow FD (1998) Thin film technology handbook. McGrow-Hill

Eytan D, Marom S (2006) Dynamics and effective topology underlying synchronization in networks of cortical neurons. J Neurosci 26(33):8465–8476

Fejtl M, Stett A et al. (2006) On micro-electrode array revival: its development, sophistication of recording and stimulation. Advances in network electrophysiology using micro-electrode arrays. Springer, New York

Frega M, Pasquale V et al (2012) Cortical cultures coupled to micro-electrode arrays: a novel approach to perform in vitro excitotoxicity testing. Neurotoxicol Teratol 34(1):116–127

Frey U, Sanchez-Bustamante CD et al (2007) Cell recordings with a CMOS high-density microelectrode array. Conf Proc IEEE Eng Med Biol Soc 2007:167–170

Frey U, Egert U et al (2009) Microelectronic system for high-resolution mapping of extracellular electric fields applied to brain slices. Biosens Bioelectron 24(7):2191–2198

Fromherz P, Offenhausser A et al (1991) Neuron-silicon junction: a Retzius cell of the leech on an insulated-gate field-effect transistor. Science 252:1290–1293

Gramowski A, Schiffmann D et al (2000) Quantification of acute neurotoxic effects of trimethyltin using neuronal networks cultured on microelectrode arrays. Neurotoxicology 21(3):331–342

Gramowski A, Jugelt K et al (2004) Substance identification by quantitative characterization of oscillatoryactivity in murine spinal cord networks on microelectrode arrays. Eur J Neurosci 19(10):2815–2825

Gross GW, Rieske E et al (1977) A new fixed-array multi-microelectrode system designed for long-term monitoring of extracellular single unit neuronal activity in vitro. Neurosci Lett 6:101–105

Gross GW, Williams AN et al (1982) Recording of spontaneous activity with photoetched microelectrode surfaces from mouse spinal neurons in culture. J Neurosci Methods 5(1–2): 13–22

Gross G, Rhoades B et al (1992) Neuronal networks for biochemical sensing. Sens Actuators 6:1–8

Harrison R (1907) Observations on the living developing nerve fiber. Anat Rec 1:116–118

Harrison R (1912) The cultivation of tissues in extraneous media as a method of morphogenetic study. Anat Rec 6:181–193

Imfeld K, Neukom S et al (2008) Large-scale, high-resolution data acquisition system for extracellular recording of electrophysiological activity. IEEE Trans Biomed Eng 55(8):2064–2073

Jimbo Y, Tateno Y et al (1999) Simultaneous induction of pathway-specific potentiation and depression in networks of cortical neurons. Biophys J 76:670–678

Johnstone AF, Gross GW et al (2010) Microelectrode arrays: a physiologically based neurotoxicity testing platform for the 21st century. Neurotoxicology 31(4):331–350

Kandel E, Schwartz J et al (2000) Principles of neural science, 4th edn. McGrawHill, pp 5–8, 14

Keefer EW, Norton SJ et al (2001) Acute toxicity screening of novel AChE inhibitors using neuronal networks on microelectrode arrays. Neurotoxicology 22(1):3–12

Kettenmann H, Grantyn R (1992) Practical electrophysiological methods: a guide for in vitro studies in vertebrate neurobiology. Wiley-Liss Inc., New York, p 12

Kriegstein AR, Dichter MA (1983) Morphological classification of rat cortical neurons in cell culture. J Neurosci 3(8):1634–1647

Lambacher A, Vitzthum V et al (2010) Identifying firing mammalian neurons in networks with high-resolution multi-transistor array (MTA). Appl Phys A 102:1–11

Martinoia S, Bonzano L et al (2005) Electrophysiological activity modulation by chemical stimulation in networks of cortical neurons coupled to micro-electrode arrays: a biosensor for neuropharmacological applications. Sens Actuators B Chem 108(1–2):589–596

Meister M, Pine J et al (1994) Multi-neuronal signals from the retina: acquisition and analysis. J Neurosci Methods 51(1):95–106

Morefield SI, Keefer EW et al (2000) Drug evaluations using neuronal networks cultured on microelectrode arrays. Biosens Bioelectron 15(7–8):383–396

Murray MR, Barber JH et al (1977) Introduction of recording booklets in general practice teaching. Med Educ 11(3):192–196

Parviz M, Gross GW (2007) Quantification of zinc toxicity using neuronal networks on microelectrode arrays. Neurotoxicology 28(3):520–531

Peterson ER, Murray MR (1955) Myelin sheath formation in cultures of avian spinal ganglia. Am J Anat 96(3):319–355

Pine J (1980) Recording action potentials from cultured neurons with extracellular microcircuit electrodes. J Neurosci Methods 2(1):19–31

Pine J (2006) A history of MEA development. In: Taketani M, Baudry M (eds) Advances in network electrophysiology using micro-electrode arrays. Springer, New York

Regehr WG, Pine J et al (1989) Sealing cultured invertebrate neurons to embedded dish electrodes facilitates long-term stimulation and recording. J Neurosci Methods 30(2):91–106

Robinson HPC, Kawahara M et al (1993) Periodic synchronized bursting in intracellular calcium transients elicited by low magnesium in cultured cortical neurons. J Neurophysiol 70(4):1606–1616

Streit J (1993) Regular oscillations of synaptic activity in spinal networks in vitro. J Neurophysiol 70(3):871–878

Thomas CA Jr, Springer PA et al (1972) A miniature microelectrode array to monitor the bioelectric activity of cultured cells. Exp Cell Res 74(1):61–66
Wheeler BC, Novak JL (1986) Current source density estimation using microelectrode array data from the hippocampal slice preparation. IEEE Trans Biomed Eng 33(12):1204–1212
Xia Y, Gross GW (2003) Histiotypic electrophysiological responses of cultured neuronal networks to ethanol. Alcohol 30(3):167–174

Chapter 3
In Vitro Neuronal Networks

In the previous chapter, I outlined the evolution of MEA electrophysiology, starting from the very first applications to the most recent developments. Here, I will present an overview of different types of neuronal networks coupled to MEAs. I will start with homogeneous neuronal networks (cf. Sect. 3.1); then I will introduce confined or patterned neuronal networks coupled to MEAs (cf. Sect. 3.2). Finally I will present an overview of the advantages and limitation of this in vitro bi-dimensional model (cf. Sect. 3.3).

3.1 Homogeneous Neuronal Networks

Large random networks of dissociated neurons developing in vitro and chronically coupled to Micro-Electrode Arrays devices (MEAs) represent a valid experimental model for studying the universal mechanisms governing the formation and conservation of neuronal cell assemblies (Marom and Shahaf 2002). In vitro cultured neurons coupled to MEA represent a reduced neurobiological structure where, at a simplified level, the collective and functional properties of the nervous system emerge and can be experimentally investigated for basic neuroscientific studies. In this kind of preparation, unlike other experimental models such as acute and cultured slices, neurons self-organize during development creating networks which exhibit complex spatio-temporal patterns of activity (Van Pelt et al. 2004a, b; Wagenaar et al. 2006; Rolston et al. 2007). Networks of neurons extracted from the developing central nervous system and cultured on MEA chips remain spontaneously active and stable for many weeks. These networks are cultured in healthy conditions for a long time, and show complex patterns of spike and burst electrophysiological activity. Such recurring activation patterns have been demonstrated to remain stable over long-term recordings of spontaneous activity (Beggs and Plenz 2004) and, at the

M. Frega, *Neuronal Network Dynamics in 2D and 3D in vitro Neuroengineered Systems*, Springer Theses, DOI 10.1007/978-3-319-30237-9_3

same time, to change in response to the application of appropriate stimulations (Brewer et al. 2009a, b).

Micro-electrode arrays are non-invasive and permit to monitor the electrophysiological activity of neurons for a long period of time, do not require external manipulations, allow multi-site recordings (typically with 60 microelectrodes) and provide a simpler approach than conventional electrophysiological techniques. The use of MEAs coupled to neuronal cultures offers the unique opportunity of recording and stimulating, simultaneously and non-invasively, the electrophysiological activity at many sites, allowing detailed investigations on the dynamics of the neuronal system. By utilizing this model it is rather easy to control network parameters, such as cell density, and it is possible to perform almost one-to-one recordings in conjunction with high-density devices (cf. Sect. 2.6). With these experimental models, patterning of modular architectures is relatively easy to be implemented (cf. Sect. 3.2).

In recent years the demand for efficient neuropharmacological and neurotoxicological test in vitro is increasing, as there are new European directives that restrict animal use for laboratory tests (Johnstone et al. 2010). New experimental strategies based on alternative methods, in which the use of time, materials, and animals is reduced and refined or animal use is completely replaced, are required. Cultured neuronal networks coupled to MEA devices can be used as test-bed for preliminary assessment before in vivo experimentation. Within this context, MEA technology is recognized as an useful approach for in vitro long-term spatio-temporal neuropharmacological and neurotoxicological investigations (cf. Sect. 2.7.1).

3.1.1 Spontaneous Activity

Using dissociated neuronal networks coupled to MEA device, it is possible to study the network electrophysiological activity and it is interesting to study how the electrophysiological activity changes during development. It is demonstrated that the firing patterns change with respect to the structural changes in the network during the in vitro maturation (Chiappalone et al. 2006; Brewer et al. 2009a, b).

In this thesis, I made mainly use of primary cultures of hippocampal and cortical dissociated neurons from rat embryos during their mature stage (i.e., fourth *week* in vitro).

Mature cultures exhibit a rich synchronized and distributed bursting activity. The percentage of random spike is very low and the electrophysiological activity is dominated by network bursting activity patterns (Chiappalone et al. 2006; Gandolfo et al. 2010). The correlation and synchronization among all the possible pairs of channels is very high. This fact indicates that also “far” connections are explored, as a possible consequence of the rapid chemical synaptogenesis during the second week in culture (Lin et al. 2002).

I performed experiments using hippocampal and cortical neuronal networks during the mature phase of development. Figure 3.1 shows two raster plots

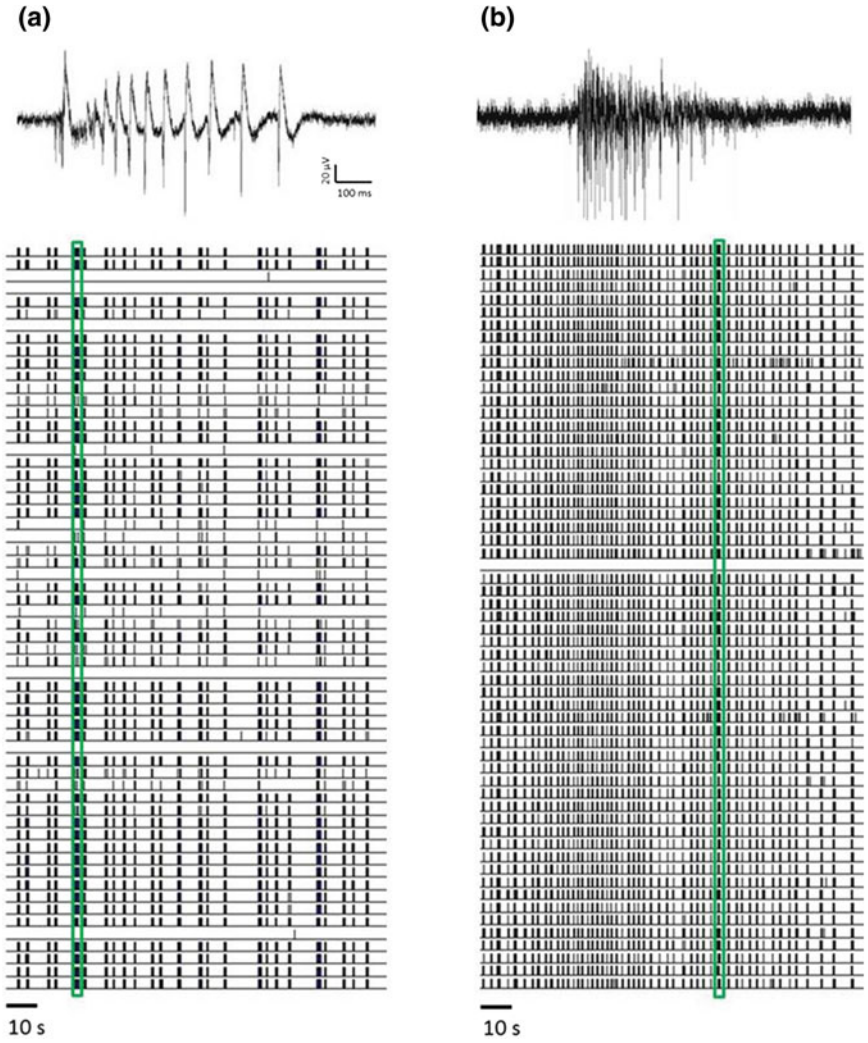

Fig. 3.1 Electrophysiological activity of a dissociated neuronal network (4 *week* in vitro). **a** Hippocampal neuronal network single channel burst and raster plot showing 120 s of spontaneous activity recorded from 60 MEA channels. **b** Cortical neuronal network single channel burst and raster plot showing 120 s of spontaneous activity recorded from 60 MEA channels. The green box indicated a network burst

(i.e. activity recorded from 60 channels) of a 2D hippocampal culture (Fig. 3.1a) and a 2D cortical culture (Fig. 3.1b) during the fourth *week* in vitro. Thanks to this plot it is possible to observe the electrophysiological activity of the network recorded from all the electrodes during 2 min. As anticipated, we can observe the quasi-synchronous activity and network dynamics composed mainly of network bursts.

There are synchronized events which involve most of the recording channels interspersed by period of time in which almost no activity is recorded (see green boxes). By looking at the single channel raw data it is possible to observe an hippocampal and a cortical burst.

3.2 Patterned Neuronal Networks

Brain architecture is inherently modular, being composed of local networks that are embedded in networks of networks, which are sparsely connected to each other. Several studies on cultured cells devoted to elucidate neurophysiological mechanisms are based on homogenous neuronal networks. Besides clear advantages related to observability reported above (cf. Sect. 3.1), such 2D neuronal model systems have major limitations as they might be inherently unable to exhibit characteristics of in vivo systems. This kind of preparation is far to the real brain structure: neurons belongs to the same population, the network is casually connected and the majority of the connections is short. In order to approaching and mimicking natural assemblies in the brain and to characterize the activity dynamics in modular networks, the possibility of designing specific network architectures forcing neurons to follow a pre-defined structure is required. This can be implemented by the combined use of bio-patterning technologies to spatially control neuronal network growth.

Cultured neurons on planar substrates with "well defined" two-dimensional network architectures (i.e. patterned networks) could give valuable insights into the cell-to-cell communication and network dynamics versus topology. Since the pioneering works of Letourneau (1975), many studies have been presented using various methods for constructing patterned network such as surface modification by silane chemistry (Georger et al. 1992), photolithographic techniques (Torimitsu 1990; Corey et al. 1996), deep-UV lithography (Dulcey et al. 1991), soft lithography (Branch et al. 1998). Another method working at the nanometer scale, is the dip-pen nanolithography which relies on the use of Atomic Force Microscope (AFM) to create nano-patterns of proteins with a dimension of about 30 nm (Piner et al. 1999; Wilson et al. 2001). This method was used to create high-resolution protein arrays to control cell attachment (Lee et al. 2002). Although various nano- micro-patterning techniques were developed and used for patterning neuronal cell cultures, only few authors (Ma et al. 1998; Vogt et al. 2005) demonstrated, for mammalian neurons, the functional electrophysiological characterization of these networks.

Other authors (Jimbo et al. 1993; Suzuki et al. 2004, 2005; Macis et al. 2007; Marconi et al. 2012) proposed to couple micro-patterning techniques to extracellular recordings by means of MEAs. In this case, micromachining or patterning is used to define the network architecture by arranging cell bodies and cell processes onto the microelectrodes.

In particular, Macis and coworkers developed a system for neuronal network patterning on MEA devices (Macis et al. 2007). By using this technique it is possible to change the architecture of the network. The automated micro-drop delivery system

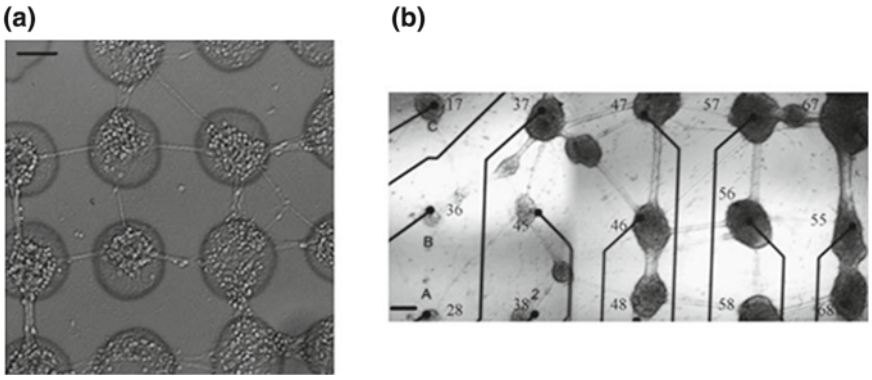

Fig. 3.2 Spatially distributed neuronal sub-populations constructed by using the automated microdrop delivery system. **a** Superimposition of the fluorescence image of the Fitc-labeled polyl-lysine spots deposited on a glass coverslip surface with the differential interference contrast (DIC) image of interconnected neuronal systems grown on them. If the distance between two clusters is 100 μm or less, they tend to collapse; on the contrary, for sufficient distance the clusters remain not-connected. Scale bar is 100 μm. **b** DIC image of a neuronal network at 20 DIV on a MEA (30 μm contact pad diameter, 500 μm spaced). Scale bar is 100 μm. From Macis et al. (2007)

which it is used allows designing and realizing spatially distributed neuronal sub-populations by depositing sub-nanoliter volumes of adhesion molecules on which neurons grow and develop. The patterned neuronal ensembles spontaneously connect each others with no need for specific patterning for neurites outgrow and guidance. In Fig. 3.2 it is possible to observe two examples of spatially distributed neuronal sub-population. In the first case (Fig. 3.2a) spots are deposited on a glass coverslip surface: it is possible to observe that interconnected neuronal systems (among 60 neurons for sub-population) grow on them. In the second case spots are deposited on MEA surface (Fig. 3.2b): each subpopulation of neurons is plated on a single electrode. The spontaneous electrophysiological activity of patterned network shows a particular dynamics that appears different from the one obtained with randomly grown cultures at the same stage of development. This would imply that forcing specific interconnected sub-population of neurons, the spontaneous activity could be driven in a more asynchronous state.

Another work in which is proposed to couple micro-patterning techniques to extracellular recordings by means of MEAs is the one of Marconi and coworkers (Marconi et al. 2012). In this work, they achieved patterning and growth of neuronal cultures for more than 20 *days* in vitro (DIV) by coupling the microcontact printing of an adhesion promoter with the use of an agarose repulsive layer and investigated the electrophysiological features of these preparations at both synaptic and network levels with respect to random cultures. In Fig. 3.3 is shown an hippocampal culture on a grid mesh and on a node. It is possible to observe that the synaptic connections are mainly formed at the nodes of the grid pattern.

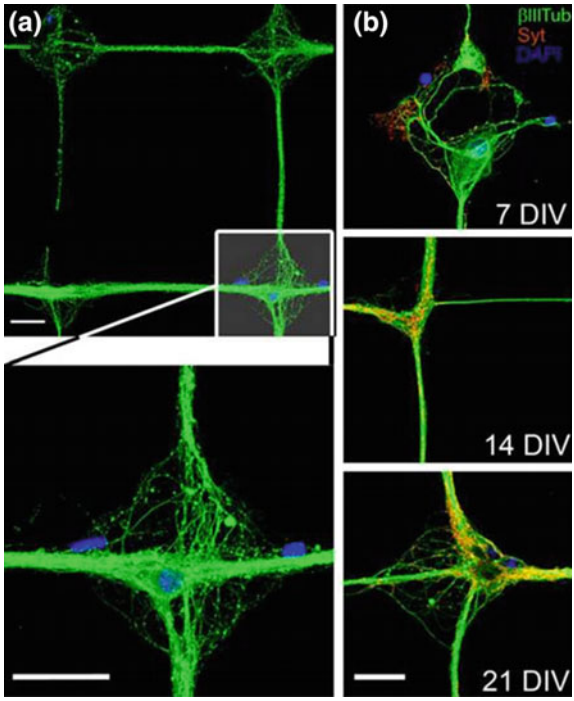

Fig. 3.3 Close-ups of patterned neuronal networks and assessment of synaptic development. **a** Close-up of a 21 DIV culture on a grid mesh (*top*) and on a node (*bottom*). **b** Synaptotagmin (Syt) staining performed at 7, 14 and 21 DIV reveals the formation of synaptic contacts concentrated on the neuronal cell bodies and proximal dendrites at the nodes. From Marconi et al. (2012)

They found that, the basic properties of synaptic transmission, the overall network development and the emerging overall network activity were not altered with respect to control random cultures. Notably, the grid topology imposed to the networks was associated with a reinforcement of functional connectivity along orthogonal directions, shorter connectivity links and an increased spiking probability in response to focal stimulation.

Another example of confined/segregated/interconnected neuronal network is the developed experimental system with microfluidic separated dual compartments coupled to microelectrode arrays (MEAs) reported by Kanagasabapathi et al. (2011, 2012).

The system integrates two closed interconnected micro-chambers on planar MEA that allow the compartmentalization of neuronal cells and the control of fluidicmicro-environments (Kanagasabapathi et al. 2012). The micro-chambers (100 μm high, 1.5 mm long) are able to segregate the two sub-populations, while an array of thin microchannels (10 μm width, 3 μm high and 150 μm length) connecting the two micro-chambers allows neurite outgrowth between the two sub-populations. By exploiting such features, it is possible to realize co-cultures of dissociated neurons.

They demonstrated that, with the micro-channels offering the necessary physical isolation between the compartments, the cells were observed to be plated uniformly along the compartment length. In addition, the small feature size of the microchannels also provided the necessary somatic and fluidic isolation between the compartments. The best evidence of the good quality of the neuronal network was the electrophysiological recording of spontaneous activity by means of a planar micro-electrodes array (MEA). They found that the spontaneous activity of an isolated culture is markedly different from those observed in a co-culture model.

3.3 Beyond the State of the Art: 3D Neuronal Networks

As recently pointed out (Muramoto et al. 1993; Hasselmo 1995; Kamioka et al. 1996; Chub and O'Donovan 1998; Timofeev et al. 2000a, b; Ben-Ari 2001; Shahaf and Marom 2001; Wagenaar et al. 2005; Eytan and Marom 2006; Gal et al. 2010; Cullen et al. 2011; Dranias et al. 2013), besides clear advantages related to controllability and observability reported above, such 2D neuronal networks have major limitations as they might be inherently unable to exhibit characteristics of in vivo systems.

Three concepts, recently introduced in network neuroscience, allow us to justify the introduction of a complementary model system constituted by 3D neuronal networks. At the same time they introduce possible intrinsic limitations of 2D models pointing to the fact that they are inherently too far away from the in vivo situation.

1. *The brain's structural connectivity exhibits peculiar features of complex network topologies* (Sporns 2011).
   Recent studies demonstrated that cortical areas are neither completely connected with each other, nor randomly linked; instead, their interconnections show a specific and intricate organization. Graph analyses of structural and functional data from the human brain have demonstrated an abundance of characteristic, nonrandom attributes. Large-scale structural networks derived from noninvasive diffusion imaging exhibit a high propensity for clustering of nodes (i.e. neurons) into structural communities, or modules (Fig. 3.4). This tendency toward modularity is coupled with a high capacity for global information flow.
2. *Brain structure and dynamics are highly interdependent* (Sporns and Tononi 2001).
   The brain is a complex system that exhibit characteristic patterns of temporal correlations that emerge as the result of functional interactions within structured network. The activity of the neuronal units of the brain gives rise to dynamic states that are characterized by specific patterns of neuronal activation and co-activation. Which patterns arise depends on the anatomical structure of the underlying network. Different connection topologies can generate different modes of neuronal dynamics: the structural features of brain networks contribute

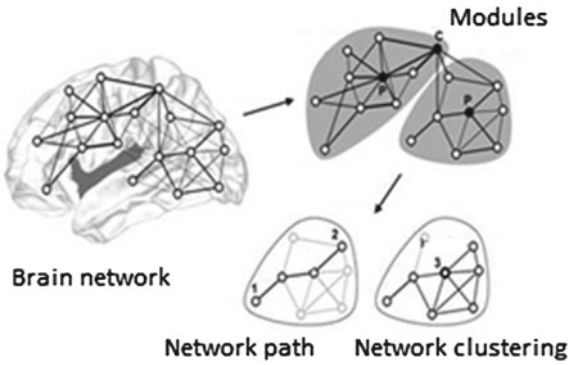

Fig. 3.4 Schematic representation of the basic concepts of graph theory. The diagram at the left shows an undirected weighted brain network such as might result from diffusion imaging and tractography. Thresholding removes weak connections, and further analysis reveals two network communities or modules that are interlinked via a highly connected and highly central node. Each module also contains highly connected nodes with mainly intramodular connections. The diagrams at the bottom illustrates the concepts of a network path (between nodes 1 and 2) and clustering (around node 3). Adapted from Sporns (2011)

to drive the network towards dynamic states characterized by synchronous/asynchronous features.

3. *The capability of neural systems to encode and process incoming stimuli is affected by both structure and ongoing dynamics* (Marguet and Harris 2011). Neuronal assemblies are usually spontaneously active, i.e. without applying any kind of electrical or chemical stimulation they present an ongoing activity which configures the brain as a noisy-entity. Such ongoing activity is strongly influenced by the underlying connectivity. Although the presence of such a strong intrinsic dynamics, the brain is able to perform useful information processing. Recent studies suggested that the synchronized state of a network leads to increased adaptation to prolonged or rapidly repeated stimuli. When the ongoing dynamic is desynchronized, instead, the system is putted under progressively greater control of sensory stimuli. The role of intrinsic dynamics in shaping population activity is toned down.

In any case it should be underlined that, generally, neuronal network preparations are far to the real brain structure: networks do not follow a specific architecture and any peculiar brain structure architecture is missing. Nevertheless basic mechanism of development and of self-organization can be investigated. The introduction of 3D in vitro models go in the direction of implementing more physiological environmental conditions for cells to grow and to mimic more similar in vivo conditions.

Morphological and electrophysiological properties of neural cells are substantially influenced by their immediate extracellular surroundings, yet the features of this environment are difficult to mimic in vitro. In 2D in vitro model the structure is constrained by the presence of a rigid planar substrate. The morphology of neurons

is rather flat and the interaction with glial cells and extracellular matrix are limited by the planar substrate on which cells grown. In this kind of preparation soma and growth cones in are unrealistically flattened and the axons-dendrites outgrowth cannot occur in all directions (Cullen et al. 2011).

The brain and more in general neuronal networks are complex systems, which exhibit characteristic patterns of temporal correlations that emerge as the result of functional interactions within a structured network. With particular reference to the electrophysiological activity, a long-lasting debate has taken place over the years and various criticisms have been introduced on the validity of such 2D experimental reduced models in order to investigate mechanisms of coding and information transmission (Gal et al. 2010), network plasticity and functional connectivity (Shahaf and Marom 2001; Eytan and Marom 2006), and memory (Dranias et al. 2013). Although these model systems are somehow widely accepted, one of the major issues raised has often been related to the poor dynamics exhibited by such networks often dominated by bursting activity encompassing most of the neurons in the network (Wagenaar et al. 2005). As it is known from the literature (Muramoto et al. 1993; Kamioka et al. 1996; Chub and O'Donovan 1998; Ben-Ari 2001), burst activity is a peculiar behavior of the developing brain and plays an important role in establishing appropriate connections. Bursting activity represents an exploring dynamics of the close in vitro systems that, missing the natural input–output pathways of the in vivo brain, have to find a stable state with properly formed synapses (Wagenaar et al. 2005). This particular behavior has been partly justified with the absence of afferent inputs (Hasselmo 1995; Timofeev et al. 2000a, b) as compared to the wide repertoire of electrical activity patterns found in wake conditions in in vivo studies (Timofeev et al. 2000a, b).

Under this prospective, it is clear that a bi-dimensional model for studying the characteristic of the in vivo system is too reduced. There is a tremendous need to develop culture systems that more closely model the complexity of nervous tissue. As reported in Sect. 2.2.1, brain slices are a brain preparation in which the morphological and functional structure of the brain is preserved. Besides the clear advantage of this type of preparation, it is really difficult to perform studies about how the network dynamic is related to the connectivity. Moreover, it is hard to try to understand which is the role of different layers of neurons in the activity generation.

It is needed to scale up from 2D neuronal network model to 3D neuronal network model, trying to overcome the limitations of the brain slice preparation. The development of a true 3D engineered in vitro neuronal model could certainly be seen as a complementary-alternative and an interesting tool for neurophysiological investigations.

References

Beggs JM, Plenz D (2004) Neuronal avalanches are diverse and precise activity patterns that are stable for many hours in cortical slice cultures. J Neurosci 24:5216–5229

Ben-Ari Y (2001) Developing networks play a similar melody. Trends Neurosci 24(6):353–360

Branch DW, Corey JM et al (1998) Microstamp patterns of biomolecules for high-resolution neuronal networks. Med Biol Eng Comput 36:135–141

Brewer GJ, Boehler MD et al (2009a) Chronic electrical stimulation of cultured hippocampal networks increases spontaneous spike rates. J Neurosci Methods 184(1):104–109

Brewer GJ, Boehler MD et al (2009b) Neuron network activity scales exponentially with synapse density. J Neural Eng 6(1):014001

Chiappalone M, Bove M et al (2006) Dissociated cortical networks show spontaneously correlated activity patterns during in vitro development. Brain Res 1093(1):41–53

Chub N, O'Donovan MJ (1998) Blockade and recovery of spontaneous rhythmic activity after application of neurotransmitter antagonists to spinal networks of the chick embryo. J Neurosci 18(1):294–306

Corey JM, Brewer GJ et al (1996) Micrometer resolution silane-based patterning of hippocampal neurons: critical variables in photoresist and laser ablation process for substrate fabrication. IEEE Trans Biomed Eng 43:944–955

Cullen DK, Wolf JA et al (2011) Neural tissue engineering and biohybridized microsystems for neurobiological investigation in vitro (part 1). Crit Rev Biomed Eng 39(3):201–240

Dranias MR, Ju H et al (2013) Short-term memory in networks of dissociated cortical neurons. J Neurosci Off J Soc Neurosci 33(5):1940–1953

Dulcey CS, George JM et al (1991) Deep UV photochemistry of chemisorbed monolayers: patterned coplanar molecules assemblies. Science 252:551–554

Eytan D, Marom S (2006) Dynamics and effective topology underlying synchronization in networks of cortical neurons. J Neurosci 26(33):8465–8476

Gal A, Eytan D et al (2010) Dynamics of excitability over extended timescales in cultured cortical neurons. J Neurosci 30(48):16332–16342

Gandolfo M, Maccione A et al (2010) Tracking burst patterns in hippocampal cultures with high-density CMOS-MEAs. J Neural Eng 7(5):056001

Georger JH, Stenger DA et al (1992) Coplanar patterns of self-assembled monolayers for selective cell-adhesion and outgrowth. Thin Solid Films 210(11):716–719

Hasselmo ME (1995) Neuromodulation and cortical function: modeling the physiological basis of behavior. Behav Brain Res 67(1):1–27

Jimbo Y, Robinson HP et al (1993) Simultaneous measurement of intracellular calcium and electrical activity from patterned neural networks in culture. IEEE Trans Biomed Eng 40(8): 804–810

Johnstone AF, Gross GW et al (2010) Microelectrode arrays: a physiologically based neurotoxicity testing platform for the 21st century. Neurotoxicology 31(4):331–350

Kamioka H, Maeda E et al (1996) Spontaneous periodic synchronized bursting during formation of mature patterns of connections in cortical cultures. Neurosci Lett 206(2–3):109–112

Kanagasabapathi TT, Ciliberti D et al (2011) Dual-compartment neurofluidic system for electrophysiological measurements in physically segregated and functionally connected neuronal cell culture. Front Neuroeng 4:13

Kanagasabapathi TT, Massobrio P et al (2012) Functional connectivity and dynamics of cortical-thalamic networks co-cultured in a dual compartment device. J Neural Eng 9(3):036010

Lee KB, Park SJ et al (2002) Protein nanoarrays generated by dip-pen nanolithography. Science 295(5560):1702–1705

Letourneau P (1975) Possible roles of cell to substratum adhesion in neuronal morphogenesis. Dev Biol 44:77–91

Lin YC, Hung Z-H et al (2002) Development of excitatory synapses in cultured neurons dissociated from the cortices of rat embryos and rat pups at birth. J Neurosci Res 67:484–493

Ma W, Liu QY et al (1998) Central neuronal synapse formation on micropatterned surfaces. Dev Brain Res 111:231–243
Macis E, Tedesco M et al (2007) An automated microdrop delivery system for neuronal network patterning on microelectrode arrays. J Neurosci Methods 161(1):88–95
Marconi E, Nieus T et al (2012) Emergent functional properties of neuronal networks with controlled topology. PLoS ONE 7(4):e34648
Marguet SL, Harris KD (2011) State-dependent representation of amplitude-modulated noise stimuli in rat auditory cortex. J Neurosci 31(17):6414–6420
Marom S, Shahaf G (2002) Development, learning and memory in large random networks of cortical neurons: lessons beyond anatomy. Q Rev Biophys 35(1):63–87
Muramoto K, Ichikawa M et al (1993) Frequency of synchronous oscillations of neuronal activity increases during development and is correlated to the number of synapses in cultured cortical neuron networks. Neurosci Lett 163(2):163–165
Piner RD, Zhu J et al (1999) "Dip-Pen" nanolithography. Science 283(5402):661–663
Rolston JD, Wagenaar DA et al (2007) Precisely timed spatiotemporal patterns of neural activity in dissociated cortical cultures. Neuroscience 148(1):294–303
Shahaf G, Marom S (2001) Learning in networks of cortical neurons. J Neurosci 21(22):8782–8788
Sporns O (2011) The human connectome: a complex network. Ann NY Acad Sci 1224:109–125
Sporns O, Tononi G (2001) Classes of network connectivity and dynamics. Complexity 7(1):28–38
Suzuki I, Sugio Y et al (2004) Modification of a neuronal network direction using stepwise photothermal etching of an agarose architecture. J Nanobiotechnol 2(1):7
Suzuki I, Sugio Y et al (2005) Stepwise pattern modification of neuronal network in photothermally-etched agarose architecture on multi-electrode array chip for individual-cell-based electrophysiological measurement. Lab Chip 5(3):241–247
Timofeev I, Grenier F et al (2000a) Origin of slow cortical oscillations in deafferented cortical slabs. Cereb Cortex (New York, NY: 1991) 10(12):1185–1199
Timofeev I, Grenier F et al (2000b) Impact of intrinsic properties and synaptic factors on the activity of neocortical networks in vivo. J Phys Paris 94(5–6):343–355
Torimitsu KKA (1990) Selective outgrowth of sensory nerve fibers on metal oxide pattern in culture. Dev Brain Res 51:128–131
Van Pelt J, Corner MA et al (2004a) Longterm stability and developmental changes in spontaneous network burst firing patterns in dissociated rat cerebral cortex cell cultures on multi-electrode arrays. Neurosci Lett 361(1–3):86–89
Van Pelt J, Wolters PS et al (2004b) Long-term characterization of firing dynamics of spontaneous bursts in cultured neural networks. IEEE Trans Biomed Eng 51(11):2051–2062
Vogt AK, Wrobel G et al (2005) Synaptic plasticity in micropatterned neuronal networks. Biomaterials 26(15):2549–2557
Wagenaar DA, Madhavan R et al (2005) Controlling bursting in cortical cultures with closed-loop multi-electrode stimulation. J Neurosci 25(3):680–688
Wagenaar DA, Nadasdy Z et al (2006) Persistent dynamic attractors in activity patterns of cultured neuronal networks. Phys Rev E: Stat, Nonlin, Soft Matter Phys 73(5 Pt 1):051907
Wilson DL, Martin R et al (2001) Surface organization and nanopatterning of collagen by dip-pen nanolithography. Proc Natl Acad Sci USA 98(24):13660–13664

Part II
A New In Vitro Model: 3D Neural Networks Coupled to MEA Devices

Chapter 4
3D Neuronal Networks: State of the Art

In the previous Chap. 1 showed advantages and limitations of the 2D in vitro model. By taking into account the limitations of such a model, it is an evidence that there is a tremendous need to develop culture systems that more closely mimic the complexity of nervous tissue. It is required to scale up from 2D neuronal network model to 3D neuronal network model.

In this Chap. 1 will introduce the state of the art about 3D neuronal networks. Firstly I will compare 2D and 3D models (cf. Sect. 4.1); then I will show two works as examples of methods for 3D networks construction (cf. Sect. 4.2).

4.1 2D Versus 3D Models

Cells in the brain interact within a complex, multicellular environment with tightly coupled 3D cell-cell/cell–extracellular matrix (ECM) interactions; yet most in vitro models utilize planar systems lacking in vivo–like ECM. Although in vitro models are invaluable in the systematic elucidation of cell behavior in a highly controlled setting, the interpretation of cellular responses in traditional planar 2D models may be confounded by critical deviations in the cellular microenvironment (e.g., access to soluble factors), atypical cellular morphology (Balgude et al. 2001; Grinnell 2003), and altered cell-cell/cell-matrix interactions (Cukierman et al. 2001, 2002; Schmeichel and Bissell 2003; Yamada et al. 2003). Culture models in 3D, in which cells are grown within a scaffold, allow investigation of cellular behavior in a more physiologically relevant state by mimicking the cytoarchitecture of in situ tissue to a higher degree than cells grown on nonphysiologic rigid surfaces. Moreover, these systems preserve the primary advantages of traditional in vitro systems, such as control of cellular environment, accessibility for repeated imaging, and elimination of systemic effects. A 3D environment provides a high surface area for growth and migration, which can be tuned to support other cell behaviors, such as differentiation

M. Frega, *Neuronal Network Dynamics in 2D and 3D in vitro Neuroengineered Systems*, Springer Theses, DOI 10.1007/978-3-319-30237-9_4

or maturation. The scaffold may act to protect cells from environmental disturbances, such as media changes, and can be designed for physiological structural stability. Scaffolds can also be designed for optimal mass exchange for both nutrient and waste diffusion.

There are fundamental differences between cells cultured in monolayer versus 3D configurations (i.e. types, quantity, and distribution of cell-cell and cell-matrix interactions) (Cukierman et al. 2001, 2002; Schmeichel and Bissell 2003; Yamada et al. 2003). For example, the matrix surrounding cells has been shown to have widespread effects on cellular function for a variety of cell types (Cukierman et al. 2001; Schindler et al. 2006) including neural cells (Venstrom and Reichardt 1993; Kiryushko et al. 2004; Loers and Schachner 2007). Cell-cell and cell-matrix interactions are, by definition, constrained in planar cultures: cells in 2D configurations may experience such interactions in only a single plane, since a majority of the cell surface is exposed. These phenomena, in turn, may have ramifications on morphology (Grinnell 2003), growth and proliferation (Granet et al. 1998), viability (Fawcett et al. 1995), gene and protein expression (Masi et al. 1992; Berthod et al. 1993), and in the response to biochemical (Hofmann 1993) and/or mechanical stimuli (LaPlaca et al. 2005). In particular, from a physical perspective, cells grown in 3D versus 2D environments have a starkly different morphology and cytostructure (Grinnell 2003). Cells stay more spherical when embedded within a scaffold than 2D cultures and, in the case of neurons and other process-extending cells, outgrowth can occur in all directions. The somata and growth cones of neurons in 2D are unrealistically flattened compared to cells in 3D or in vivo, which present a rounder, more bulbous shape (Balgude et al. 2001).

Differences in gene expression, growth characteristics, and viability are found when comparing cells cultured in 3D and 2D to cells in vivo (Schindler et al. 2006; Smalley et al. 2006). Specifically, cells cultured in a 3D environment have been shown to better represent in vivo cellular behavior than cells cultured in monolayer, for both neural and non-neural cells (Fawcett et al. 1989, 1995; Granet et al. 1998; Wang et al. 1998; Grinnell 2000).

A growing body of evidence suggests that cells grown in planar cultures do not have the same morphology (Cukierman et al. 2001), proliferation rates (Hindie et al. 2006; Willerth et al. 2006), migration (Friedl et al. 1998), gene expression (Birgersdotter et al. 2005; Liu et al. 2006), differentiation (Chun et al. 2006; Willerth et al. 2006), cellular signaling (Pedersen and Swartz 2005), or pathological susceptibility (Behravesh et al. 2005; Hindie et al. 2006; Smalley et al. 2006) as in 3D culture or in vivo. 3D cultures have been shown to result in longer neurites, higher levels of survival, and different patterns of differentiation as compared to 2D monolayers (Choi et al. 1993; Horie and Akahori 1994; Bellamkonda et al. 1995; Blackshaw et al. 1997; Pardo and Honegger 2000). Cells cultured in 2D have also exhibited an increase in sensitivity to chemical treatments independent of changes in surface area (Miller et al. 1985), challenging the suitability of 2D models for studies evaluating pharmacological responses.

Neural culture systems in 3D may also be more appropriate for electrophysiological studies than planar counterparts. For example, in 3D culture, Na^+/H^+

exchangers have been shown to have polarized expression to the apical membrane, which is difficult to maintain in monolayer cultures (Castillon et al. 2002). In addition, neurons in a 2D culture environment have exaggerated Ca^{2+} dynamics in comparison to 3D cultures (Mao and Kisaalita 2004; Desai et al. 2006; Xu et al. 2006).

Collectively these findings raise questions about the appropriateness of employing monolayer 2D culture models to study certain cell, tissue, or systems level phenomena.

Carefully designed and optimized 3D models, with sufficient mass transport and appropriate cell and matrix elements, may more faithfully recapitulate aspects of native tissue than 2D models. Cells are influenced by complex environmental stimuli, central to which is the local extracellular microenvironment. Inherent differences in cell-cell/cell-matrix interactions coupled with corresponding alterations in cell morphology and alterations in the cellular microenvironment may have a profound impact on intracellular signaling and gene expression. Thus, due to fundamental deviations in planar cell culture from the in vivo environment, cells cultured in 2D may be inherently unable to recapitulate certain traits exhibited in vivo, whereas properly designed and regulated 3D systems may represent a step closer to in vivo.

4.2 Engineered 3D Neuronal Networks

Three dimensional neuronal cell systems present a degree of experimental control not possible in vivo. The engineering of neuronal constructs in vitro creates many advantages, including spatial and temporal control of cellular composition, matrix/scaffold properties, mechanical environment, and exogenous factors. For cellular composition, neural and non-neural cell types may be selected, and the constructs can be further customized by considering special cell sources (e.g., transgenic labeling of all neurons or a particular neuronal subtype). These cells may be added in a controlled ratio temporally and spatially, and at a prescribed 3D density. The matrix/scaffold constituent(s) may also be designed with control over concentration, porosity, mechanical factors (e.g., stiffness), and degree of bioactivity.

Although many of these attributes are shared with traditional two-dimensional (2D) cell culture models, it is important to note that cells retained in engineered 3D systems have the added benefit of enhanced micro-environmental fidelity to the in vivo situation. This degree of experimental control makes 3D tissue engineered neuronal constructs superior for 2D preparations for most facets of neurobiological investigation.

In the following paragraphs two works about 3D neural network construction are reported. In the first work (Cullen et al. 2011) (cf. Sect. 4.2.1) Cullen and co-authors used an hydrogel scaffold; in the second work (Pautot et al. 2008) (cf. Sect. 4.2.1) Pautot and co-workers used a micro-beads based scaffold.

4.2.1 Bioactive Extracellular Matrix-Based Scaffold

In (Cullen et al. 2011) the authors engineered a novel 3D neuronal construct composed of neurons and/or astrocytes within a bioactive extracellular matrix-based scaffold. They applied these engineered neural tissue surrogates as in vitro investigational platforms to study and manipulate neurobiological responses within 3D micro-environments.

They developed and optimized a series of 3D cell culture models to study neurobiological phenomena within 3D cyto-environments. These models consist of neurons and glia distributed throughout ECM and/or hydrogel scaffolds (500–600 μm thick). Tissue engineered 3D neural cell cultures constructed with this method are shown in Fig. 4.1. A volumetric rendering of live neurons in 3D culture is reported in Fig. 4.1a; an image in which it is visible the network formation throughout the thickness of the 3D cultures is presented in Fig. 4.1b.

The motivation for the development of these cultures is that most studies evaluating in vitro survival, neurite outgrowth, network formation, synaptogenesis, and functionality have been done in planar culture lacking significant amounts of ECM. However, they postulate that the presence of 3D growth/interactions and bioadhesive ligands are crucial to studying these phenomena in vitro. These 3D cellular systems present a degree of experimental control and precision not attainable in vivo.

Cullen and co-authors made a comparison between 3D and 2D neuronal culture: the main results are summarized below.

1. *Culture architecture*
   Cells plated in 3D extended numerous processes at all orientations, while cells plated in 2D remained nearly planar, as expected.
2. *Neurite outgrowth*
   There was not a statistically significant difference in the mean number of neurites departing the soma per neuron for neurons plated in 2D compared to 3D

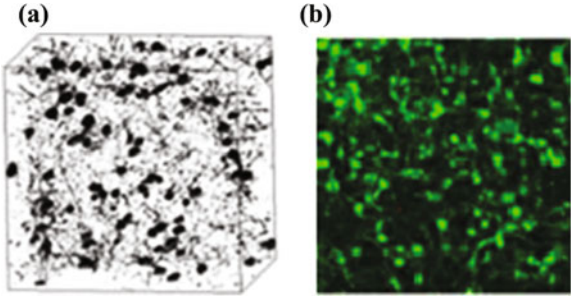

Fig. 4.1 Tissue engineered 3D neuronal cell cultures for neurobiological investigations in vitro. **a** Volumetric rendering of live neurons in 3D culture. Neurobiological studies of neural cells within 3-D matrices provide enhanced fidelity to in vivo while affording all advantages of traditional (*planar*) in vitro systems. **b** Live neurons (*green*) demonstrating survival and network formation throughout the thickness of the 3D cultures. Adapted from Cullen et al. (2011)

configurations. There is a similar dendritic outgrowth in 2D versus 3D, but a 3D configuration results in an increase in axonal length/caliber or an enhanced state of neuronal maturation compared to a 2D configuration. Altogether, there are differences in neuronal cytoarchitecture and neurite outgrowth in 3D versus 2D cultures. Processes within 2D cultures were constrained to a nearly planar morphology, while those in 3D constructs traversed much longer z distances, more representative of in vivo cytoarchitecture. Neurons within 3D constructs assumed complex 3D morphologies with rich neurite arborization in all spatial dimensions expressed mature cytoskeletal proteins, and demonstrated network connectivity.

3. *Morphology*
   The study reveals distinct morphological differences between cells plated within a 3D matrix and cells plated on a 2D rigid substrate. Neural cells plated in 3D presented a bulbous morphology with intercellular contacts in all spatial directions (Fig. 4.2, first row). Neurons in 2D culture had a flatter base with a restricted cytostructure (Fig. 4.2, second row).
4. *Survival based on cell density*
   There was a parabolic relationship between cell plating density and cell viability in the 3D neuronal cultures (Fig. 4.3). Cultures plated at lower density ($\leq$2500 cells/mm^3) or higher density ($\geq$6250 cells/mm^3) exhibited poor viability (<50 % for each). Neuronal death in low cell density 3D cultures was likely independent of mass transport limitations. However, mass transport limitations were likely the predominant reason that 3D neuronal cultures exhibited poor viability at high cell densities ($\geq$6250 cells/mm^3). Increasing the cell density in 3D effectively decreases the available area for diffusion, increases tortuosity factors, and increases the overall rates of nutrient consumption and waste product production. There was an optimum viability of 90 % for cultures plated at 3750–5000 cells/mm^3. The optimized cell density range yielded cultures with extensive neurite arborization, robust neuronal survival, and active outgrowth.
   Overall, viability in 3D neuronal cultures was highly dependent on cell density, with optimal viability at an initial plating density of 3750 cells/mm^3 for 500 to 600 μm thick cultures.

In conclusion, neurons within a 3D structure assumed complex 3D morphologies with rich neurite arborization and clear indications of network connectivity, including synaptic junctures. Interestingly, there were no significant differences in culture viability, number of neurites per neuron, or neuron/astrocyte composition when comparing optimized 3D conditions to similar 2D cultures. However, there was an increase in axonal outgrowth in 3D compared to 2D. Also, there were stark morphological/cytostructural differences in neurons cultured in 2D, which present a flat morphology, compared to cells distributed throughout a matrix, which present a bulbous morphology with cell-matrix contact in all spatial dimensions.

Plating density was a critical parameter for neurons in 3D, with an optimal cell viability obtained at 3750 cells/mm^3. This optimal value of cell density is a strong limitation of this model. The density that Cullen and co-workers are able to achieve

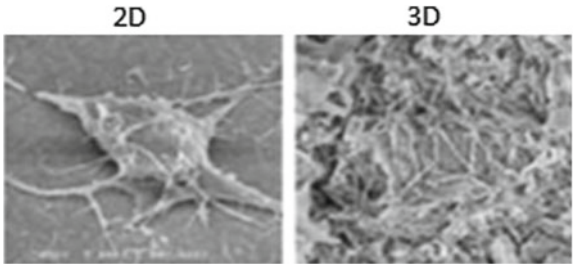

Fig. 4.2 Electron micrographs of neuronal cultures in 3D and 2D. Neurons in a 3D matrix present a rounded morphology with matrix interactions possible in all spatial dimensions, while neurons in 2D have a flattened morphology. Adapted from Cullen et al. (2011)

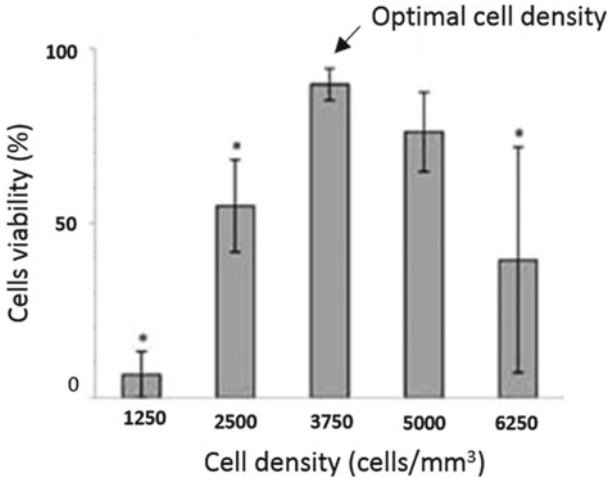

Fig. 4.3 Neuronal survival in 3D depends on cell density. In this culture model, cell density was found to be a significant factor in neuronal survival (data presented as mean ± standard deviation). Neuronal cell densities >5000 cells/mm^3 and <2500 cells/mm^3 result in poor survival. *Groups varied significantly from the peak cell viability attained at a cell density of 3750 cells/mm^3 ($P < 0.05$). Thus, there were thresholds in survival of thick, 3D neural cultures based on cell density when supported by passive diffusion, potentially related to biomass transport limitations at higher cell densities. Adapted from Cullen et al. (2011)

utilizing a bioactive extracellular matrix-based scaffold is very low compared with the in vivo situation. This value is far away to the cell density measured in the mouse brain cortex (91,000 cells/mm^3) (Schuz and Palm 1989).

4.2.2 Micro-Beads Based Scaffold

In (Pautot et al. 2008) the authors presented a method that makes possible to grow dissociated cultured neurons on silica beads. The beads provide a growth surface large enough for neuronal cell bodies to adhere and for their processes to grow, mature and produce pre- and post-synaptic specializations. The use of these beads allowed to move, transfect and culture highly differentiated neurons without disrupting their adhesion and without damaging their delicate processes. Moreover, they took advantage of the spontaneous assembly properties of monodispersed beads (Pusey and Vanmegen 1986; van Blaaderen et al. 1997) to form 3D layered hexagonal arrays containing distinct subsets of neurons in different layers with constrained connectivity between neurons on different beads. They layered beads coated with a chemical attractant on a coverslip to promote axonal growth and orient functional neuronal connections between different bead layers.

The authors used silica beads larger than 45 μm in diameter to provide a growth surface large enough for neuronal cell bodies and their processes.

The assembly principle is easy. They coated the bead surface with Poli-Lysin to enhance cell adhesion and to support neuronal maturation (Letourneau 1975a, b). They collected primary rat hippocampal neurons and cultured them on beads. The beads contained between one and a few neurons and glial cells. They dropped beads onto coverslips containing conventional 2D neuronal cultures upon which the monodispersed beads (Pusey and Vanmegen 1986; van Blaaderen et al. 1997) assembled spontaneously into 2D ordered arrays.

Once the neurons reached maturity on their respective beads, they carefully moved the beads carrying the cells to small wells with a coarse pipette. The beads settled under gravitational force and spontaneously assembled into 2D hexagonal arrays at the bottom of the wells. Once the first layer was fully packed, they added more beads, which formed a second ordered layer that had the same hexagonal symmetry. Successive addition of beads resulted in construction of a packed 3D assembly.

Three-dimensional self-assembly of a neuronal network is presented in Fig. 4.4. By looking at this figure it is possible to observe the assembly of five layers of microbeads. This figure shows that, when the 3D assembly is finished, there is enough space for cell bodies in the interstitial spaces between the beads. It is also possible to observe that neuronal processes are able to grow over the beads and in different layers.

The main characteristic of this 3D network are summarized below.

1. *Neuronal processes and functional connections*
   After the spontaneous assembly of the 3D hexagonal arrays, neuronal processes grew between the beads over the course of 3 weeks in culture to form highly interconnected millimeter-sized networks without the use of conditioned medium or a glial feeder layer. Neuronal processes cross from one bead to the next and observed glial cells in all the bead layers. Functional synaptic connections are present between neurons belonging from different layers.

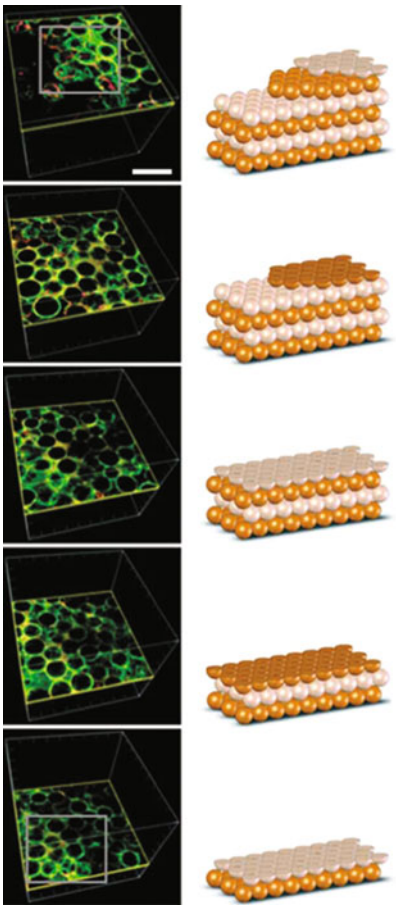

Fig. 4.4 Three-dimensional self-assembly of a neuronal network. Three week-old culture of 3D neuronal network assembly fixed and stained with the neuron-specific antibody to alpha tubulin (*green*) and the glial specific antibody to GFAP (*red*). Five layers, a 450 × 450 × 388 μm volume of the assembly, were imaged by confocal microscopy. The images extracted from the z stack for the *green* and *red* channels (*left*) are shown with schematic representations of the corresponding layer position (*right*). Scale bar, 100 μm. From Pautot et al. (2008)

The pattern of connectivity between neurons on beads within a 3D hexagonal array was spatially constrained by the 12 equidistant contacts made between each bead and its neighbors: 6 within the plane, 3 in the plane above and 3 in the plane below. For hexagonal ordered assemblies, the density of connection points depends inversely on the bead radius cubed, and the distance between contact points is linearly related to the bead radius. Thus, the neuronal connectivity of the network that forms on these bead arrays is expected to be set by bead size, with smaller beads leading to assemblies with higher connectivity.

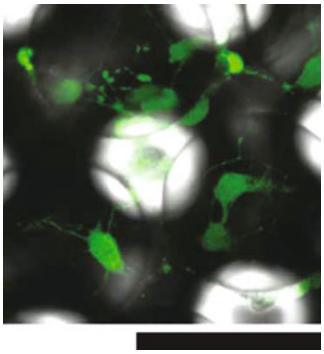

Fig. 4.5 Two-layer assembly of beads carrying GFP-expressing neurons imaged live by confocal microscopy on day 4 of in vitro culture. The image is an x-y projection of a 20 μm (10 frames) confocal z-series images overlaid with the corresponding bright-field image. Scale bars, 125 μm. From Pautot et al. (2008)

2. *Morphology*
   Neural cells plated in 3D presented a bulbous morphology with intercellular contacts in all spatial directions. In Fig. 4.5 is presented a two-layer assembly of beads. It is possible to observe that neurons exhibit a globular morphology.
3. *Cell survival*
   Despite the small number of glia on each bead, they were sufficient to maintain neuron health and support uniform and robust neuronal process outgrowth throughout the bead layers, including in the deep layers. The void spaces between the beads permitted the necessary medium exchange to maintain healthy growing conditions. The number of cells per bead and the number of neuronal processes were similar in all layers of the array, indicating that cell health is not affected by location within the assembly.
4. *Cell density*
   By varying both the density of cells during plating and the dimension of the beads, Pautot and co-workers determined the density of cells per bead and thus the number of cells per unit volume in the arrays. For a given volume, a hexagonal compact assembly of 45 μm diameter beads is composed of 19 times more beads than an assembly of 125 μm diameter beads. Hence, the most effective way to increase cell density, while allowing for a low number of cells per bead, is to use small beads. The upper limit to cell density is dictated by the free volume left by beads and is defined by bead packing order, representing 32 % of the total volume for hexagonal compact assembly.
   They achieved densities of up to 75,000 cells/mm^3 with 45 μm diameter beads, that is, close to the 91,000 cells/mm^3 measured in the mouse brain cortex (Schuz and Palm 1989).

4.2.3 Hydrogels Versus Beads Scaffolds

In recent years, scientists have used tissue engineering in attempts to create 3D neuronal cultures that emulate the high cell density and connectivity seen in vivo by using two main approaches to biomaterials: polymer gels and solid porous matrices (Schmidt and Leach 2003; Ma et al. 2004; Shany et al. 2005; Huang and Huang 2006; Baranes et al. 2007; Lee et al. 2008). Polymer gels molded to form tubes have been used successfully to provide 2D growth surfaces for peripheral neurons and to protect their processes from the inflammatory response of surrounding scar tissue (Schmidt and Leach 2003; Huang and Huang 2006). When cast as uniform blocks with cells embedded in them, they have provided supports for 3D cultures of neurospheres (neuronal stem cell aggregates) (Ma et al. 2004). Polymer gels have not been applied to isolated primary neurons. Moreover, to create layered 3D cultures from polymer gels would require gel microprinting, and it would be difficult to place cells of different types in desired 3D relations to one another.

Although the use of solid porous matrices is attractive because of their rigid mechanical properties (Shany et al. 2005; Baranes et al. 2007), these matrices have limited porosity, and thus they do not allow for deep cell migration within the matrix. This could be overcome by grinding or slicing the matrix into 'unit' modules, but the diversity of size and shape of the particles would be expected to interfere with packing into regular layered arrays.

The viability in 3D neuronal cultures was highly dependent on cell density. By using polymer gels and solid porous matrices there is a very important limitation. In this type of structure, the optimal viability is founded at an initial plating density of 3750 cells/mm^3 (for 500–600 μm thick cultures) (Cullen et al. 2011). This density value is low if it is compared to the in vivo situation.

In contrast to other methods (Schmidt and Leach 2003; Ma et al. 2004; Shany et al. 2005; Huang and Huang 2006; Baranes et al. 2007; Lee et al. 2008), Pautot's approach makes it possible to grow dissociated neurons on moveable surfaces that allow for genetic and mechanical manipulation and assembly into ordered 3D networks. They worked with silica beads that are large enough to provide an adhesion surface for neuronal cell bodies, and for growth and differentiation of axons and dendrites. The neurons can be moved by displacing the beads without disrupting cell adhesion or damaging the delicate processes. They can be transfected before transfer either into culture dishes containing conventional 2D neuronal cultures, with which they form contacts, or in such a way that they spontaneously organize into regular ordered 2D layers. Layers can be added in succession to make 3D hexagonal arrays. Some of the layers can contain beads coated with chemical guidance cues that direct process growth to create synaptic layers. Finally, by varying the beads diameter, with this method it is possible to achieve densities of up to 75,000 cells/mm^3, that are close to the 91,000 cells/mm^3 measured in the mouse brain cortex (Abeles 1991).

These properties of the colloid method make it possible to do what the earlier methods could not, namely, to build artificial layered networks out of genetically modified cells, under conditions that provide for cell densities that approach those

found in the brain, and allowing synaptic connections to be formed and their spatial distribution and strength to be assessed. Their method should pave the way for studying synapse formation and modification in the context of specific molecular interactions, chemical cues and activity patterns in designed 3D networks. Because the approach is amenable to long-term culture, it affords a unique system for cell-based assays of neuraly targeted drugs and could prove useful for developmental studies of interactions between neurons in a controlled environment.

References

Abeles M (1991) Corticonics: neural circuits of the cerebral cortex. Cambridge University Press, Cambridge

Balgude AP, Yu X et al (2001) Agarose gel stiffness determines rate of DRG neurite extension in 3D cultures. Biomaterials 22(10):1077–1084

Baranes D, Cove J et al (2007) Interconnected network of ganglion-like neural cell spheres formed on hydrozoan skeleton. Tissue Eng 13(3):473–482

Behravesh E, Emami K et al (2005) Comparison of genotoxic damage in monolayer cell cultures and three-dimensional tissue-like cell assemblies. Adv Space Res 35(2):260–267

Bellamkonda R, Ranieri JP et al (1995) Hydrogel-based three-dimensional matrix for neural cells. J Biomed Mater Res 29(5):663–671

Berthod F, Hayek D et al (1993) Collagen synthesis by fibroblasts cultured within a collagen sponge. Biomaterials 14(10):749–754

Birgersdotter A, Sandberg R et al (2005) Gene expression perturbation in vitro–a growing case for three-dimensional (3D) culture systems. Semin Cancer Biol 15(5):405–412

Blackshaw SE, Arkison S et al (1997) Promotion of regeneration and axon growth following injury in an invertebrate nervous system by the use of three-dimensional collagen gels. Proc Biol Sci 264(1382):657–661

Castillon N, Hinnrasky J et al (2002) Polarized expression of cystic fibrosis transmembrane conductance regulator and associated epithelial proteins during the regeneration of human airway surface epithelium in three-dimensional culture. Lab Invest 82(8):989–998

Choi HK, Won L et al (1993) Dopaminergic neurons grown in three-dimensional reaggregate culture for periods of up to one year. J Neurosci Methods 46(3):233–244

Chun TH, Hotary KB et al (2006) A pericellular collagenase directs the 3-dimensional development of white adipose tissue. Cell 125(3):577–591

Cukierman E, Pankov R et al (2001) Taking cell-matrix adhesions to the third dimension. Science 294(5547):1708–1712

Cukierman E, Pankov R et al (2002) Cell interactions with three-dimensional matrices. Curr Opin Cell Biol 14(5):633–639

Cullen DK, Wolf JA et al (2011) Neural tissue engineering and biohybridized microsystems for neurobiological investigation in vitro (Part 1). Crit Rev Biomed Eng 39(3):201–240

Desai A, Kisaalita WS et al (2006) Human neuroblastoma (SH-SY5Y) cell culture and differentiation in 3-D collagen hydrogels for cell-based biosensing. Biosens Bioelectron 21(8): 1483–1492

Fawcett JW, Barker RA et al (1995) Dopaminergic neuronal survival and the effects of bFGF in explant, three dimensional and monolayer cultures of embryonic rat ventral mesencephalon. Exp Brain Res 106(2):275–282

Fawcett JW, Housden E et al (1989) The growth of axons in three-dimensional astrocyte cultures. Dev Biol 135(2):449–458

Friedl P, Zanker KS et al (1998) Cell migration strategies in 3-D extracellular matrix: differences in morphology, cell matrix interactions, and integrin function. Microsc Res Tech 43(5):369–378

Granet C, Laroche N et al (1998) Rotating-wall vessels, promising bioreactors for osteoblastic cell culture: comparison with other 3D conditions. Med Biol Eng Comput 36(4):513–519

Grinnell F (2000) Fibroblast-collagen-matrix contraction: growth-factor signalling and mechanical loading. Trends Cell Biol 10(9):362–365

Grinnell F (2003) Fibroblast biology in three-dimensional collagen matrices. Trends Cell Biol 13(5):264–269

Hindie M, Vayssade M et al (2006) Interactions of B16F10 melanoma cells aggregated on a cellulose substrate. J Cell Biochem 99(1):96–104

Hofmann RM (1993) To do tissue culture in two or three dimensions? That is the question. Stem Cells 11(2):105–111

Horie H, Akahori Y (1994) Three-dimensional cell aggregation enhances growth-promoting activity of NGF in adult DRG. NeuroReport 6(1):37–40

Huang YC, Huang YY (2006) Biomaterials and strategies for nerve regeneration. Artif Organs 30(7):514–522

Kiryushko D, Berezin V et al (2004) Regulators of neurite outgrowth: role of cell adhesion molecules. Ann N Y Acad Sci 1014:140–154

LaPlaca MC, Cullen DK et al (2005) High rate shear strain of three-dimensional neural cell cultures: a new in vitro traumatic brain injury model. J Biomech 38(5):1093–1105

Lee J, Cuddihy MJ et al (2008) Three-dimensional cell culture matrices: state of the art. Tissue engineering Part B, Reviews 14(1):61–86

Letourneau P (1975a) Possible roles of cell to substratum adhesion in neuronal morphogenesis. Dev Biol 44:77–91

Letourneau PC (1975b) Cell-to-substratum adhesion and guidance of axonal elongation. Dev Biol 44(1):92–101

Liu H, Lin J et al (2006) Effect of 3D scaffold and dynamic culture condition on the global gene expression profile of mouse embryonic stem cells. Biomaterials 27(36):5978–5989

Loers G, Schachner M (2007) Recognition molecules and neural repair. J Neurochem 101(4):865–882

Ma W, Fitzgerald W et al (2004) CNS stem and progenitor cell differentiation into functional neuronal circuits in three-dimensional collagen gels. Exp Neurol 190(2):276–288

Mao C, Kisaalita WS (2004) Characterization of 3-D collagen hydrogels for functional cell-based biosensing. Biosens Bioelectron 19(9):1075–1088

Masi L, Franchi A et al (1992) Adhesion, growth, and matrix production by osteoblasts on collagen substrata. Calcif Tissue Int 51(3):202–212

Miller BE, Miller FR et al (1985) Factors affecting growth and drug sensitivity of mouse mammary tumor lines in collagen gel cultures. Cancer Res 45(9):4200–4205

Pardo B, Honegger P (2000) Differentiation of rat striatal embryonic stem cells in vitro: monolayer culture vs. three-dimensional coculture with differentiated brain cells. J Neurosci Res 59(4): 504–512

Pautot S, Wyart C et al (2008) Colloid-guided assembly of oriented 3D neuronal networks. Nat Methods 5(8):735–740

Pedersen JA, Swartz MA (2005) Mechanobiology in the third dimension. Ann Biomed Eng 33(11): 1469–1490

Pusey PN, Vanmegen W (1986) Phase-behavior of concentrated suspensions of nearly hard colloidal spheres. Nature 320:340–342

Schindler M, Nur EKA et al (2006) Living in three dimensions: 3D nanostructured environments for cell culture and regenerative medicine. Cell Biochem Biophys 45(2):215–227

Schmeichel KL, Bissell MJ (2003) Modeling tissue-specific signaling and organ function in three dimensions. J Cell Sci 116(Pt 12):2377–2388

Schmidt CE, Leach JB (2003) Neural tissue engineering: strategies for repair and regeneration. Annu Rev Biomed Eng 5:293–347

Schuz A, Palm G (1989) Density of neurons and synapses in the cerebral cortex of the mouse. J Comp Neurol 286(4):442–455

Shany B, Vago R et al (2005) Growth of primary hippocampal neuronal tissue on an aragonite crystalline biomatrix. Tissue Eng 11(3–4):585–596

Smalley KS, Lioni M et al (2006) Life isn't flat: taking cancer biology to the next dimension. In Vitro Cell Dev Biol Anim 42(8–9):242–247

van Blaaderen A, Ruel R et al (1997) Template-directed colloidal crystallization. Nature 385:321–324

Venstrom KA, Reichardt LF (1993) Extracellular matrix. 2: Role of extracellular matrix molecules and their receptors in the nervous system. FASEB J 7(11):996–1003

Wang F, Weaver VM et al (1998) Reciprocal interactions between beta1-integrin and epidermal growth factor receptor in three-dimensional basement membrane breast cultures: a different perspective in epithelial biology. Proc Natl Acad Sci U S A 95(25):14821–14826

Willerth SM, Arendas KJ et al (2006) Optimization of fibrin scaffolds for differentiation of murine embryonic stem cells into neural lineage cells. Biomaterials 27(36):5990–6003

Xu T, Gregory CA et al (2006) Viability and electrophysiology of neural cell structures generated by the inkjet printing method. Biomaterials 27(19):3580–3588

Yamada KM, Pankov R et al (2003) Dimensions and dynamics in integrin function. Braz J Med Biol Res 36(8):959–966

Chapter 5
3D Neuronal Networks Coupled to MEAs

In the previous chapter I presented the state of the art of 3D neuronal network models: no attempt has been presented in the literature related to functional multisite electrophysiological measurements on 3D neuronal networks.

In this chapter, I will present the results coming from 3D networks coupled to Micro-Electrode Arrays devices (MEAs). Firstly, I will report the imaging characterization (cf. Sect. 5.2) of such networks. Then, I will show the 3D hippocampal neuronal network dynamics (both spontaneous, stimulus-evoked, and after chemical manipulation) and I will prove how the recorded activity is enhanced with respect to the corresponding 2D model (cf. Sect. 5.3). Finally, I will show preliminary results about the spontaneous activity exhibited by 3D cortical neuronal networks (cf. Sect. 5.4).

5.1 3D Neuronal Networks Coupled to MEA Devices

The potential advantages of 3D neuronal engineered constructs are evident as they can be used as a more accurate investigational in vitro platform or as the basis for developing living bio-hybrid neuro-electronic microsystems in vitro or in vivo (Cullen et al. 2011). Thus the design and implementation of 3D engineered neuronal networks with embedded sensors and recording-stimulating electrodes, would certainly open new opportunities for investigation in the neuroscientific domain. On the other hand, the development of such 3D cellular constructs coupled to the possibility of functional electrophysiological recordings poses various challenges in terms of integration between scaffolds and recording-stimulating systems, long-term cell survival, exchange of nutrients, cell coupling with micro-electrodes and micro-sensors, etc.

Up to now, most of the efforts have been devoted to the development of new materials (Lee et al. 2008), passive (Irons et al. 2008; Kunze et al. 2011) and active

M. Frega, *Neuronal Network Dynamics in 2D and 3D in vitro Neuroengineered Systems*, Springer Theses, DOI 10.1007/978-3-319-30237-9_5

scaffolds (Rowe et al. 2007), and new experimental procedures to guarantee the development of 3D cultured networks. However, multi-site electrophysiological recordings in such 3D neuronal preparations are still lacking.

In this paragraph the innovative method for constructing 3D neuronal networks coupled to MEA devices is reported. By using this model multi-site electrophysiological recordings of 3D neuronal preparations can be performed.

In literature a lot of works are presented describing different methods utilized to create 3D neuronal cultures that emulate the high cell density and connectivity seen in vivo (cf. Sect. 4.2) (Pautot et al. 2008; Cullen et al. 2011). By comparing advantages and limitation of these methods, we decided to take inspiration from the Pautot's one (Pautot et al. 2008). The procedure used for constructing a 3D neuronal network coupled to MEA is reported in what follows.

The basic structure for designing and implementing 3D neuronal networks is constituted by layers of glass micro-beads of a selected dimension. In order to build the hippocampal assembly, we used micro-beads of 40 ± 2 μm in diameter that self-assemble in a compact hexagonal geometry and that provide a reasonable growth surface for neurites and a large enough interstitial space for cell bodies (Parviz and Gross 2007).

To allow cell plating preferentially onto the active electrode area of the device and to ensure a good communication between the substrate embedded micro-electrodes and the 3D assembly, two preliminary steps are to be performed. These steps are reported in what follows.

1. *Confinement of the active area of MEA device*
   The active area of the MEA device is delimited by coupling a Poly-dimethyl-siloxane (PDMS) structure to the MEA substrate. The confinement is used to

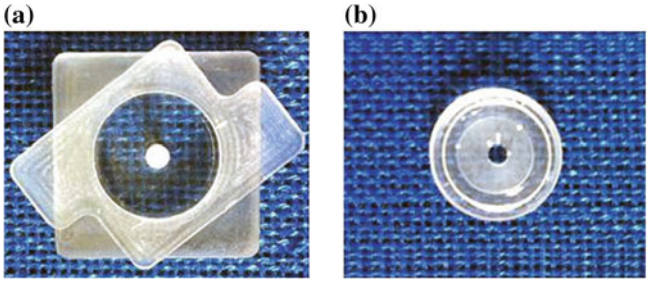

Fig. 5.1 First step for the construction of 3D neuronal networks: confinement of the active area of the device. **a** Molder used to build the confinement structure. **b** PDMS structure allowing to confine microbeads and neurons on the recording site area

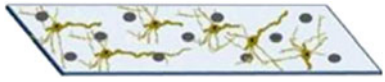

Fig. 5.2 Sketch of 2D neuronal network coupled to MEA device

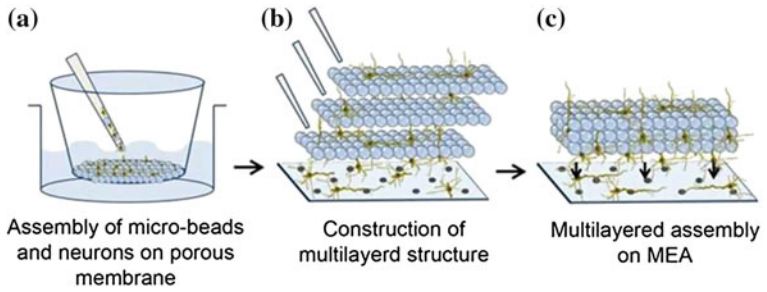

Fig. 5.3 Main steps for building a 3D neuronal network. **a** Micro-beads were placed onto a porous Transwell® membrane where they self-assembled in a hexagonal geometrical structure; dissociated hippocampal or cortical cells were plated on such coated micro-beads. **b** To obtain a 3D structure, the suspension of neurons and micro-beads was then moved from the membrane to the MEA surface several times. **c** Final configuration: multilayered assembly of micro-beads and neurons on MEA

allow cell plating preferentially onto the active electrode area of the device and subsequently to accommodate the glass micro-beads stacks with adherent neurons. The PDMS structure is constituted by a simple cylinder (built with the molder shown in Fig. 5.1a) with an external and internal diameter of 22.0 and 3.0 mm respectively and with a height of 650 µm. The confinement is shown in Fig. 5.1b.

2. *2D network on MEA*
   Hippocampal or cortical neurons were plated onto the MEA surface, which was previously pre-coated with adhesion factors (Laminin and Poly-Lysine both at 0.05 µg/ml) and delimitated by the PDMS constraint. It should be noted that the 2D neuronal network (cell density of 1800–2000 cells/mm^2) directly coupled to the active area of the MEA is fundamental to ensure a good communication between the substrate embedded micro-electrodes and the 3D assembly. A sketch of a 2D neuronal network coupled to MEA is reported in Fig. 5.2.

When the preliminary steps are performed, it is possible to start with the 3D neuronal network construction. The other steps required for the 3D neuronal network construction are described below and are reported in the sketch in Fig. 5.3.

1. *Assembly of micro-beads and neurons on porous membrane*
   The micro-beads were sterilized and pre-treated with a mixture of adhesion factors Laminin and Poly-D-Lysine (both 0.05 µg/ml) at 37 °C for 12 h. At this stage, about 30,000 micro-beads were placed onto a Transwell® porous membrane where they self-assembled forming a uniform layer. Then, for the direct coupling with neurons, dissociated hippocampal or cortical cells (concentration of 700 cells/µl) were seeded on such coated monolayer of micro-beads (Fig. 5.3a) and cultured them in Neurobasal medium supplemented with B27. The cell seeding concentration was chosen in order to obtain a final density of

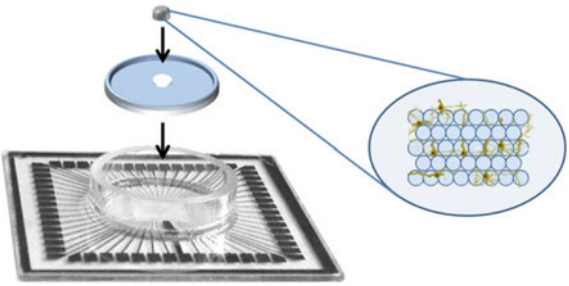

Fig. 5.4 Cartoon illustrating the final configuration of 3D neuronal networks: multi-layers of micro-beads and neurons confined by a PDMS structure onto the active area of the Micro-Electrode Array device

about 1500 cells/mm^2 covering the micro-beads surface and approaching a confluent monolayer.

2. *Construction of multilayered structure*
   After 8–10 h, the suspension of neurons and micro-beads was moved from the Transwell® membrane and deposited over the 2D neuronal network previously plated onto the area defined by the PDMS structure. With respect to the original density, we estimate a loss of about 20–30 % of cells due to mechanical manipulations and to cell bodies that remain on the Transwell® membrane surface.
   Once the first layer was deposited, we replicated the same operation to obtain a packed 3D assembly (Fig. 5.3b). The resulting 3D structure rearranges itself to form a colloidal crystal that self-assembles in a (theoretically) hexagonal structure composed on average by 5–8 layers of micro-beads and cells (Fig. 5.3c).
   The final configuration, made up of MEA, PDMS structure, micro-beads and neurons layers, is shown in Fig. 5.4.

Once all the layers were spontaneously assembled, neuronal processes grew over the micro-bead scaffold resulting in a high-density physically connected 3D neuronal network with an estimated (on the basis of the actual volume and total number of transferred neurons) final cell density of about 80,000 cells/mm^3, a value in the range of the interstitial density computed for glass micro-beads of 40 μm in diameter (1×10^5 mm^{-3}). It is worth noting that this value is not far from 92,000 cells/mm^3, the average neuronal density estimated in the mouse brain cortex (Schuz and Palm 1989). Indeed, by adjusting the micro-beads dimension we could change-control the density of the neurons and partly control the average connectivity degree of the network (Pautot et al. 2008).

By coupling 3D neuronal network to MEAs, it is possible to record the electrophysiological activity. By exploiting the electrodes of the device, it is also possible to stimulate the network from the bottom layer. The final stimulation-recording configuration is represented in the cartoon of Fig. 5.5. In addition, the developed set-up allowed us to deliver an electrical stimulation both from the bottom layer through the MEA electrodes and from the top layers by using a conventional tungsten electrode. The stimulus utilized is a rectangular biphasic pulse with a frequency of 0.2 Hz and an amplitude of 1.5 V_{pp} or 3 V_{pp} (for the bottom or top layer stimulation, respectively).

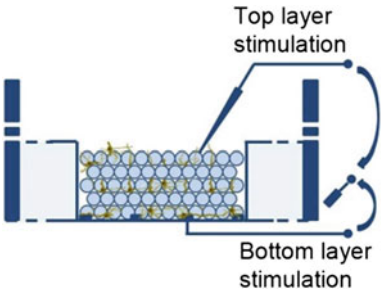

Fig. 5.5 Sketch depicting the recording/stimulation configuration: the electrophysiological activity of the 3D network is recorded from the substrate MEA electrodes (*bottom layer*); the network can be stimulated both from MEA and tungsten electrodes (*bottom* and *top layers*)

5.2 Imaging Characterization

In order to prove in vivo like cell morphology and demonstrate that we are partly controlling the development of a 3D network, we gathered structural information on fixed 3D hippocampal cultures by indirect immunofluorescence techniques. The use of antibodies directed against specific neuronal proteins allowed us to recognize the distribution of neuron types, glia and synaptic connections. For this purpose we prepared sister cultures on glass coverslips that were fixed with PFA 4 % together with the 3D cultures coupled to MEAs at the end of each recording session. We treated the different coverslip-grown cultures with a selected panel of primary and secondary antibodies in sequence. The use of coverslip (thickness 0.13–0.14 mm) coupled 3D cultures was necessary to overcome the limitation introduced by the relatively high thickness (1 mm) of the MEA glass substrate that precluded the possibility of using high numerical aperture objectives with an inverted confocal microscope. The configuration of the coverslip coupled cultures was identical to the final structure of the hippocampal 3D network on MEAs. Hippocampal neurons were plated with the same procedures and for the same period of time. We used an upright confocal microscope to complete our tridimensional optical analysis. The selected objective is immersed inside the MEA reservoir where the multilayered structure of micro-beads is assembled. In this scenario, we used long-working distance objectives, to observe the morphology of the neuronal network within the deepest layers with a Z-stack exceeding 400 μm.

The pictures presented in this paragraph show the different configurations investigated from 2D cultured hippocampal neurons to 3D networks coupled to MEAs. The main characteristic of this 3D network are summarized below.

1. *Cell morphology*
   Neural cells plated in 3D presented a bulbous morphology with intercellular contacts in all spatial directions (Fig. 5.6).
   Figure 5.6a shows a close-up of a few cells cultured on a planar substrate relative to a 2D neuronal network,. In this in vitro model the structure is constrained by the presence of a rigid planar substrate. The morphology of neurons is rather flat and the interaction with glial cells and extracellular matrix are limited by the

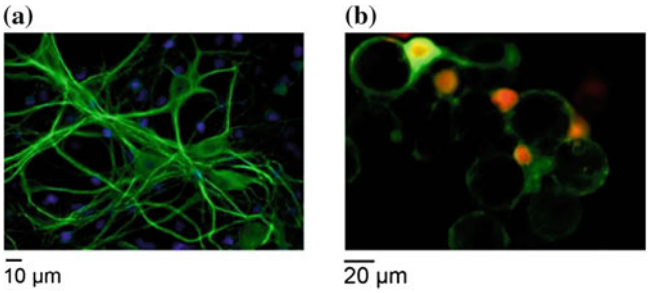

Fig. 5.6 **a** Mature hippocampal neurons (4 *week* in vitro), cultured on a planar substrate (i.e., 2D standard model, positive for Map-2 and Dapi nuclear dye). **b** Small cluster of neurons and microbeads closely linked together by a GABA interneuron (*green*/*red*) and four Nuclear Neuronal protein NeuN positive neurons (*red*)

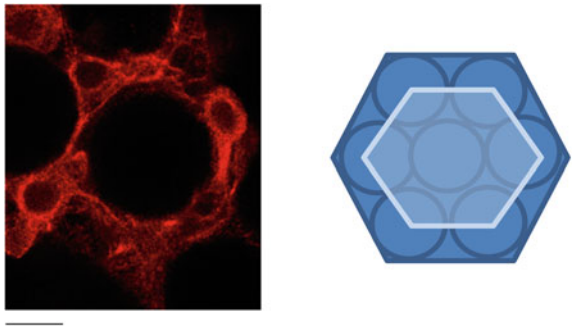

Fig. 5.7 Compact hexagonal geometry of the structure. A micro-bead is surrounded by six other micro-beads. Neurons lie in the interstitial space among beads. Scale bar: 20 µm

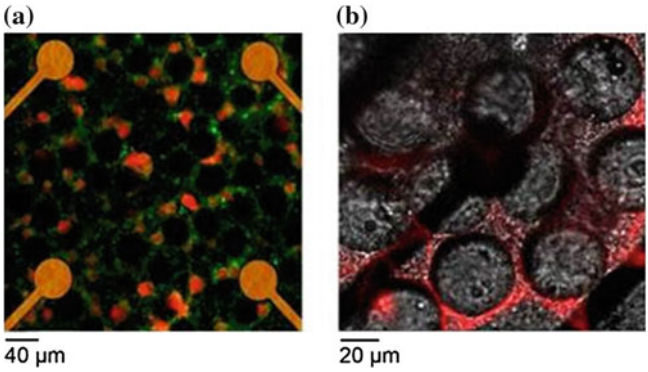

Fig. 5.8 **a** 3D culture on MEAs, labeled with Map-2 and NeuN. **b** The first layer of microbeads directly coupled on top of a single micro-electrode

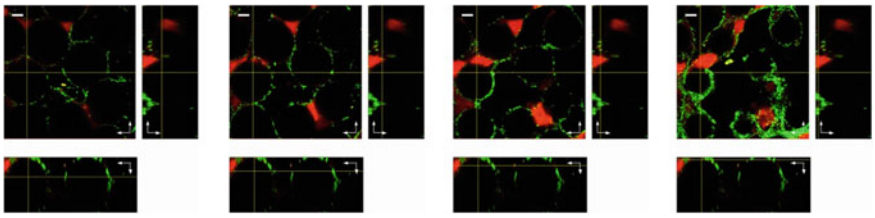

Fig. 5.9 Z-stack sequence of 3D cultured hippocampal neurons fixed at DIV 28 and immunolabeled for the pre-synaptic marker Synapsin (*green*) and NeuN (*red*). Scale bar: 10 μm

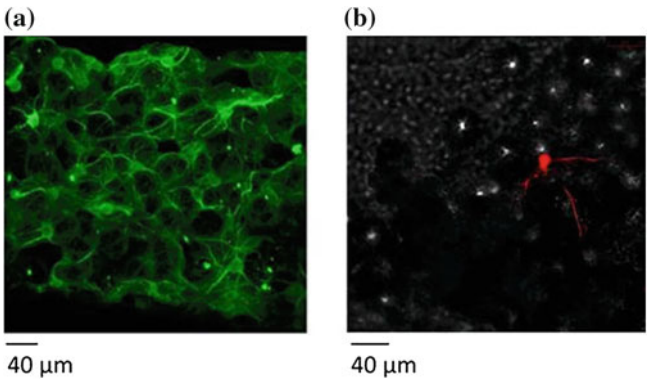

Fig. 5.10 **a** 3D rendering of 261.4 μm Z-stack of the hippocampal network on MEA device showing a high density of neuronal processes, exposed to dendritic marker Map-2. **b** Transfected neuron. Projection of about 80–120 μm on the z-axis

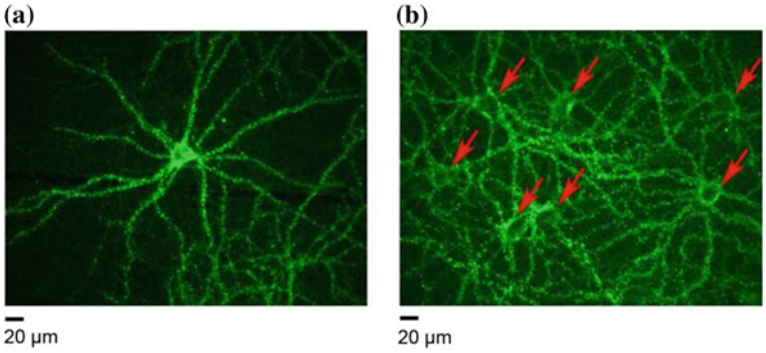

Fig. 5.11 Synaptic density of 2D neuronal network. **a** Immunostaining of a single neuron of a representative 2D hippocampal network immunolabeled for the pre-synaptic marker Synapsin. **b** Immunostaining of seven neurons (indicated with the *red arrows*) of a representative 2D hippocampal network immunolabeled for the pre-synaptic marker Synapsin

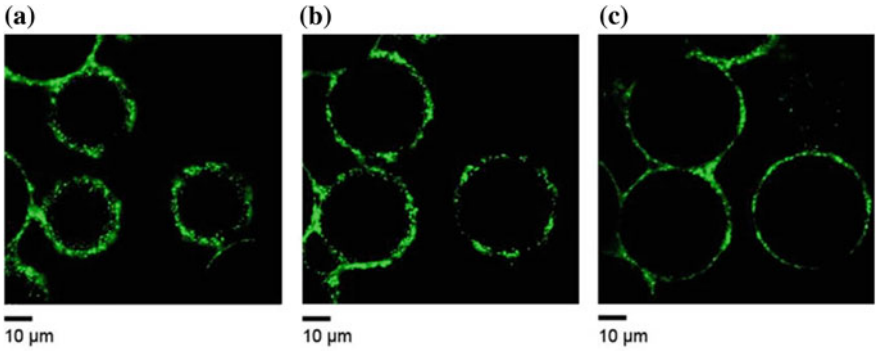

Fig. 5.12 Synaptic density of 3D neuronal networks. **a–c** Immunostaining of the 3D network close to three beads shown at different z-stacks. 3D cultured hippocampal neurons are immunolabeled for the pre-synaptic marker Synapsin

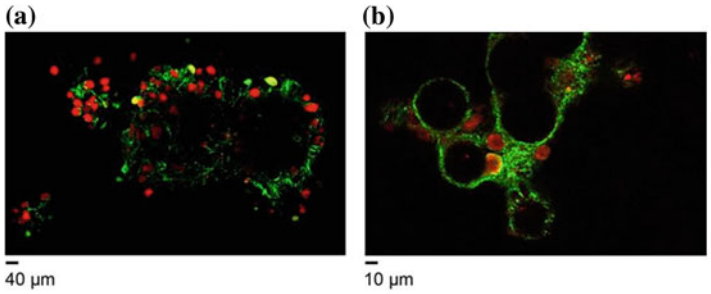

Fig. 5.13 Excitatory/inhibitory balance in 2D and 3D model. **a** Clusters of seven GABA interneurons (*green*) and among 35 Nuclear Neuronal protein NeuN positive neurons (*red*) belonging to a 2D neuronal network are shown. **b** Small cluster of neurons and microbeads closely linked together by a GABA interneuron (*green*/*red*) and four Nuclear Neuronal protein NeuN positive neurons (*red*)

planar substrate on which cells grow. By looking at the picture reported it is possible to see that in this kind of preparation soma and growth cones in are unrealistically flattened and the axons-dendrites outgrowth cannot occur in all directions.

In the picture representing neurons belonging to a 3D neuronal network (Fig. 5.6b), a small cluster of neurons with embedded micro-beads are shown. In this picture a GABA positive neuron (top left) and four NeuN positive (putative excitatory) neurons can be observed. It is possible to observe that cells stay more spherical when embedded within a scaffold than 2D cultures and, in the case of neurons and other process-extending cells, outgrowth can occur in all directions. It should be noted the round shape of the cell bodies with respect to the flattened shape of surface plated neurons.

2. *Compact geometry*
   To construct 3D neuronal network, we utilized micro-beads of 40 μm of diameter. These micro-beads self-assembled in a compact hexagonal geometry and the chosen diameter provides a growth surface large enough for neuronal cell bodies and their processes.
   By looking at the picture shown in Fig. 5.7, it is possible to observe the compact hexagonal geometry of the structure. It is possible to see a central micro-bead surrounded by six other micro-beads: this configuration is very ordered and compact. By looking at this picture it is also possible to observe some neurons lied in the interstitial space among beads: there a reasonable space for cell bodies. Pictures reported in Fig. 5.8 show the first layer of micro-beads directly coupled to micro-electrodes. By looking at these picture it is possible to observe a good assembly of the glass micro-beads onto the MEA surface plated with neurons. The pictures show that on the MEA surface there is nice occupancy of the interstitial space by soma and extensive arborizations connecting the neurons.
3. *Cell bodies in the interstitial spaces among beads in 3D*
   Figure 5.9 shows a sequence of the micro-bead and neurons stack on a glass coverslip. On the orthogonal projection of the Y-axis it can be observed that some neuronal soma lie on the glass surface while others remain entrapped among the micro-beads in the interstitial spaces. The beads diameter chosen for this structure provides a growth surface large enough for neuronal cell bodies to adhere and to stay in the interstitial spaces among beads.
4. *Neuronal processes and connections*
   After the spontaneous assembly of the 3D hexagonal arrays, neuronal processes grew between the beads to form highly interconnected networks. Neuronal processes cross from one bead to the next and observed glial cells in all the bead layers. The picture depicted in Fig. 5.10a shows extensive encapsulation by neuritic processes around the micro-bead scaffold indicating a high-density of potential connectivity among neurons. Neurites develop in a 3D space and form extensive arborizations connecting the neurons. By looking at this picture it is possible also to observe that in this configuration processes are able to grow over the beads, forming connection in different layers. In order to prove that connections between neurons belonging from different layers are formed, it has been transfected a neuron (Fig. 5.10b), where it is possible to observe that such a neuron projects for about 80–120 μm (i.e. 2–3 layers): it indicates that connections among neurons in different layers are feasible.
   Compared to the 2D model, this new network configuration gains a wide range of extension and, although constrained by the presence of the micro-beads ordered reticulum, each neuron can, in principle, have a site density of connecting points that is inversely dependent on the beads radius cubed (Pautot et al. 2008). To prove that 3D neuronal network exhibits an high connectivity degree, the synaptic connectivity in both uniform 2D and 3D models is quantified.
   In Fig. 5.11 images of peripheral regions of 2D cultures at very-low density are reported. By using these peripheral regions, the synapses density could be estimated and then the average synapses per neuron could be derived. 2D hippo-

campal networks are immunolabeled for the pre-synaptic marker Synapsin. A representative single neuron is reported in Fig. 5.11a; seven neurons are shown in Fig. 5.11b.

By counting and averaging the synaptic puncta in different regions, I could estimate a synaptic density of about 10^4 synapses/mm^2 (Ichikawa et al. 1993). From this number, and considering the low density of neurons in these peripheral regions I obtained, on average, 600 synapses per neuron, value that is comparable with other works (e.g., Cullen et al. 2010).

In order to quantify our 3D neuronal network synaptic density, I counted the number of synaptic puncta around single beads (Fig. 5.12a–c) in different picture along the z-axis with a step of 2 μm (value that should allow to count a single synapse only once). The synaptic puncta are contained within an annulus of 2 μm of width. I counted about 1200 synapses in a volume of 4.5×10^{-5} mm^3 (volume of the sphere containing the synaptic puncta). It is possible to roughly estimate a synaptic density of 2.6×10^7 synapses/mm^3, value that is comparable with previous works (Koch 1999). By considering an average neuronal density of 80×10^3 cells/mm^3, with this synaptic density value we obtain about 500 synaptic connections per neurons on average. This value is not far from the average synaptic connectivity measured in the mouse brain ($1–8 \times 10^8$ synapses/mm^3, Koch 1999).

5. *Excitatory/inhibitory neuronal balance*
   The proportion between GABAergic and glutammatergic populations is likely to remain similar in both 2D and 3D models (with about a 1:5 ratio). In Fig. 5.13a, a representative clusters of seven GABA interneurons (green) and among 35 Nuclear Neuronal protein NeuN positive neurons (red) belonging to a 2D neuronal network are shown. This result is comparable to what is reported in the literature for similar experimental models (Marom and Shahaf 2002; Bonifazi et al. 2005). Regarding 3D neuronal network, in Fig. 5.13b we can see a representative cluster of neurons and microbeads closely linked together by a GABA interneuron (green/red) and four Nuclear Neuronal protein NeuN positive neurons (red). From this very preliminary estimate (performed on different regions of our neuronal cultures) it is possible to say that is likely that the ratio of about 1:5 is conserved also in the 3D structure.
6. *Cell survival*
   In this type of configuration neuron health is maintained and uniform and robust neuronal process outgrowth throughout the bead layers, including in the deep layers, is supported. The void spaces between the beads permitted the necessary medium exchange to maintain healthy growing conditions.

In summary, by performing the imaging characterization I demonstrated that I was able to construct a physically connected 3D neuronal network.

I can underline two fundamental differences between cells cultured in monolayer versus 3D configurations. I found differences in soma morphology (neurons lying on a planar surface are flat while neurons growing within the 3D structure have got a more realistic morphology). Another fundamental difference regards the

development of the axo-dendritic processes. The growth of 3D network shows patterns of tangled ramifications both across and along different layers (5–8 layers), and around the single micro-bead. Moreover, by comparing 2D and 3D neuronal networks models, the synaptic connectivity degree is higher in the 3D one. The synaptic density is in the range of the average synaptic connectivity measured in the mouse brain (Koch 1999).

5.3 3D Hippocampal Neuronal Network Dynamics

To characterize the electrophysiological activity of the 3D network, and to demonstrate how the 3D structure modulates the network dynamics, we specifically compared the expressed dynamics with traditional 2D neuronal networks grown over MEAs. The characterization of the recorded activity was mainly carried out in comparison to standard 2D neuronal cultures coupled to MEA because they represent the reference model that has always been used to study the network neurophysiology and functional properties correlated with the electrophysiological activity (Robinson et al. 1993; Gal et al. 2010).

I anticipate that the main result is a 3D neuronal network model coupled to MEA that shows a wide range of activity patterns. These patterns are variable and present striking differences from the dynamics of standard high density 2D neuronal cultures both during spontaneous and electrically stimulated activity. The results regarding spontaneous activity, stimulus-evoked activity and activity modulated by chemical treatment are reported in the following paragraphs.

5.3.1 Spontaneous Activity

Spontaneous activities of 2D (N = 28) and 3D (N = 39) neuronal networks were recorded after four weeks in culture by means of TiN 60 channels MEAs. The activities of 2D and 3D neuronal networks were analyzed and compared. In this paragraph, the characterization of the spontaneous activity of the experiments performed will be reported.

By analyzing the spontaneous activity of 2D and 3D neuronal networks, I founded differences regarding patterns of activity, correlation and synchronization level and propagation of the signal.

5.3.1.1 Pattern of Activity

2D high density hippocampal neuronal networks show a typical and stereotyped electrophysiological activity in the mature phase of their development characterized by oscillating dynamics and synchronous bursts involving most of the active

channels in the MEA (Wagenaar et al. 2005; Gandolfo et al. 2010). Mature cultures (fourth week) exhibit a synchronized and distributed bursting activity mixed with a low spiking activity. During this stage of development the percentage of random spike is very low and the electrophysiological activity is dominated by bursting activity patterns. Short bursts, encompassing simultaneously a large number of recording sites, are generated, and the percentage of spikes within a burst is high, indicating that the bursting activity dominates this stage. This phenomenon is also recognized as "network burst", a recurrent event of strong neuronal interaction at many recording sites which appears during the second week in culture and is maintained during development with changing features (Van Pelt et al. 2004, 2005; Chiappalone et al. 2005).

Figure 5.14 shows a raster plot of the spontaneous activity of a representative experiment performed on a 2D hippocampal culture during the fourth *week* in vitro. Thanks to this plot it is possible to observe the electrophysiological activity of the network recorded from all the electrodes during 4 min. As anticipated, we can observe the quasi-synchronous activity and network dynamics composed mainly of network bursts (green box). There are synchronized events which involve most of the recording channels interspersed by period of time in which almost no activity is recorded.

Similarly, Fig. 5.15 shows a raster plot of the spontaneous activity of a representative experiment of a sister culture (i.e., same batch) forming a 3D network at the same age of its development (i.e., fourth week). It can be immediately noticed that the signature of the network dynamics presents a wider repertoire of activities with less global synchrony and more pronounced spiking at a single channel-neuron level. From a preliminary qualitative observation we can see periods in which the network holds a more synchronous activity (red box), with the presence of network bursts. In this configuration the duration of the network burst is more variable: there is the presence of network burst with duration that seams similar to what observed in the 2D networks, but there are also network burst longer than the ones observed in 2D. As anticipated, the 3D neuronal network exhibits also a significant 'random spiking' and non-synchronous bursting activity (blue box).

To highlight the type of firing exhibited by 2D and 3D neuronal networks, the Instantaneous Firing Rate (IFR) profiles are computed (cf. Appendix A.2). The 2D neuronal network IFR profile evaluated within the network burst activity region is shown in Fig. 5.16a; the 3D neuronal network IFR profiles evaluated within the random spiking and network bursting activity regions are reported Fig. 5.16b, c respectively.

As reported above, 2D hippocampal neuronal networks show a stereotyped electrophysiological activity characterized by synchronous bursts involving most of the active channels in the MEA. By looking at the 2D neuronal network profile, we can observe a very high synchronous activity over all the channels and the absence of significant random spiking activity. It is possible to observe that the activity recorded from the electrodes is similar and that the onset of the network burst appears simultaneously in all the channels. Also the duration of the activity within the network burst seams the same for all the channels involved in the network burst. Another

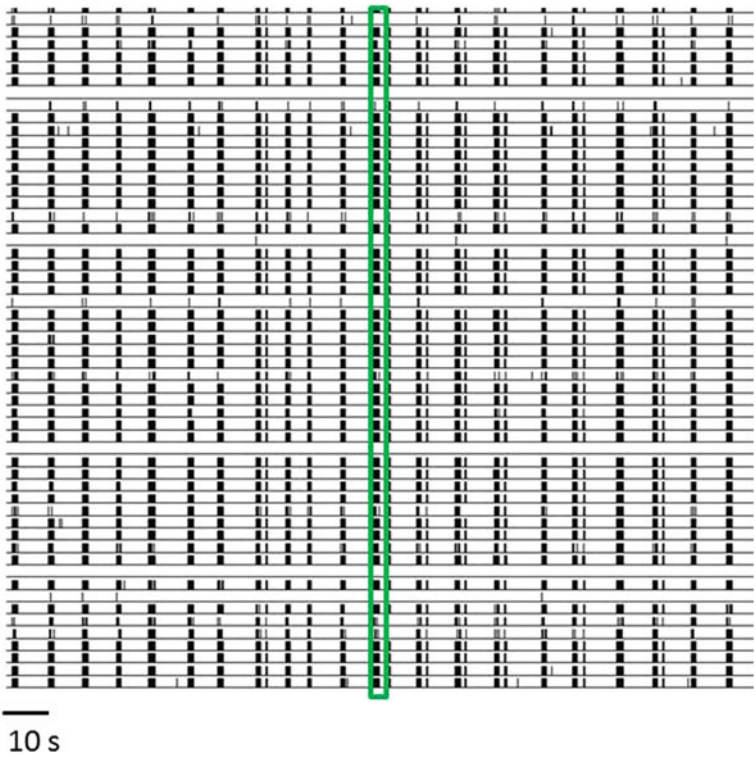

Fig. 5.14 Electrophysiological activity for a representative 2D hippocampal neuronal network. Raster plot showing 240 s of spontaneous activity. The highlighted area indicates a network bursting region (*green box*)

important feature that can be observed by the IFR profile and that characterizes the spontaneous electrophysiological activity of 2D neuronal network is the low activity recorded outside the network bursts.

By looking at the raster plot of a 3D neuronal network (Fig. 5.15), we found that the network exhibits less global synchrony and more pronounced spiking at a single channel-neuron level. Network bursting and random spiking activity are observed. To highlight these two distinct 'modes' of firing, I computed the IFR profiles (cf. Appendix A.2). By looking at the IFR profile computed within the random spike activity region (Fig. 5.16b), it is possible to observe that the network exhibits no synchronous activity and seems that only few channels work together (channels depicted in pink in the raster plot reported in Fig. 5.15). Regarding the IFR profile computed within the network burst region (Fig. 5.16c), it is possible to observe that the onset of the network burst appears not simultaneously in all the channels. In this case the activity recorded from the electrodes is similar but the amplitude of the network burst is not the same in all the recorded channels. Looking closer at the IFR

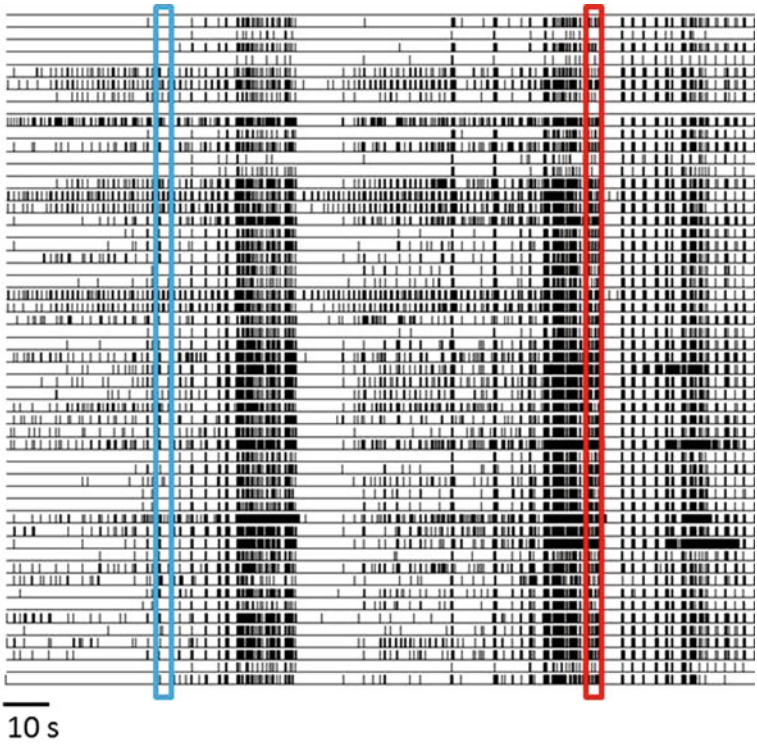

Fig. 5.15 Electrophysiological activity for a representative 3D neuronal network. Raster plot showing 240 s of spontaneous activity. The highlighted areas indicate the random spiking and the network bursting activity regions (*blue* and *red box* respectively)

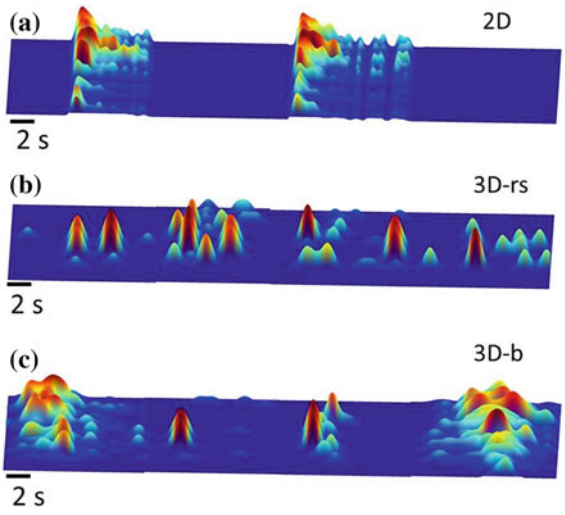

Fig. 5.16 Electrophysiological activity for a representative 2D and 3D neuronal networks. IFR profiles showing 40 s of activity are reported. **a** 2D neuronal network IFR profile is computed within the network bursting rate activity region. **b** 3D neuronal network IFR profiles computed within the random spiking activity region. **c** 3D neuronal network IFR profiles computed within the network bursting activity region

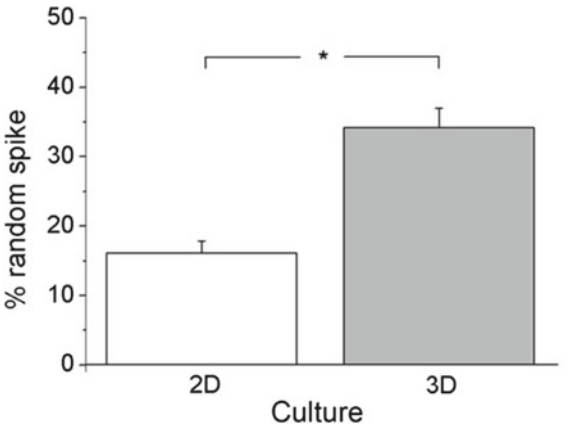

Fig. 5.17 Percentage of random spikes evaluated over the entire dataset of 2D (*white*) and 3D (*gray*) networks. *Asterisk* above the plot indicates significant difference, (P-value = 10^{-4}, Mann-Whitney U-test)

profile it is possible to see that there is the presence of random spiking activity between two network bursts.

The previous observations were further globally quantified by evaluating the Percentage of Random Spikes (i.e., the fraction of spikes outside bursts) in all the performed experiments. By looking at the bar plot of Fig. 5.17, we can see that the random spike activity is statistically different in 2D and 3D networks.

2D networks exhibit a strong synchronous bursting activity interspersed by period of time in which almost no activity is recorded. This network has got a low value of Percentage of Random Spikes [15.9 ± 2 % (mean ± standard error of the mean)].

3D networks exhibit a wide range of activity patterns, with the presence of both network burst and random spike regions. 3D neuronal networks show a significant higher level of random spiking (33.8 ± 3 %; P-value = 10^{-4}, Mann-Whitney U-test).

Both the high level of bursting activity and the low level of random spike activity exhibited by the 2D neuronal network represents the dynamics of the close in vitro systems that, missing the natural input–output pathways of the in vivo brain, have to find a stable state with properly formed synapses.

On the contrary, 3D neuronal network presents a high level of random spiking activity. This feature suggests that there are stimuli that arrive from the upper layers (i.e. external stimuli) that modulate the electrophysiological activity of the network.

By looking at the raster plot of a representative 2D and 3D neuronal networks (Figs. 5.14 and 5.15), we observed that the electrophysiological activity is composed by spiking and bursting patterns. In order to quantify the bursting activity at the single channel level, the frequency and the duration of the burst have been evaluated. The Mean Bursting Rate and the Burst Duration are evaluated over the entire dataset and are reported in Fig. 5.18. The main difference between 2D and 3D neuronal network bursting activity is the burst frequency.

2D networks exhibit a spontaneous activity that is composed mainly by burst pattern. In fact, as it is shown before, the random spiking activity is very low and the mean bursting rate is very high (19.7 ± 1.1 burst/min). 3D networks, instead,

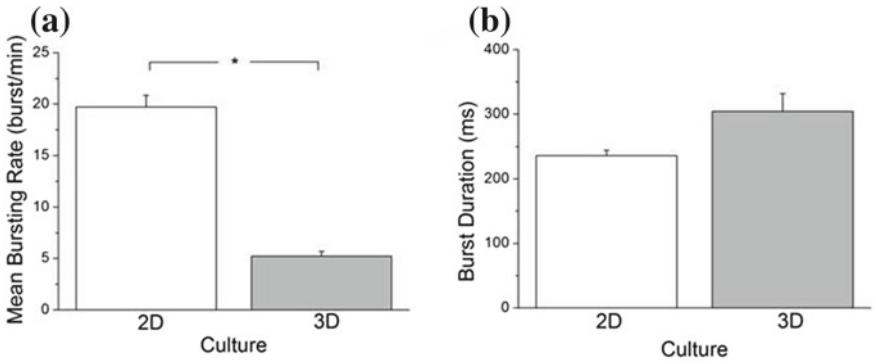

Fig. 5.18 **a** Mean bursting rate and **b** Burst Duration evaluated over the entire dataset of 2D (*white*) and 3D (*gray*) networks. *Asterisk* above the plot indicates significant difference, (P-value = 10^{-4}, Mann-Whitney U-test)

exhibit an high random spike activity. Accordingly to this result, the bursting rate exhibited by this type of network is low (5.2 ± 0.4 burst/min).

At single channel level, the 2D and 3D neuronal networks burst duration are not significantly different (Fig. 5.18b).

The bursting behavior exhibited by the 2D neuronal network is stereotyped, as qualitative depicted by the raster plot of Fig. 5.14, while in the 3D one the bursting behavior is more variable (Fig. 5.15).

To quantify this evidences, the Inter Burst Interval (IBI) of 3D and 2D neuronal networks have been evaluated over the entire dataset. 2D and 3D neuronal networks exhibit different Inter Burst Interval distributions (see Fig. 5.19). In the case of the 2D neuronal network, the values of the IBI span from 1 to 5 s (white bars in Fig. 5.19): 90 % of the IBI is distributed within the first 2.5 s and only 1 % is detected after 5 s. In the case of 3D neuronal network there are also periods in which the bursting activity is high: 40 % of the IBI distribution is within the first 0.25 s. In this type of configuration there are periods in which the network exhibits random spiking activity. During this period the timing between two burst is high: for this reason IBI spans from 10 to 15 s are detected. Globally, in this configuration 90 % of the IBI distribution is reached after 5 s and among 10 % of IBI is detected after 10 s.

Even if network bursting remains a common signature for both preparations, the shift from 2D to 3D does also affect the network bursting behavior. The main effects are observed both in frequency and duration.

I estimated the Mean Network Bursting Rate and Network Burst Duration evaluated over the entire dataset (Fig. 5.20).

Regarding 2D neuronal networks, I observed a quasi-synchronous activity and network dynamics composed mainly of network bursts: the number of network burst detected is very high the Network Burst Duration seams similar for all the network burst detected. By evaluating the Mean Network Bursting Rate over the entire dataset I found a very high value (22.3 ± 3.8 NB/min) (Fig. 5.20a). Regarding the network

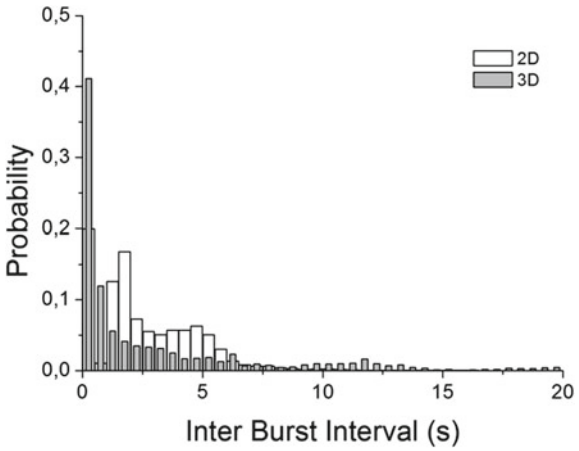

Fig. 5.19 Inter Burst Interval distribution evaluated over the entire dataset of 2D (*white*) and 3D (*gray*) networks. Bin size: 0.5 ms

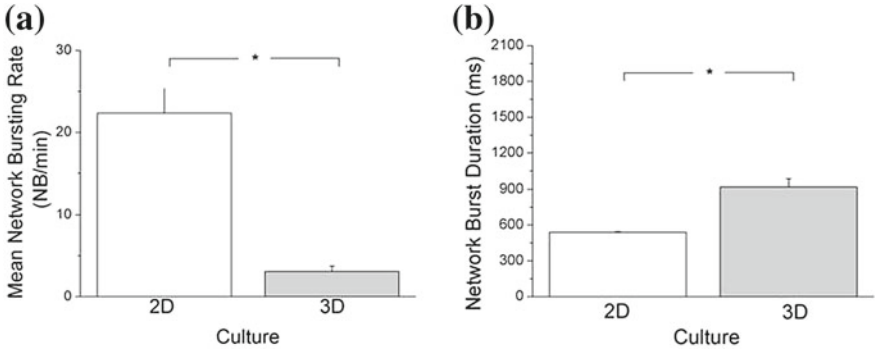

Fig. 5.20 **a** Mean Network Bursting Rate and **b** Network Burst Duration evaluated over the entire dataset of 2D (*white*) and 3D (*gray*) networks. *Asterisk* above the plot indicates significant difference, (P-value = 9×10^{-4}, Mann-Whitney U-test)

burst duration evaluated over the entire dataset I found that the mean value of Network Burst Duration is 540 ± 5 ms (Fig. 5.20b).

3D neuronal networks, instead, exhibited both random spike and network burst activities. I observed that in this case the number of network burst detected is low and the duration of the network burst is more variable: there is the presence of network burst with duration that seams similar to what observed in the 2D networks, but there are also network burst longer than the ones observed in 2D. By evaluating the Mean Network Bursting Rate over the entire dataset I found a very low value of this parameter (3.0 ± 0.6 NB/min) (Fig. 5.20a). In the case of the Network Burst Duration for all the experiments taken into account, I estimated a value of

919 ± 65 ms (Fig. 5.20b). The high value of the standard error for the 3D networks suggests a much higher variability of bursting activity. 2D and 3D network bursting rate and burst durations are statistically different (P-value $= 9 \times 10^{-4}$, Mann-Whitney U-test).

5.3.1.2 Correlation and Synchronization

To quantify the level of correlation and synchronization of the network activity we computed the Cross-Correlation (CC) function for 2D and 3D neuronal networks with a time window of 2 s and a bin size of 5 ms (cf. Appendix 5). For 3D neuronal networks CC is also specifically evaluated within the random spike activity and within the burst activity regions.

As anticipated, 2D mature cultures exhibit a synchronized and distributed bursting activity. During this stage of development the percentage of random spike is very low and the electrophysiological activity is dominated by bursting activity patterns. During the mature phase of development, the correlation and synchronization among all the possible pairs of channels is very high. This fact indicates that also "far" connections are explored, as a possible consequence of the rapid chemical synaptogenesis during the second week in culture.

Figure 5.21a shows the CC functions evaluated during 1 min of recording. The correlation between one channel and all the other recording electrodes for a representative experiment is reported. CC functions for 2D networks underline the high level of correlation among all the recording channels. By looking at this plot, it is possible to observe that the CC functions evaluated for all the channels are similar. All the functions are centered and peaked on the central bin; also the profile of the functions seem similar.

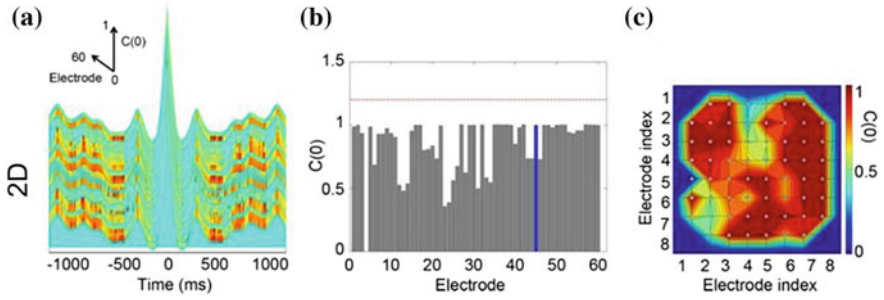

Fig. 5.21 Cross-Correlation analysis relative to 2D network. The analysis are performed during 1 min of recording. The Cross-Correlation function is evaluated between one representative channel and all the other recording channels. Only a single representative experiment is taken into account. **a** Cross Correlation function evaluated for the 2D neuronal networks. CC is computed with a time window of 2 s and a bin size of 5 ms. **b** C(0) values for 2D networks. The blue bar identifies the autocorrelation value. **c** Colormap that show the C(0) values in a 8×8 layout

The C_{Peak} values (i.e., maximum values of the CC function) for all the active channels are close to one (0.85 ± 0.03). This fact indicates that the level of activity correlation is very high for 2D neuronal networks.

I have further characterized the level of synchronization of the 2D network activity by computing the values of the CC function presented in Fig. 5.21a in the central time bin (i.e., C(0)). C(0) values are evaluated for all the recording channels and are shown in Fig. 5.21b. By looking at this figure it is clear that 2D neuronal networks exhibit a high level of synchronization as the normalized C(0) values are close to one for the majority of the recording channels. To better identify the synchronized electrodes, I plot the C(0) values over an 8×8 color map layout that represents the physical position of the MEA channels (see Fig. 5.21c). Observing this figure we can see a network that is highly synchronized (all the channels present a C(0) value close to one): network activity is always the same, the activity patterns are reliable and all the subpopulations of neurons belonging from the network work together. This fact represents an exploring dynamics of the close in vitro systems that, missing the natural input–output pathways of the in vivo brain, have to find a stable state with properly formed synapses.

As anticipated, 3D mature cultures exhibit an enhanced dynamic in which both network burst and random spike activity region are present.

In this case there is the presence of synchronized and distributed bursting activity mixed with spiking activity. During this stage of development the percentage of random spike is very high and the electrophysiological activity is various. During the mature phase of development, the correlation and synchronization among all the possible pairs of channels is high when it is computed within the network burst activity region while it is low if it is computed within the random spike activity region.

By analyzing the activity of 3D neuronal networks I obtained a low level of correlation among the active channels in the random spike activity region. Figure 5.22a shows the CC functions evaluated during 1 min of random spiking activity recording. The correlation between one channel and all the other recording electrodes for a representative experiment is reported. It is clear that in this case there is a low correlation and synchronization of the network activity. The mean C_{Peak} value is low (0.42 ± 0.02) and the peaks values are shifted with respect to the central bin suggesting possible causal relationships mediated by the neuronal population above the read-out neuronal layer coupled to the MEA substrate.

I have further characterized the level of synchronization of the 3D network activity within the random spike activity by computing the values of the CC functions reported in Fig. 5.22a in the central time bin (i.e., C(0)). C(0) values are shown in Fig. 5.22b. By looking at this figure it is clear that 3D neuronal networks exhibit a very low level of synchronization. The normalized C(0) values are lower than 0.5 for the majority of the recording channels. In order to better identify the synchronized channels within this region, we compared the C(0) value with a threshold related to the average C(0) values (cf. Appendix A.5). Only five channels present a value of C(0) higher than the threshold (these channels are highlighted in pink in the raster of Fig. 5.15) and they represent a group of spatially confined electrodes that could

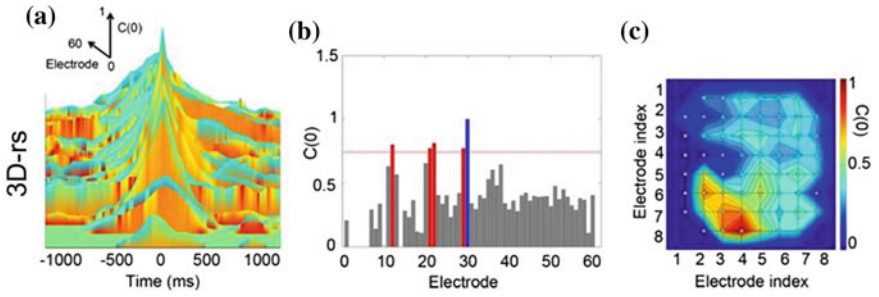

Fig. 5.22 Cross-Correlation analysis relative to 3D neuronal networks. The analysis are performed during 1 min of random spiking activity recording. The Cross-Correlation function is evaluated between one representative channel and all the other recording channels. Only a single representative experiment is taken into account. **a** Cross Correlation functions evaluated for the 3D neuronal networks within the random spike activity region. CC is computed with a time window of 2 s and a bin size of 5 ms. **b** C(0) values for 3D networks. These values are compared with a threshold (*red dashed line*). The blue bar identifies the autocorrelation value; the electrodes that show a C(0) value higher than the threshold are visualized with *red bars*. **c** Colormap that show the C(0) values in a 8×8 layout. 3D neuronal network within the random spike activity region exhibits only one channel with maximum C(0) value (autocorrelation) and there are few channels with a C(0) value major than 0.5

underline a synchronized sub-population. To better identify the synchronized electrodes, I plot the C(0) values over an 8×8 color map layout that represents the physical position of the MEA channels (see Fig. 5.22c). By looking at this plot it is clear that there is a very low synchronization level, and that there is a sub-group of synchronized electrodes that work together.

The CC function is also evaluated within the network burst activity region. The function is similar for all the recording channels (see Fig. 5.23a). In this case the level of correlation among channels is high (mean C_{Peak} value of 0.70 ± 0.02), with the majority of peaks centered in the central bin.

The level of synchronization of the 3D neuronal network activity is high during the period of bursting. By looking at Fig. 5.23b it is possible to observe that C(0) values are close to one for all the recording channels as for the 2D networks. To better identify the level of synchronization, I plot the C(0) values over an 8×8 color map layout that represents the physical position of the MEA channels (see Fig. 5.23c). By looking at this plot it is clear that there is an high synchronization level in all the network. The few channels that are synchronized during the random spike activity region remain with an high synchronization level and are the ones with the higher values compared with the other electrodes.

The previous observations were globally quantified by evaluating the C(0) values for all the performed experiments (see Fig. 5.24).

2D neuronal networks present a mean C(0) value close to one (0.81 ± 0.02), suggesting a very high synchronization among all the channels.

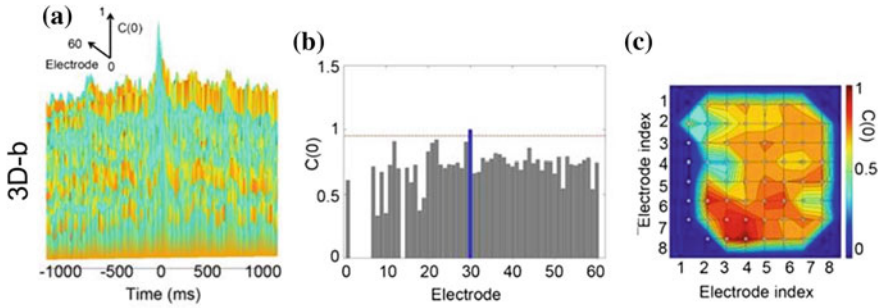

Fig. 5.23 Cross-Correlation analysis relative to 3D neuronal networks. The analysis are performed during 1 min of network bursting activity recording. The Cross-correlation function is evaluated between one representative channel and all the other recording channels. Only a single experiment is taken into account. **a** Cross Correlation functions evaluated for the 3D neuroal networks within the burst activity region. CC is computed with a time window of 2 s and a bin size of 5 ms. **b** C(0) values. The *blue bar* identifies the autocorrelation value. **c** Colormap that show the C(0) values in a 8×8 layout. 3D neuronal network within the burst activity region presents only one channel with maximum C(0) value (autocorrelation) and almost all the other channels exhibit a C(0) value major than 0.7

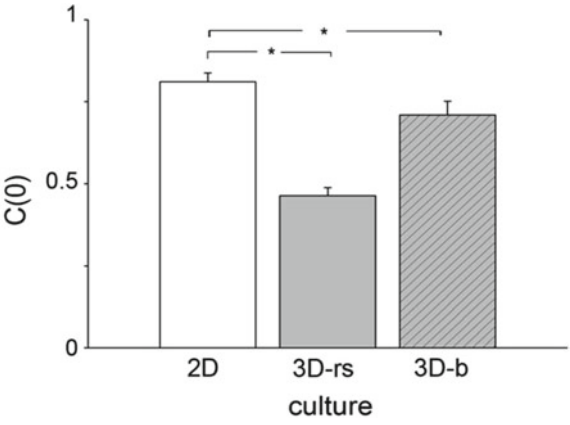

Fig. 5.24 C(0) values evaluated for 2D networks (*white*), 3D networks within the random spike activity region (*gray*) and 3D networks within the burst activity region (*striped gray*). *Asterisk* above the plot indicates significant differences (P-value $< 10^{-6}$, Mann-Whitney U-test)

The level of synchronization in 3D neuronal networks is high within the burst activity region (mean C(0) value of 0.71 ± 0.04) and low within the random spike activity region (mean C(0) value of 0.46 ± 0.02). Data differences are significant (P-value $< 10^{-6}$, Mann-Whitney U-test).

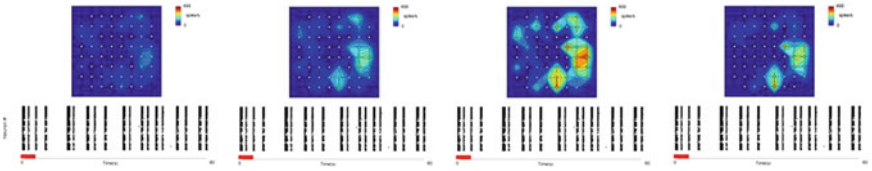

Fig. 5.25 Four time stamps of 2D neuronal network activity. Each panel is composed by an 8×8 color map layout (representing the physical position of the MEA channels) and by a raster plot representing 80 s of activity recorded from the electrodes

5.3.1.3 Signal Propagation

To demonstrate whether the layers are effectively connected, we studied and characterized the propagation of the signal (cf. Appendix A.6).

In 2D neuronal network, the signal propagation is continuous. In Fig. 5.25 different time stamps where it is possible to observe the signal propagation are reported. Each panel is composed by a raster plot of 80 s and by an 8×8 color map layout (representing the physical position of the MEA channels) in which the firing rate recorded by the electrodes is shown.

In this type of structure the signal starts from one source and propagates rapidly and in a continuous way in all the network. We can observe that the intensity of the signal increases smoothly. The first panel of Fig. 5.25 indicates a low signal intensity. Than the intensity of the firing rate starts to increase reaching its maximum value in the third panel, after about 40 ms. Then the signal intensity starts to decrease gradually in all the network. In order to know if this behavior is reliable, the coefficient of variation (i.e. standard deviation/mean) is evaluated on the network inter burst interval. This parameter allows to evaluate the values dispersion with respect to the mean. In the case of 2D neuronal network the value of the coefficient of variation is of 0.5. It indicates a low value of standard error: the dispersion of the values is low. In this type of configuration the behavior observed is reliable: we are in the presence of a very organized system that without external inputs continues to repeat the same pattern of activity.

In 3D neuronal network, the signal that starts from one site propagates in the network in a discontinuous way.

In Fig. 5.26 different time stamps in which it is possible to observe the signal propagation are reported. Each panel is composed by a raster plot of 80 s and by an 8×8 color map layout (representing the physical position of the MEA channels) in which the electrophysiological activity recorded from the electrodes is shown.

By looking at this figure it is clear that in this type of structure the signal starts from one source and propagates in a discontinuous way to the other parts of the network. The signal starts with a low level of intensity in one part of the network and gradually increases reaching a maximum value visible in the third plot reported in Fig. 5.26. Then the intensity of the signal starts to decrease. The firing rate is not increasing in all the network but only in a sub-network. When the intensity of the

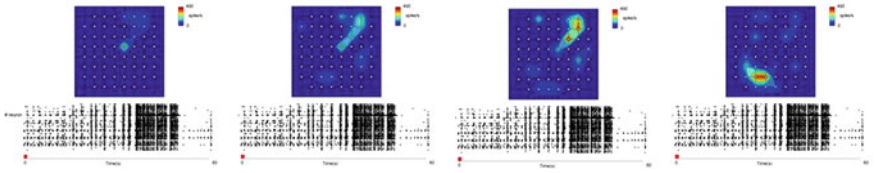

Fig. 5.26 Four time stamps of 3D neuronal network activity. Each panel is composed by an 8×8 color map layout (representing the physical position of the MEA channels) and by a raster plot representing 80 s of activity recorded from the electrodes

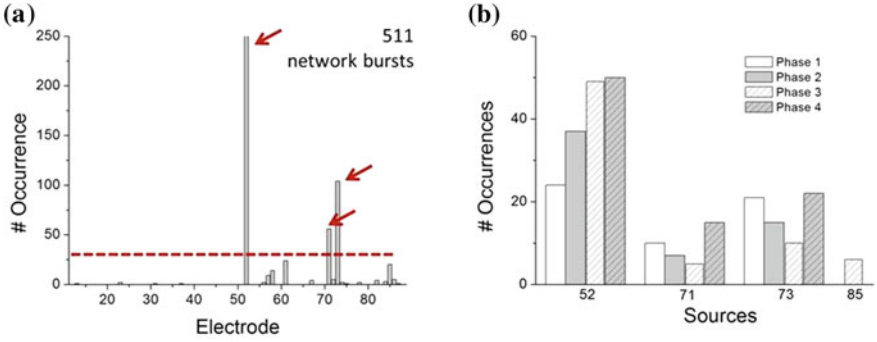

Fig. 5.27 **a** Signal sources evaluated in a recording phase of 30 min. The number of occurrence of the site where burst initiated is reported. The sources are the electrodes from which the signal starts in at least 5 % of all network burst (n = 511). The threshold is indicated by a dashed *red line* and the three sources are indicated with *arrows*. **b** Signal sources evaluated in four recording phases of 5 min each. The number of occurrence for each source is reported

signal reached a minimum value in one part of the network, another signal appears in another part, as it is visible in the last panel of Fig. 5.26. It starts to increase in intensity, it reaches the maximum value and then the intensity decreases and another signal starts in another sub-network. Also in this case, in order to know if this behavior is reliable, the coefficient of variation is evaluated on the network inter burst interval. The value of the coefficient is of 2.2, indicating an high value of standard error with respect to the mean: the dispersion of the network inter burst interval is high. Therefore, in this type of configuration the behavior observed is not reliable: we are in the presence of a very complex system that with external inputs (i.e. from top layers) continues to change the pattern of activity.

Three main results regarding the signal propagation have been achieved.

1. *Signal sources*
   As shown before, in 2D neuronal network the signal that initiates from one site propagates to the other parts of the network in a continuous way ("sliding" propagation).

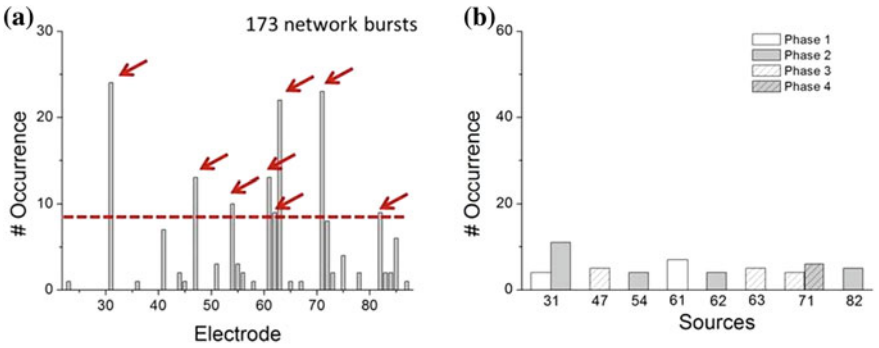

Fig. 5.28 **a** Signal sources evaluated in a recording phase of 30 min. The number of occurrence of the site where burst initiated is reported. The sources are the electrodes from which the signal starts in at least 5 % of all network burst (n = 173). The threshold is indicated by a dashed *red line* and the eight sources are indicated with *arrows*. **b** Signal sources evaluated in four recording phases of 5 min each. The number of occurrence for each source is reported

In order to know if 2D neuronal network system exhibits a simple and stereotyped dynamic, I evaluated the sites from which the signal (i.e. network burst) initiated during 30 min of recording of a representative experiment. I evaluated the sources of the signal as the sites where bursts were initiated in at least 5 % of all network bursts (cf. Appendix A.6) (Streit et al. 2001; Tscherter et al. 2001).

In 2D neuronal network there are few sources that appears with high occurrence. By looking at Fig. 5.27a it is possible to observe that there are a lot of network burst but only three sources are present. The signal starts 250 times from the electrode 52 and among 50 and 100 times from the electrodes 71 and 73 respectively.

In order to know if in this system there is a reliability of the sources, I evaluated the signal sources in different phases (5 min for each phase). The result is presented in Fig. 5.27b. It is clear that sources are always the same in different experimental phases. The electrodes 52, 71 and 73 are sources in all the four experimental phases taken into account. The system is organized and there is reliability of the sources.

In 3D neuronal network structure the signal that initiates from one site propagates in the other parts of the network in a discontinuous way ("jumping" propagation).

In order to know if 3D neuronal network system exhibits a complex and not reliable dynamic, I evaluated the sites from which the signal (i.e. network burst) starts during 30 min of recording (Fig. 5.28a). I evaluated the sources of the signal as the sites where bursts were initiated in at least 5 % of all network bursts.

In this 3D neuronal network representative experiment, there are a lot of sources that appear with a low occurrence. By looking at Fig. 5.28a it is possible to observe that there are few network burst and that a lot of sources are present.

In order to know if in this system there is a reliability of the sources, I evaluated the signal sources in different phases (5 min for each phase). By looking at

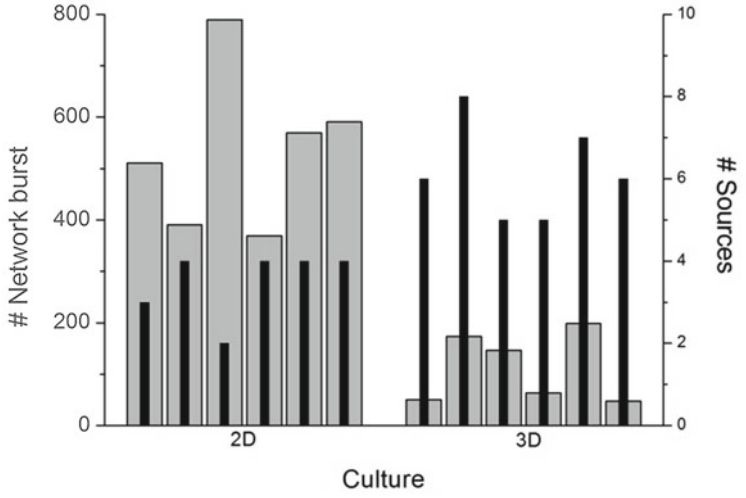

Fig. 5.29 Number of network burst (*grey bars*) and number of sources (*black bars*) evaluated in 30 min of recording. Each bar represent a single experiment (six experiment for the 2D neuronal network and six experiment for the 3D one)

Fig. 5.28b it is clear that sources change in different experimental phases. In the first phase the sources are the electrodes 31 and 61; in the second phase the electrodes 31 remains a source, but other sources appear (electrodes 54, 62, 82); in the third phase three new sources appear (electrodes 47, 63, 71); in the last phase only the source 71 remains.

This system presents a complex organization in which the sources are not reliable. This is an indirect proof of the fact that there is the presence of real sources in the upper layers.

The previous results evaluated taking into account a single representative experiment, were further globally quantified by evaluating the number of network burst and the relative sources detected in different experiments. In Fig. 5.29 are represented the network burst number and the sources detected in six experiments during 30 min of recordings.

By looking at the grey bars (i.e. number of network burst detected in 30 min of recording) it is possible to observe that the number of network burst exhibited by the 2D neuronal network is very high (mean value of 537 ± 62 network burst). In the 3D neuronal network, instead, only few network burst can be detected in 30 min of recording (mean value of 113 ± 27 network burst). By looking at the black bars (i.e. number of sources evaluated in 30 min of recording), 3D neuronal network exhibits more sources than the 2D one.

Summarizing, 2D neuronal network exhibits a lot of network burst and few sources; in the 3D neuronal network, on the contrary, few network burst and more sources are detected.

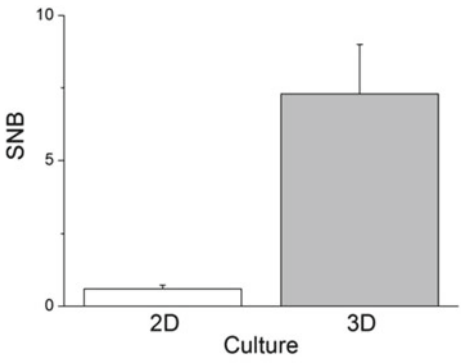

Fig. 5.30 SNB values (percentage of sources within respect to the number of network burst) evaluated in 30 min of recording for all the experiment performed

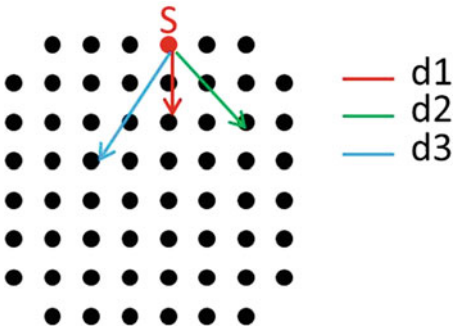

Fig. 5.31 Sketch that represents the 8×8 MEA electrode layout. A source is depicted with a *red* electrode. The *arrows* indicated three different distance that the signal travels with relative latencies

In order to compare this behavior, the percentage of sources related to the number of network burst (i.e. SNB) is evaluated (Eq. 5.1).

$$SNB = \frac{\#Sources}{\#NetworkBurst} * 100 \tag{5.1}$$

The SNB values evaluated for all the performed experiments are reported in Fig. 5.30. 2D neuronal network exhibit a very low value of SNB (0.6 ± 0.1): it indicates the presence of a lot of network burst with respect to the number of sources. The value of SNB evaluated for the 3D neuronal network is higher than the one shown by the 2D neuronal network (7.3 ± 1.6). It means that there are a lot of sources with respect to the number of network burst detected.

It is possible to observe that in the relationship between the sources detected in 2D neuronal network and the ones exhibited by the 3D neuronal network is 1:11.

Summarizing, in 2D neuronal network the propagation of the signal is continuous. This system is simple and stereotyped and there is a reliability of the sources. These features indicates a close system in which no external inputs arrives to modulate the activity.

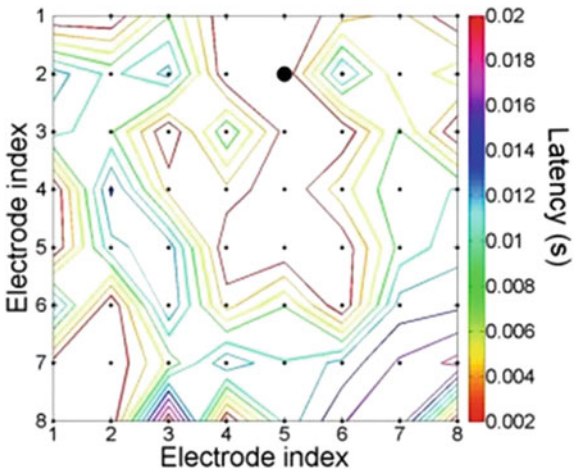

Fig. 5.32 Timing that the signal needs for propagating from one source to the other parts of the 2D neuronal network. The source is indicated with a *bold point* (electrode 52). The latency spans from 2 to 20 ms

3D neuronal network, instead, is a more complex system. The signal propagation is discontinuous and the sources are not reliable. These features indicates that the activity of this system is modulated by external input: there are real sources in the upper layers, from which the signal starts and reaches the sub-networks coupled to the MEA device modulating their activity.

2. *Latency*
   As shown before, the source is the site from which the signal (i.e. network burst) starts. In Fig. 5.31 the MEA electrode layout is depicted: one source is represented with a red electrode. The distance that the signal travels is evaluated as the physical distance from the source electrode to the other electrode involved in the network burst (cf. Appendix A.6). The time that the signal needs to reach another electrode involved into the network burst starting from the source (i.e. d1) is the latency of the signal (cf. Appendix A.6) (Streit et al. 2001; Tscherter et al. 2001).
   By computing the latency values and relating it with the distance that the signal travels, it is possible to quantify the speed propagation of the signal. The average of the latencies over all bursts from the same source was calculated for each electrodes (Streit et al. 2001; Tscherter et al. 2001).
   Regarding 2D neuronal network, the signal propagation is continuous and short. Figure 5.32 represents the timing that the signal needs for propagates from one representative source to the other parts of the network. The colors of the lines presented in the figure indicate how long it takes the wave-front of the burst to reach the different electrodes. It is noticeable that the propagation is continuous and fast. The signal starts from the source and reaches immediately the electrode that are closer. Then, in a continuous way, the wave-front of the signal arrives to the distant sites.

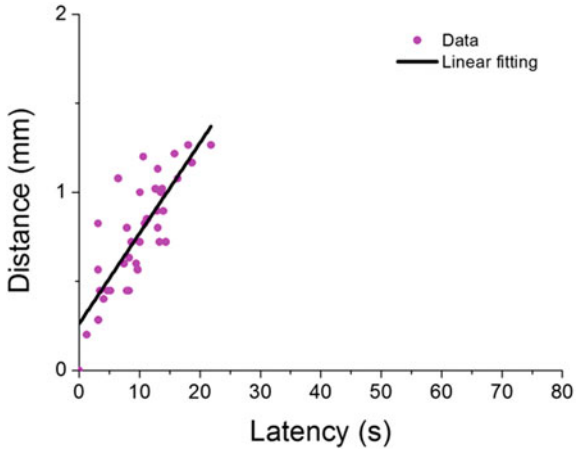

Fig. 5.33 Distance-latency correlation

In this case there is a clear (i.e. linear) correlation between latency and distance. As reported in Fig. 5.33, the wave-front of the signal arrives immediately at the sites that are close to the initiation site, than (after among 20 ms) it reaches the more distant sites. The speed of the propagation of the signal is of about 50 mm/s (RMSE = 0.18), value that is comparable with previous results (Bonifazi et al. 2005; Pasquale et al. 2008).

Regarding 3D neuronal network, the propagation of the signal is discontinuous and long. Figure 5.34 represents the timing that the signal needs for propagates from one representative source to the other parts of the network. By looking at this plot it is clear that the propagation is discontinuous. The signal starts from the source and reaches in a random way other parts of the network.

The propagation of the signal is long: it is possible to observe latencies of among 50 ms. In the case of 3D neuronal network there is a random relationship between latency and distance (see Fig. 5.35): the signal that starts from one site could perform the same distance both in a very fast way and with high latency. Because of the not clear latency-correlation ratio, it is not possible to evaluate the speed of the signal propagation.

By comparing the timing that 2D and 3D neuronal networks need to perform the same distance (i.e. 1 mm) it is possible to observe that in the 3D network the latency is longer (i.e. 10 ms for 2D neuronal network and 40 ms for 3D network). It is because of the variability in the connectivity pathway that are present in the 3D structure: the signal can pass through possible paths going up and down to the 3D micro-bead layers.

The previous results evaluated taking into account a single representative experiment, were further globally quantified by evaluating the latency-distance ratio in

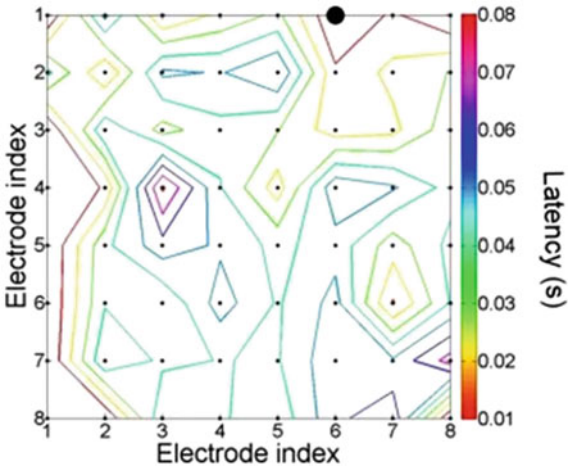

Fig. 5.34 Timing that the signal needs for propagating from one source to the other parts of the 3D neuronal network. The source is indicated with a *bold point* (electrode 16). The latency spans from 10 to 80 ms

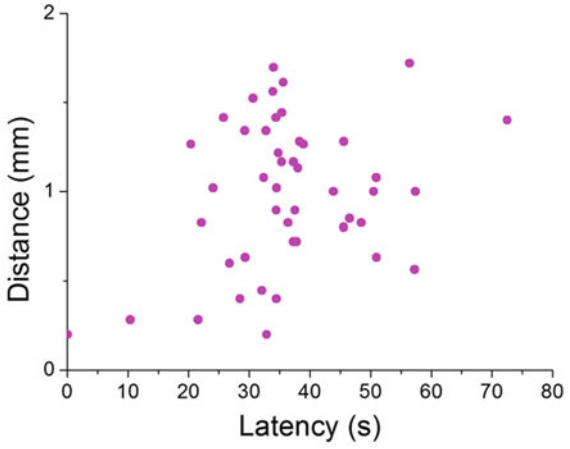

Fig. 5.35 Distance-latency correlation

different recordings. In Fig. 5.36 the latency-distance values for 2D and 3D neuronal networks are reported.

By looking at the graph relative at the 2D neuronal network (Fig. 5.36a), it is possible to observe that for each experiment the maximum value of latency is of about 20 ms: there is a fast propagation of the signal. Furthermore, a linear correlation between latency and distance is maintained. The linear fittings for each experiment are reported with lines with different colours in the inset of the figure. It is possible

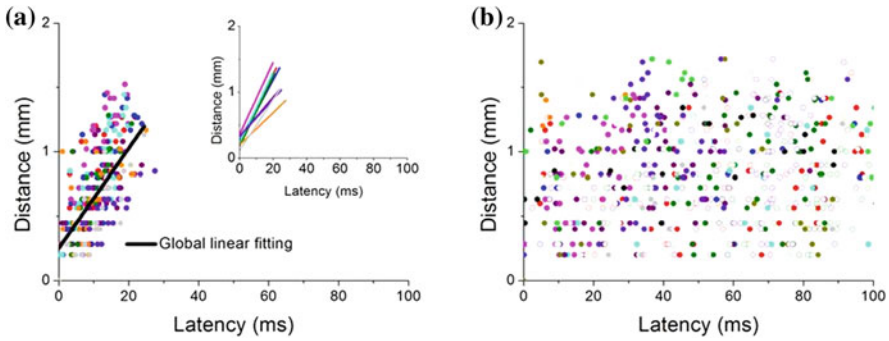

Fig. 5.36 Distance-latency correlation evaluated for 9 experiments of 2D and 3D neuronal network activity recordings. **a** Distance-latency ratio of 2D neuronal networks. Each colour represents an experiment. The *black line* indicates the global fitting of the data. Within the inset the fittings of all the experiments are reported. **b** Distance-latency ratio of 3D neuronal networks. Each experiment is represented by a *colour*. Because of the non-linear relationship between latency and distance it is not possible to fit the data

to evaluate a global fitting (RMSE = 0.17), that is shown with a black line in Fig. 5.36a. The speed of the propagation computed for all the experiment is of 42 ± 3.5 mm/s, value that is comparable with previous works (Streit et al. 2001; Tscherter et al. 2001; Bonifazi et al. 2005; Pasquale et al. 2008).

Regarding 3D neuronal network, by looking at the graph reported in Fig. 5.36b, it is possible to observe that latency values are higher than the ones detected for the 2D neuronal network. In this case there are values of latency close to 100 ms: the 3D neuronal signal propagation is lower than the 2D one. Moreover, there is a non-linear relationship between latency and distance which does not allow to estimate the signal propagation speed.

5.3.1.4 Controls Systems

To prove that enhanced activity was due to the developed 3D architecture, I compared the expressed 3D dynamics with the activity of the two additional controls.

The first control system (Control 1) was realized to verify whether the electrical activity generated only by 3D networks assembled onto the micro-beads were possibly captured by the substrate MEA. In this configuration the neurons are not directly coupled to the microelectrodes: the network is constructed over the beads and 2D neuronal network is not coupled to the device (Fig. 5.37a).

The second control (Control 2) is constituted by high density 2D neuronal networks plated onto MEAs assembled (2D neuronal network) with around 5–8 layers (i.e. without neurons) of bare micro-beads on top (Fig. 5.37b). This configuration is required to verify whether electrophysiological activity of 2D network is affected by the presence of a micro-bead stack on top of the cell culture.

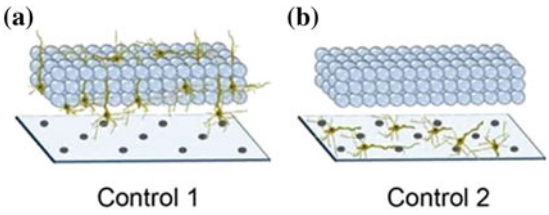

Fig. 5.37 Experimental configurations. **a** Control 1: network constructed among beads plated on MEA. **b** Control 2: 2D network plated onto MEA with bare beads on top

The electrophysiological activity of Control 1 (N = 5) and Control 2 (N = 5) was recorded and analyzed.

In the case of Control 1, almost no activity was recorded. By looking at the raster plot representing the electrophysiological activity of a representative experiment of Control 1 (Fig. 5.38a) it is possible to see that only few spikes are detected from the MEA electrodes. This fact indicates that to ensure a good communication between the substrate embedded micro-electrodes and the 3D assembly the 2D neuronal network is needed.

In the case of Control 2, the electrophysiological activity was, as expected, not distinguishable from the 2D neuronal network. The raster plot reported in Fig. 5.38b shows 300 s of spontaneous activity for a representative experiment related to Control 2. By looking at this plot it is possible to observe a good network activity with the presence of network bursts.

To understand if the electrophysiological activity of Control 2 is different from the one exhibited from 2D neuronal network, I evaluated the Percentage of Random Spikes, the Network Burst Duration and the C(0) values for all the performed experiments.

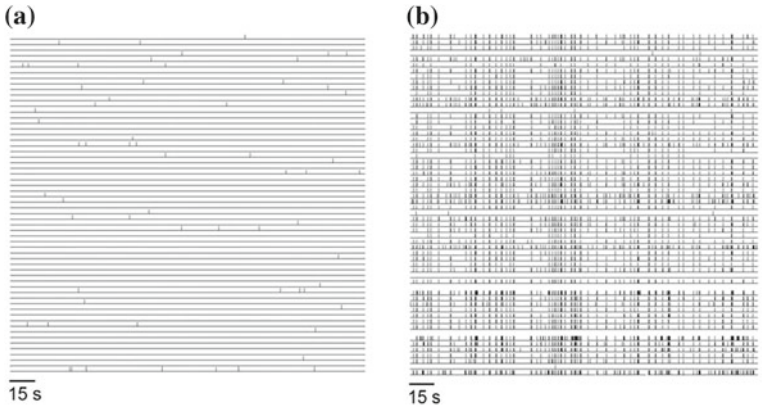

Fig. 5.38 **a** Raster plot showing 300 s of spontaneous activity for a representative experiment related to Control 1: 3D networks coupled to MEA not plated with a 2D network (bare MEA). **b** Raster plots showing 300 s of spontaneous activity for a representative experiment related to Control 2: 2D network covered with 5–8 layers of bare micro-beads

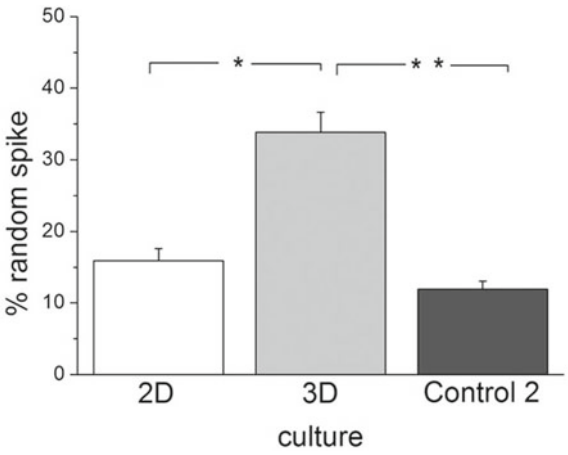

Fig. 5.39 Percentage of random spikes evaluated over the entire dataset of 2D (*white*), 3D (*gray*) and Control 2 (*dark gray*) networks. *Asterisks* above the plot indicate significant differences, (*) P-value = 10^{-4} and (**) P-value = 8×10^{-5}, Mann-Whitney U-test

As already shown, 2D neuronal networks exhibit a synchronized and distributed bursting activity. During this stage of development the percentage of random spike is very low. 3D neuronal networks, instead, exhibit a wide range of activity patterns, with the presence of both network burst and random spike regions. In this case the random spike activity level is high.

Control 2 exhibit a spontaneous activity similar to the one observed in 2D networks. The level of random spiking activity is low. By looking at Fig. 5.39, we can observe that Control 2 exhibit a percentage of random spike level that is statistically different from the 3D network one; this level is not statistically different from the 2D network one.

Even if network bursting remains a common signature for both preparations, the shift from 2D to 3D does also affect the bursting behavior. The main effects are observed both in frequency and duration. As it is already shown, 2D neuronal network exhibits burst with a short duration while 3D network exhibits burst longer and with a more variable duration.

Control 2 exhibits network burst with short duration. The mean value is statistically different from the 3D neuronal network one but it is not statistically different from the 2D network one (see Fig. 5.40).

As already shown, another difference between 2D and 3D neuronal network activity is the synchronization level. 2D neuronal network exhibit a high synchronization level with C(0) values close to one. In the case of 3D neuronal network there is a high level of synchronization during the network burst activity region and a very low level of synchronization within the random spike activity region.

By looking at Fig. 5.41, it is clear that Control 2 exhibit a very high synchronization level. The mean value is statistically different from the ones evaluated from 3D neuronal network. It is not statistically different from the C(0) value evaluated for 2D neuronal networks.

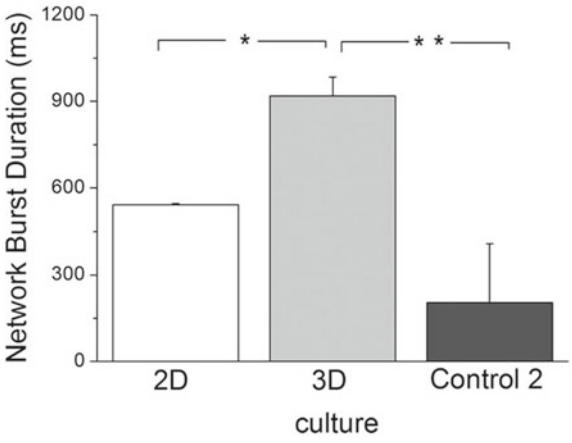

Fig. 5.40 Network Burst Duration evaluated over the entire dataset of 2D (*white*), 3D (*gray*) and Control 2 (*dark gray*) networks. *Asterisks* above the plot indicate significant differences, (*) P-value = 9×10^{-4} and (**) P-value = 3×10^{-6}, Mann-Whitney U-test

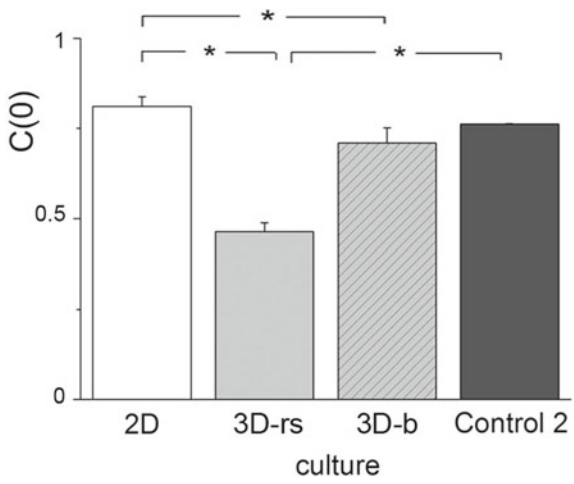

Fig. 5.41 C(0) values evaluated over the entire dataset of 2D networks (white), 3D network within the random spike activity region (*gray*) and within the burst activity region (*striped gray*), Control 2 (*dark gray*). *Asterisk* above the plot indicate significant difference, P-value < 10^{-6}, Mann-Whitney U-test

These results clearly indicate that the presence of a 3D network organization enhances the electrical activity by inducing partly synchronized sub-populations and breaking down (Leondopulos et al. 2013) the uniform and stereotyped behavior of standard high density 2D neuronal networks.

5.3.2 Stimulus-Evoked Activity

By using immunofluorescence imaging techniques we characterized the developed 3D assemblies constituted, on average, by 5–8 layers with a cell density of 80,000 cells/mm^3 and clear structural connections among neurons belonging to

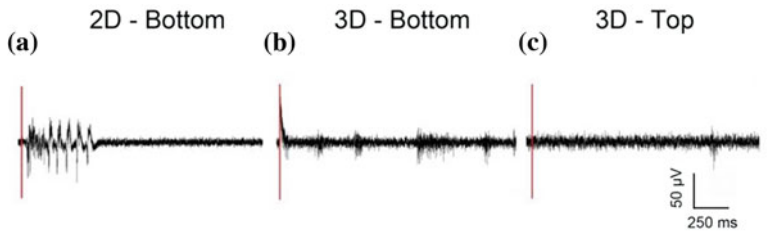

Fig. 5.42 Raw data showing the response of a sample electrode to stimulation (*red bar*) in case of: **a** 2D neuronal network and **b** 3D neuronal network stimulated from the *bottom layer*; **c** 3D neuronal network stimulated from the *top layer*

different layers. The spontaneous activity showed by such 3D networks supports the hypothesis that the interconnections are functional, thus determining a new 3D topological connectivity with a completely different electrophysiological dynamic behavior.

To further support the previously presented results and to demonstrate whether the layers are clearly functionally connected (i.e., synaptic pathways cross the assembly in all the direction of the 3D space), I performed experiments by delivering electrical stimulation with two different experimental protocols-settings.

I stimulated from the bottom layer 3D (N = 15) and 2D (N = 7) cultures by using one of the electrodes of the substrate MEA; I performed top-layer stimulation on 3D cultures (N = 3) by means of a bi-polar tungsten electrode. The experimental configuration is illustrated in Fig. 5.5.

In order to have a qualitative idea of the network response to stimulation, we can observe a single channel raw data (Fig. 5.42). The red bar depicted in the plot represents the stimulation.

Regarding 2D neuronal network stimulated from the bottom layer, the response to the stimulation is very fast. By looking at the raw data in Fig. 5.42a we can observe that the network response appears immediately after the stimulation.

3D neuronal network stimulated from the bottom layer exhibits different type of responses. By looking at the raw data shown in Fig. 5.42b we can observe both fast responses and delayed responses.

3D neuronal network stimulated from the top layer exhibit a delayed response. By looking at the raw data presented in Fig. 5.42c, we can observe a network response after 1 s.

In order to study the different evoked activities that the network exhibits in response to the applied stimulation, the Post Time Stimulus Histogram (PSTH) is evaluated (cf. Appendix A.4). Then, to examine the network response characteristics to the delivered stimulation, I evaluated the time in which the 60 % of the PSTH area occurs (t_{60}).

The 2D neuronal network response to the stimulation delivered from the bottom layer (i.e. one MEA electrode, indicated with the black cross) is shown in Fig. 5.43. The PSTH profile is depicted over a 4×4 grid, representing a subset of channels of

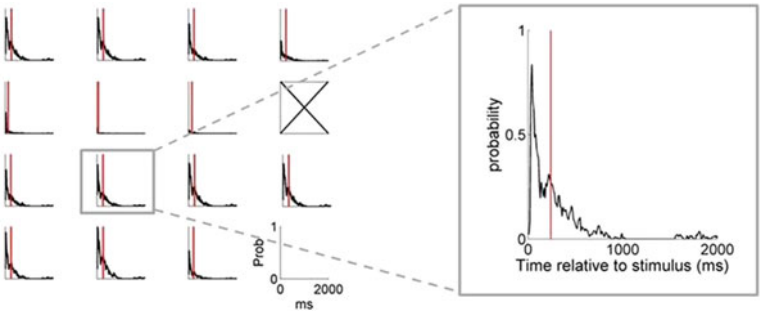

Fig. 5.43 2D neuronal network response to electrical stimulation and single channel PSTH profile. The PSTH profiles are depicted over a 4 × 4 grid, representing a subset of the most responsive electrodes of the MEA. The *red vertical bar* indicates the time instant in which the 60 % of the PSTH area occurs. The crossed cell indicates the electrode from which the stimulus is delivered

the 8 × 8 MEA layout. The vertical red bars reported in the figure indicate the t_{60} value.

In 2D network the neuronal response to the stimulation delivered by the bottom layer (2D-Bottom) is, as expected (Chiappalone et al. 2008) similar for all the responding channels. By looking at a single channel zoom, it is clear that the highest response probability is detected immediately after the stimulation; than the profile exhibits a decreasing trend. By observing the position of the red bar (i.e., t_{60}), a strong confinement of the network response in the first hundreds of milliseconds can be identified. This is the typical network behavior found in 2D neuronal cultures under electrical stimulation (Jimbo et al. 1999; Kermany et al. 2010; Leondopulos et al. 2013).

In order to prove the fact that the network is highly connected, I evaluated the network response to stimulation delivered by different electrodes. 2D neuronal network response to electrical stimulation delivered from three MEA electrodes is shown in Fig. 5.44. Figure 5.44a presents the PSTH profiles for all the recording electrodes; the profiles are reported in a 8 × 8 maps showing the physical position of the electrodes. The red profiles indicate the network response to the stimulation delivered from the electrode 46 (i.e. el 1); the black profiles indicate the network response to the stimulation delivered from the electrode 28 (i.e. el 2); the blue PSTH profiles indicate the response to the stimulation delivered from the electrode 51 (i.e. el 3). By looking at this figure it is clear that 2D interconnected hippocampal networks stimulated by different electrodes show a relatively fast and synchronized response depending on the stimulating site. The site of stimulation causes an almost uniform response (for the high-connectivity of the network) in all the active sites. The response time is relatively fast and confined below the first 250 ms. In Fig. 5.44b a 2D neuronal network response to single channel stimulation is reported. PSTH profiles of all the channels are depicted in gray and the mean PSTH profile is shown in red, dark and blue (stimulation delivered from electrode 1, 2 and 3 respectively). The PSTH profiles depicted in gray are similar,

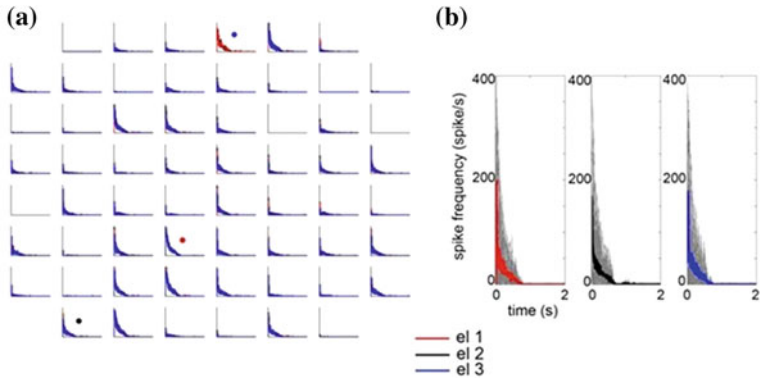

Fig. 5.44 2D neuronal network response to electrical stimulation delivered from 3 MEA electrodes. *Red*, *dark* and *blue lines* represent the response to the stimulation delivered from three different electrodes of the MEA. The *red*, *dark* and *blue points* depicted in the PSTH 8 × 8 maps show the position of the stimulating electrodes. **a** 2D neuronal network PSTH profiles represented over a 8 × 8 grid. **b** 2D neuronal network response to single channel stimulation. PSTH profiles of all the channels are depicted in *gray* and the mean PSTH profile is shown in *red, dark* and *blue* (stimulation delivered from electrode 1, 2 and 3 respectively)

indicating the uniform network response to the stimulation. By comparing the mean PSTH profiles it is possible to see that the network response to the stimulation delivered from different electrodes is similar. This results indicates that 2D neuronal network is highly connected.

The PSTH profile of the 3D neuronal network response to the stimulation delivered from the bottom layer is depicted over a 4 × 4 grid, representing a subset of channels of the 8 × 8 MEA layout (Fig. 5.45). The vertical red bars reported in the figure indicate the t_{60} value.

In the case of 3D neuronal networks stimulated through the MEA, PSTH profiles present a more pronounced variability. By looking the subset of PSTH profiles shown in Fig. 5.45, it is clear that some electrodes display a large response immediately after the stimulation. In other cases the response peak is up to 1 s after the stimulation. The single channel PSTH profile indicates the 60 % of response is within the first 700 ms. These results prove by themselves that additional synaptic pathways are involved and elicited when stimulating from the bottom layer (MEA substrate) and that possible reverberating paths going up and down to the 3D micro-bead layers contribute to the observed delayed responses.

In order study if the network is highly connected, I evaluated the network response to stimulation delivered by different electrodes. 3D neuronal network response to electrical stimulation delivered from three MEA electrodes is shown in Fig. 5.46a. In this figure PSTH profiles for all the recording electrodes are depicted on a 8 × 8 map showing the physical position of the electrodes. The red profiles indicate the network response to the stimulation delivered from the electrode 55 (i.e. el 1); the black profiles indicate the network response to the stimulation delivered from the

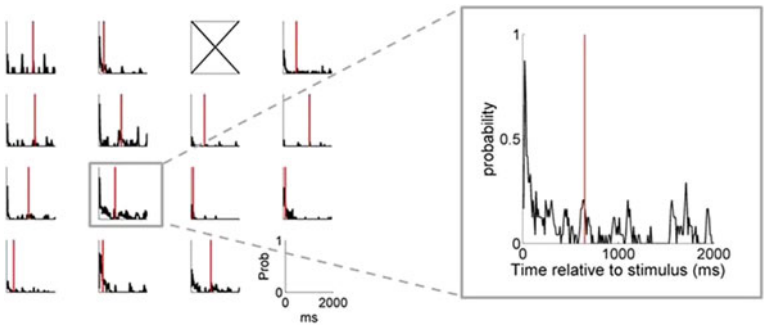

Fig. 5.45 3D neuronal network response to the stimulation delivered by the bottom layer and single channel PSTH profile. The PSTH profiles are depicted over a 4 × 4 grid, representing a subset of the most responsive electrodes of the MEA. The *red vertical bar* indicates the time instant in which the 60 % of the PSTH area occurs. The crossed cell indicates the electrode from which the stimulus is delivered

electrode 47 (i.e. el 2); the blue PSTH profile indicates the response to the stimulation delivered from the electrode 63 (i.e. el 3). By looking at this figure it is clear that 3D networks stimulated from the bottom layer exhibit various types of synchronized response often generating a uniformly distributed response delay. In Fig. 5.46b a 3D neuronal network response to single channel stimulation is reported. PSTH profiles of all the channels are depicted in gray and the mean PSTH profile is shown in red, dark and blue (stimulation delivered from electrode 1, 2 and 3 respectively). The PSTH profiles depicted in gray are different, indicating the that the response of the network is more variable. By comparing the mean PSTH profiles it is possible to see that the response of the network is generated with an uniformly distributed delay.

The last analyzed case is the 3D neuronal network response to stimulation delivered by the top layer (Fig. 5.47). The PSTH profiles are depicted over a 4 × 4 grid, representing a subset of channels of the 8 × 8 MEA layout. The vertical red bars reported in Fig. 5.47 indicate the t_{60} value.

As it might be expected, in this configuration not many channels (less than 50 %) detect the neuronal responses, suggesting that the recruitment of many neurons on the read-out layer is prevented by the combined action of this kind of stimulation (less coupling with neurons) together with the hypothesis that a reduced number of synaptic pathways reach the bottom layer. However, for the responsive channels, the evoked activity is quite different from the previous ones. The t_{60} (i.e., red bars) spans over a wide time window and electrodes exhibit a t_{60} value exceeding 1 s.

To prove that the top stimulation propagates downward to the MEA layer only thanks to the axonal and/or dendritic excitation, I performed experiments in which the synaptic transmission has been blocked by introducing in the culture medium a cocktail made up of BIC, APV and CNQX (25, 50 and 50 μM respectively).

In Fig. 5.48 a raster plot showing the stimulus-evoked activity of an hippocampal network before and after the synaptic blockade is reported. By looking at the raster

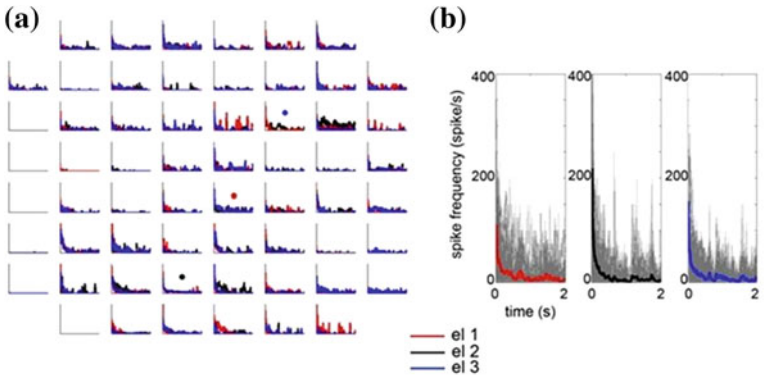

Fig. 5.46 3D neuronal network response to electrical stimulation delivered from 3 MEA electrodes. *Red*, *dark* and *blue lines* represent the response to the stimulation delivered from three different electrodes of the MEA. The *red*, *dark* and *blue points* depicted in the PSTH 8 × 8 maps show the position of the stimulating electrodes. **a** 3D neuronal network PSTH profiles represented over a 8 × 8 grid. **b** 3D neuronal network response to single channel stimulation. PSTH profiles of all the channels are depicted in gray and the mean PSTH profile is shown in *red*, *dark* and *blue* (stimulation delivered from electrode 1, 2 and 3 respectively)

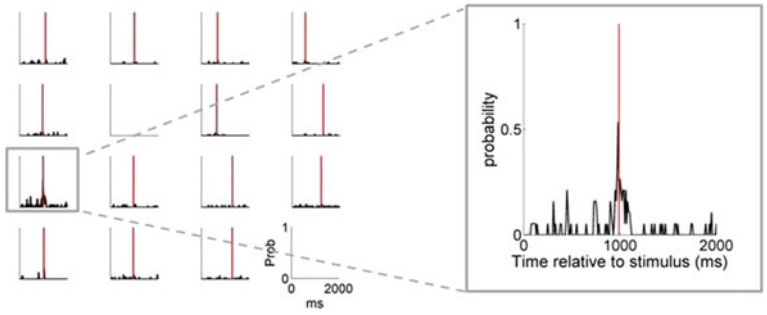

Fig. 5.47 3D neuronal network response to the stimulation delivered by the top layer and single channel PSTH profile. The PSTH profiles are depicted over a 4 × 4 grid, representing a subset of the most responsive electrodes of the MEA. The *red vertical bar* indicates the time instant in which the 60 % of the PSTH area occurs

plot relative the network stimulus-evoked activity before the synaptic blockade (Fig. 5.48a), it is possible to observe that the top layer stimulation generates a response of the network. This is a prove of the fact that the network is functionally connected. After the synaptic blockade, no network response to the stimulation can be detected (Fig. 5.48b).

To study the evoked activities that the network exhibits in response to the applied stimulation, the PSTH is evaluated.

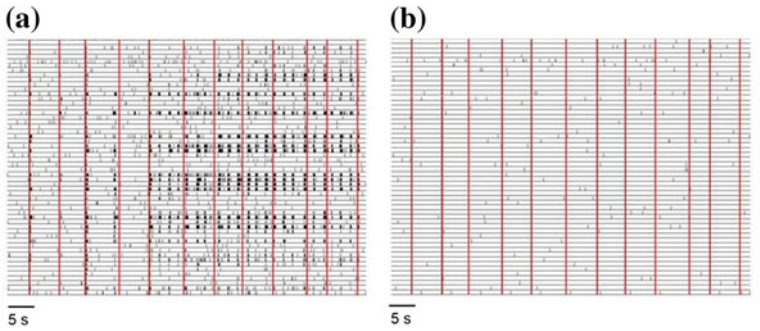

Fig. 5.48 Raster plot showing 4 min of stimulus-evoked activity of an hippocampal neuronal network (24 DIV) when the stimulation (*red lines*) is delivered from the top layer. **a** Stimulus-evoked activity before the synaptic transmission blockade. **b** Stimulus-evoked activity after the synaptic transmission blockade

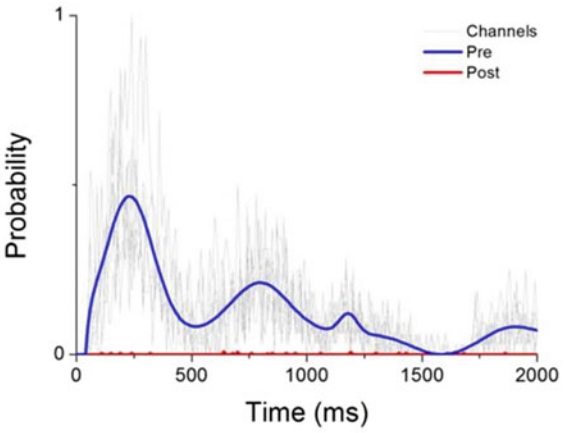

Fig. 5.49 PSTH showing the response to the top layer stimulation. The *gray lines* are the PSTH profiles of the responsive channel before the synaptic blockade. The *blue line* is the average PSTH profile before the synaptic blockade. The *red line* shows the average PSTH profile after the synaptic blockade

In Fig. 5.49 the PSTH profiles of the responsive channels to the top layer stimulation are reported (gray lines). As it might be expected, in this configuration less than 50 % of the electrodes detect the neuronal responses. However, for the responsive channels, we can observe that the network response spans from 200 ms to 2 s. The average of the PSTH profile of the responsive channel before and after the synaptic blockade is reported (blue and red lines respectively). By looking at the red line, it is clear that if the transmission is pharmacologically blocked no neuronal network response can be detected.

What I found is that no direct evoked activity is (on average) elicited in the bottom layer, meaning that direct connections from top layer to the surface of our MEA are unlikely.

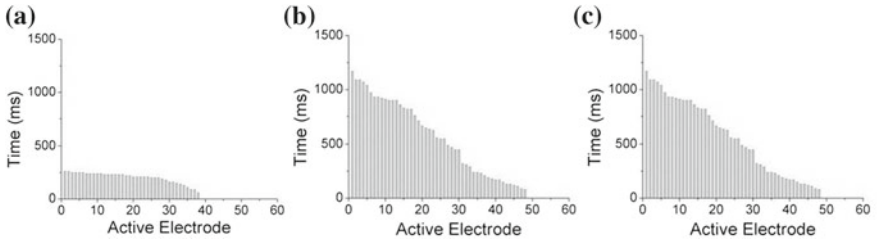

Fig. 5.50 Time instants in which the 60 % of the PSTH area occurs for all the recording channels in case of **a** 2D neuronal network stimulated from the *bottom layer*; **b** 3D neuronal network stimulated from the *bottom layer*; **c** 3D neuronal network stimulated from the *top layer*

To quantify and compare the neuronal network responses to electrical stimulation, I plotted the t_{60} values for all the recording channels of a representative experiment.

Figure 5.50a represents the time that the 2D neuronal network needs to generate 60 % of the response when it is stimulated from the bottom layer. This value is reported for all the active channels. In the case of 2D neuronal networks stimulated from the bottom layer, the responses appear close to the stimulation time: for the majority of the channels the 60 % of the PSTH area is detected within the first 250 ms with an almost uniform distribution.

Regarding the 3D neuronal networks stimulated from the bottom layer, there is a high variability of time values and a complex evoked activity: neuronal responses appear both immediately after the stimulation time but also after few hundreds of milliseconds. Time values of the t_{60} distribute within an interval that spans from 100 ms up to 1200 ms (see Fig. 5.50b).

Finally, in the case of 3D neuronal network stimulated from the top layer, the response to stimulation is very much delayed as the recorded evoked responses are related to neurons on the MEA substrate and to reach the bottom layer they might involve few-several neurons and synaptic connections. Time values distribute in an interval that ranges from 500 to 1400 ms (Fig. 5.50c). The cut-off value observed around 500 ms might indicate that only poly-synaptic pathways reach the substrate MEA and no direct functional connections cross this culture in the z-direction.

I present also the averaged results of all the performed measurements (Fig. 5.51). The electrophysiological specificity of 3D networks is further demonstrated by the analysis and comparison, in all the performed experiments, of the t_{60} and t_{90} (time that is necessary to generate 90 % of response to stimulation). Time values are reported for 2D and 3D networks stimulated from the bottom layer (P-value $= 9 \times 10^{-4}$, Mann-Whitney U-test) and for 3D network stimulated from the top layer (P-value $= 2 \times 10^{-4}$, Mann-Whitney U-test).

2D neuronal networks display a reliable response time (also qualitatively found in previous works (Jimbo et al. 1999; Chiappalone et al. 2008; Kermany et al. 2010) in which the 60 % of the PSTH area occurs (200 ± 5 ms). The values detected for the 3D neuronal networks are higher and more variable. In the case of the bottom layer stimulation t_{60} value is 680 ± 28 ms, while in the case of the top layer stimu-

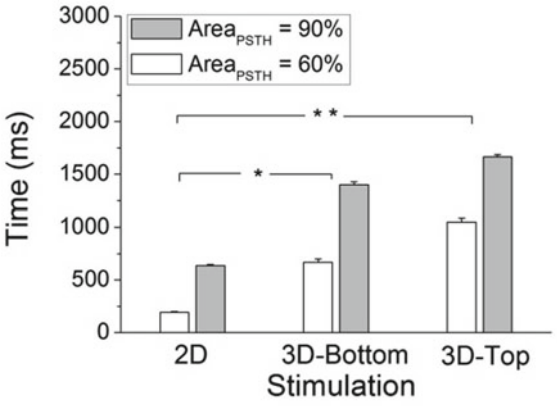

Fig. 5.51 Time occurring to generate 60 and 90 % of response to stimulation for 2D and 3D networks. *Asterisks* above the plot indicate significant differences, (*) P-value = 9×10^{-4} and (**) P-value = 2×10^{-4}, Mann-Whitney U-test

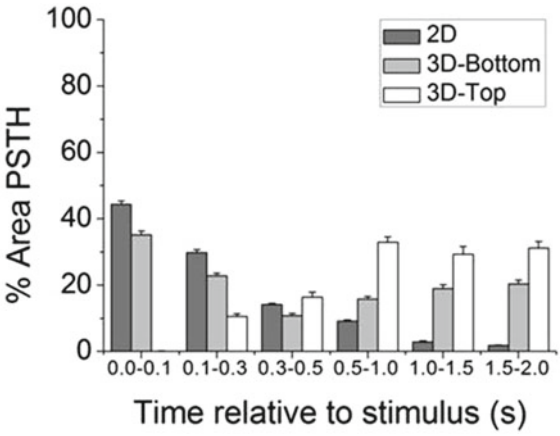

Fig. 5.52 Percentage of PSTH area values evaluated within different temporal windows

lation t_{60} shifts to 1050 ± 38 ms. The time that networks need to generate 90 % of the total response to stimulation (t_{90}) is obviously higher than such time values, but it follows the same trend.

Finally, I evaluated the percentage of PSTH area generated after electrical stimulation in different time windows to quantify the different response modes of the networks.

By looking at the dark gray bars in Fig. 5.52, it is clear that the response to stimulation of 2D networks is very fast: among 90 % of the PSTH area is reached within the first 500 ms.

3D neuronal networks stimulated from the bottom layer exhibit a similar response to stimulation within all the time windows: by looking at the light gray bars, we can observe both a fast response (35 % of PSTH area reached within the first 100 ms) and also a slow response (among 30 % of the response to stimulation is detected between 1 and 2 s). This result is really interesting because it proves that the 3D

neuronal network is effectively connected. In general the evoked activity can be thought as the combination of two types of response. The first type is fast: it is generated by subsets of neurons in the 2D layer that are connected with subgroups of neurons in the same layer. The second type of response is delayed: it is generated by subset of neurons in the 2D layer connected with sub-networks of neurons in the upper layers.

In the case of 3D networks stimulated from the top layer, I am able to detect a response of the network. This is a prove of the fact that the network is functionally connected. In this case the fast response is not detected (no response is detected in the first 100 ms, only about 10 % of PSTH area is within the first 300 ms) suggesting that no direct pathways are present. The responses generated from this type of stimulation are slow: by looking at the white bars we can observe that about 90 % of PSTH area is reached between 500 ms and 2 s. The fact that the response is delayed means that the signal has to pass through all the different layers before reaching the MEA electrodes level.

5.3.3 Chemical Modulation

By using immunofluorescence imaging techniques I characterized the developed 3D assemblies and I showed clear structural connections among neurons belonging to different layers. The spontaneous activity exhibited by such 3D networks supports the hypothesis that the interconnections are functional, thus determining a new 3D topological connectivity with a completely different electrophysiological dynamic behavior. The stimulus-evoked activity showed by the 3D neuronal networks stimulated from the bottom and the top layers demonstrate that the layers are clearly functionally connected (i.e., synaptic pathways cross the assembly in all the direction of the 3D space).

To further support the previous reported results, it is important to study the balance between excitatory and inhibitory neurons. Even if both the spontaneous and the stimulus-evoked dynamics are very different, by an imaging characterization (cf. Fig. 5.13) I found that the proportion between GABAergic and glutammatergic populations is likely to remain similar in both 2D and 3D models (with about a 1:5 ratio) (Marom and Shahaf 2002; Bonifazi et al. 2005).

In order to characterize how the excitatory and inhibitory neurons balance may affect the 2D and 3D neuronal networks driving activity, I performed experiments with chemical modulation. In these experiments the $GABA_A$ receptors were blocked by introducing in the culture medium 25 μM of Bicuculline (BIC). BIC is a competitive antagonist of the $GABA_A$ receptors: it blocks the inhibitory action of $GABA_A$ receptors, generating an increment of the network activity (i.e. epileptic dynamic). By using this compound, it is possible to compare the excitatory contribute on the ongoing activity of 2D and 3D neuronal networks.

Spontaneous and chemical modulated activities of 2D (N = 3) and 3D (N = 3) neuronal networks were recorded after 4 weeks in culture by means of TiN 60 chan-

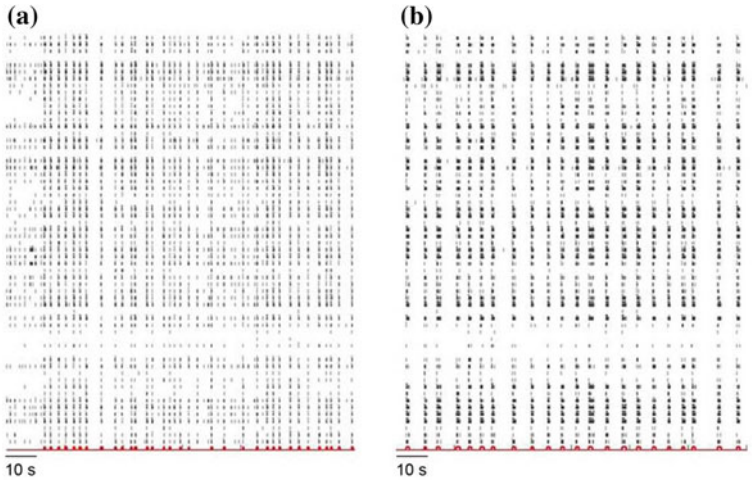

Fig. 5.53 Electrophysiological activity for a representative 2D network recorded from 60 MEA channels. **a** Raster plot showing 3 min of spontaneous activity. **b** Raster plot showing 3 min of activity modulated by BIC (concentration of 25 μM)

nels MEAs. The activities of 2D and 3D neuronal networks were analyzed and compared.

Figure 5.53a shows a raster plot of the spontaneous activity of a representative experiment performed on a 2D hippocampal culture during the fourth week in vitro. Thanks to this plot it is possible to observe the electrophysiological activity of the network recorded from all the electrodes during 3 min. As anticipated, we can observe the quasi-synchronous activity and network dynamics composed mainly of network bursts (indicated with the red line). Few random spiking activity is present.

In order to block the $GABA_A$ receptors, I applied BIC at a concentration of 25 μM. The raster plot reported in Fig. 5.53b shows the chemically modulated activity of the 2D neuronal network. It is possible to observe that the compound induce a significant change in the network activity: as expected, the introduction of BIC generates an "epileptic" network activity. BIC induced a significant increase in the network synchronization. Moreover, the random spiking activity and the burst and network burst duration increase.

3D neuronal networks exhibit a dynamic that presents a wide repertoire of activities with few global synchrony and pronounced spiking at a single channel-neuron level. 3D neuronal network exhibits both network bursting and a significant 'random spiking' and non-synchronous bursting activity. Figure 5.54a shows a raster plot of the spontaneous activity of a representative experiment performed on a 3D hippocampal neuronal network during the fourth *week* in vitro. It is possible to observe the electrophysiological activity of the network recorded from all the electrodes during 3 min. As anticipated, we can observe the presence of few network burst, an high percentage of random spiking and a low network activity synchronization.

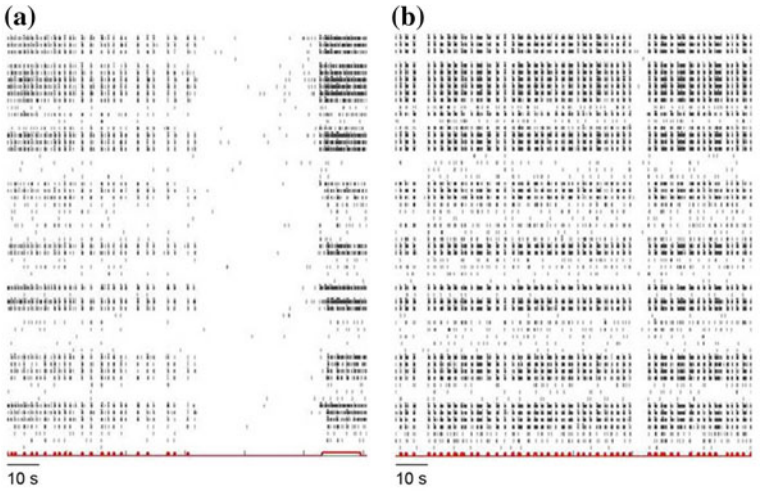

Fig. 5.54 Electrophysiological activity for a representative 3D network recorded from 60 MEA channels. **a** Raster plot showing 3 min of spontaneous activity. **b** Raster plot showing 3 min of activity modulated by BIC (concentration of 25 μM)

The raster plot reported in Fig. 5.54b shows the chemically modulated activity of the 3D neuronal network. 3D neuronal network is treated with BIC at the concentration of 25 μM. As in the case of 2D neuronal network, the compound induce a significant change in the network activity. The introduction of BIC induced a significant increase in the network synchronization and the random spiking activity decreases. There is an increment of the number of burst and network burst and the burst and network burst duration decrease.

The previous observations were further globally quantified by evaluating how the spiking activity is modulated by the introduction of the compound. In Fig. 5.55 the Percentage of Random Spike evaluated in all the performed experiments is shown. As reported above, in normal condition 2D neuronal network exhibits a very low random spiking activity (22.3 ± 2.6 %). When the network is treated with BIC, the activity of the network increases, generating also an increment of the random spiking activity (36.5 ± 2.7 %). 3D neuronal network, instead, exhibit an high value of random spiking activity during the spontaneous phase (43.2 ± 1.6 %). After the introduction of BIC, the activity of the network became more synchronized: the random spiking activity decreases (35.6 ± 1.9 %). It is interesting to observe that BIC generates a similar 2D and 3D neuronal networks spiking activity.

By looking at the raster plots reported in Figs. 5.53 and 5.54 we observe that BIC induces a change also in the bursting behavior at the single channel level. In order to support this result, the Mean Bursting Rate and the Burst Duration are evaluated for the entire dataset.

Figure 5.56a shows the Mean Bursting Rate values for 2D and 3D neuronal networks during both spontaneous and chemically modulated activities. At single

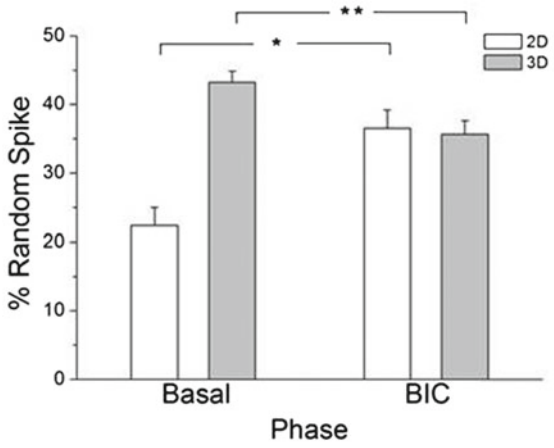

Fig. 5.55 Percentage of Random Spike evaluated over the entire dataset (N = 3). The percentage of random spike values are reported for the spontaneous activity and for the chemically modulated phases (Basal and BIC respectively). The *white bars* indicates the 2D neuronal network while 3D neuronal networks are shown with the *gray bars*. *Asterisks* above the plot indicate significant differences, (*) P-value = 0.001 and (**) P-value = $1.7 \cdot 10^{-5}$, Mann-Whitney U-test

channel level, 3D and 2D neuronal networks exhibit a similar bursting activity (12.6 ± 1.2 burst/min and 12.1 ± 0.8 burst/min respectively). When BIC is introduced within the networks, the activity starts to increase and the new burst are generated. It is possible to observe an increment of the bursting activity both in 2D and 3D neuronal networks (19.2 ± 1.8 burst/min and 24.7 ± 3.8 burst/min respectively): the increment of the burst number is more visible in the 3D neuronal network.

In Fig. 5.56b the values of Burst Duration are reported. As for the Mean Bursting Rate, during the spontaneous activity the 2D and 3D neuronal networks Burst Duration is similar (171.1 ± 3.3 ms and 176.1 ± 4.3 ms respectively). During the BIC treatment, the Burst Duration starts to increase in the 2D neuronal network (274 ± 33.5 ms), while there is a little decrement of this value in the 3D one (141.5 ± 11.9 ms).

By looking at the raster plots of a 2D and 3D neuronal networks (Figs. 5.53 and 5.54 respectively) it is also possible to observe that, at single channel level, the timing between two consecutive burst is different. The bursting behavior exhibited by the 2D neuronal network is stereotyped; in the 3D neuronal network the bursting behavior is more variable.

In order to know how BIC affects the bursting behavior, the 2D and 3D neuronal networks Inter Burst Interval is evaluated over the entire dataset during the spontaneous activity and the chemically modulated phases. The 2D neuronal network IBI distribution during the spontaneous activity phase and during the BIC treatment (black and red bars respectively) are reported in Fig. 5.57a. The same plot for the 3D neuronal network is shown in Fig. 5.57b. By looking at these graphs it is possible

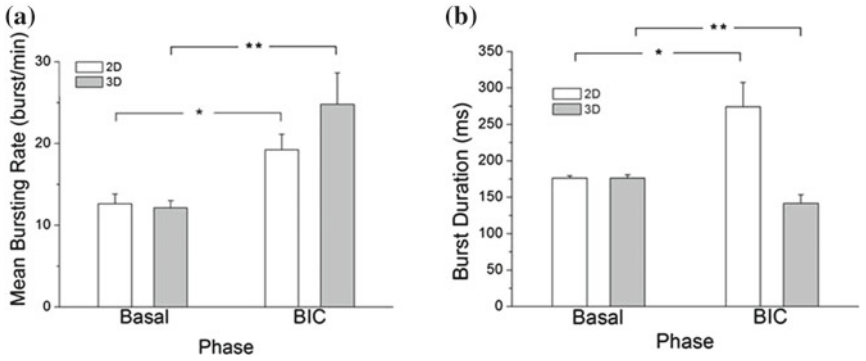

Fig. 5.56 **a** Mean Bursting Rate evaluated over the entire dataset (N = 3). *Asterisks* above the plot indicate significant differences. (*) P-value = 0.03 and (**) P-value = 0.01, Mann-Whitney U-test. **b** Mean Bursting Rate evaluated over the entire dataset (N = 3). *Asterisks* above the plot indicate significant differences, (*) P-value = 0.007 and (**) P-value = 0.004, Mann-Whitney U-test. Both the Mean bursting Rate and the Burst Duration values are reported for the spontaneous activity and for the chemically modulated phases (Basal and BIC respectively). The *white bars* indicates the 2D neuronal network while 3D neuronal networks are shown with the *gray bars*

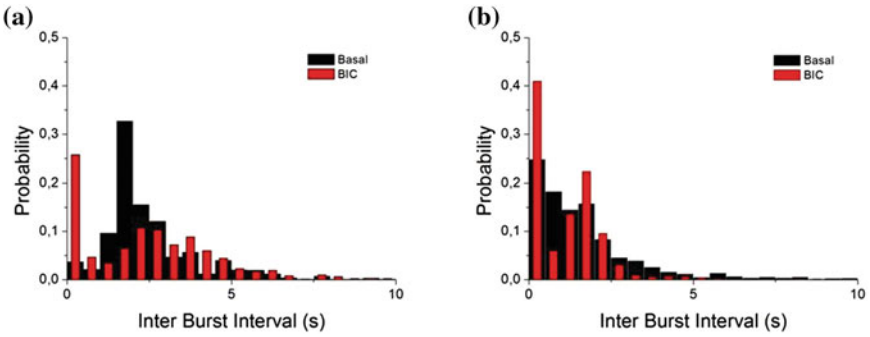

Fig. 5.57 Inter Burst Interval distribution during the spontaneous activity and the BIC treatment phases (*black* and *red bars* respectively). Bin size: 0.5 s. The IBI distribution is evaluated over the entire dataset (N = 3). **a** 2D neuronal network IBI distribution. **b** 3D neuronal network IBI distribution

to observe that the 2D and 3D neuronal networks IBI distributions are different. As already shown (cf. Fig. 5.19), during the spontaneous activity phase 2D neuronal network exhibits values of IBI that span from 1 to 5 s, with a maximum probability to detect burst within an interval of 2 s. In the case of 3D neuronal network the IBI value that is more probable to detect is 0.5 s.

When BIC is introduced in the network, the activity became more synchronized and, as it is shown before, the Mean Bursting Rate increases in both the preparations. Accordingly with these results, the probability to find values of IBI of 0.5 s increases.

2D neuronal network exhibits a maximum probability when the IBI is of about 0.5 s; the same behavior is visible in the 3D neuronal network. Moreover, both 2D and 3D neuronal network exhibit high probability values when the IBI is 2 s. BIC treatment seams to generate a similar 2D and 3D neuronal network IBI distribution.

The shift from 2D to 3D neuronal networks does affect the network bursting behavior. The main effects are observed both for in frequency and duration (cf. Fig. 5.20). 2D neuronal network exhibits an high number of network burst and the network burst duration seams similar for all the network burst detected. Regarding 3D neuronal network, instead, the number of network burst detected is low and the duration of the network burst is more variable: globally the network burst duration is higher than the one exhibited by the 2D neuronal network.

In order to quantify how BIC affect the network bursting behavior, the 2D and 3D neuronal networks Mean Network Bursting Rate and the Network Burst Duration are evaluated over the entire dataset (N = 3).

In Fig. 5.58a 2D and 3D Mean Network Bursting Rate values evaluated during both the spontaneous ant the chemically modulated activity phases are reported. Accordingly with the previous results, it is possible to observe that 2D neuronal network exhibits a high value of this parameter during the spontaneous activity phase (15.9 ± 1.3 network burst/min). In 3D neuronal network, instead, globally less network burst can be detected (6.6 ± 1.1 network burst/min). When the BIC is introduced, the number of network burst starts to decrease in the 2D preparation (14.1 ± 1.1 network burst/min) and increase in the 3D one (23.5 ± 1.2 network burst/min).

Regarding the duration of the network burst, the results are reported in Fig. 5.58b. During the spontaneous activity, the 2D neuronal Network Burst Duration is low

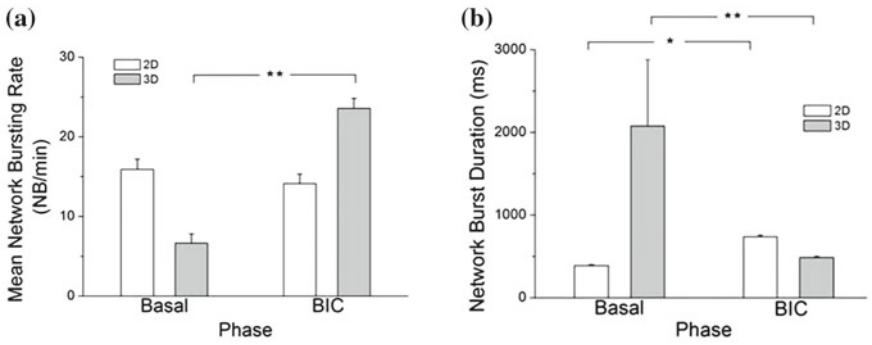

Fig. 5.58 **a** Mean Network Bursting Rate evaluated over the entire dataset (N = 3). *Asterisk* above the plot indicates significant differences. P-value = 0.009, Mann-Whitney U-test. **b** Network Burst Duration evaluated over the entire dataset (N = 3). *Asterisks* above the plot indicate significant differences, (*) P-value = 0.01 and (**) P-value = 0.02, Mann-Whitney U-test. Both the Mean Network Bursting Rate and the Network Burst Duration values are reported for the spontaneous activity and for the chemically modulated phases (Basal and BIC respectively). The *white bars* indicates the 2D neuronal network while 3D neuronal networks are shown with the *gray bars*

(388.3 ± 11.8 ms) and it is similar for all the network burst detected (i.e. very low standard error value). 3D neuronal network, instead, presents a high Network Burst Duration (2077.6 ± 804.1 ms): the duration of the network burst is more variable than the one detected for the 2D neuronal network (i.e. high standard error). When BIC is introduced, accordingly with the Mean Network Bursting Rate results, the Network Burst Duration starts to increase in the 2D neuronal network (738.7 ± 15.2 ms) while it decreases in the 3D preparation (486.7 ± 12.1 ms).

5.4 3D Cortical Neuronal Network Dynamic

In the previous chapters I presented a new experimental in vitro platform constituted by 3D neuronal cultures coupled to MEAs for network electrophysiology. During this thesis I mainly made use of hippocampal cultures. I constructed 3D hippocampal neuronal networks and I demonstrated that neurons belonging from different layers are functionally connected. The work presented in this thesis was mainly focused on the characterization of the activity of hippocampal neuronal networks. I carefully compared the spontaneous, evoked and chemically modulated electrophysiological activity in 3D hippocampal cultures with the traditional network dynamics from 2D cultures. I demonstrated that 3D hippocampal neuronal network coupled to MEA shows a wide range of activity patterns. These patterns are variable and present striking differences from the dynamics of standard density 2D neuronal cultures both during spontaneous and electrically stimulated activity.

To further support the previous results and to understand whether my experimental model really resembles the in vivo situation, I also constructed 3D neuronal network of cortical neurons. I compared the spontaneous electrophysiological activity of these networks with the dynamic exhibited by standard 2D cortical networks.

I recorded the spontaneous activities of 2D (N = 5) and 3D (N = 9) cortical neuronal networks after 4 weeks in culture by means of TiN 60 channels MEAs. The results about patterns of activity and correlation and synchronization levels are reported in what follows.

Similarly at the results about hippocampal neuronal networks (cf. Sect. 5.3.1.1), 2D cortical neuronal networks show a stereotyped electrophysiological activity in the mature phase of their development characterized by synchronous bursts involving most of the active channels in the MEA (Wagenaar et al. 2005; Gandolfo et al. 2010).

Figure 5.59 shows a raster plot of the spontaneous activity of a representative experiment performed on a 2D cortical culture during the fourth week in vitro. By looking at this plot it is possible to observe the electrophysiological activity of the network during 4 min of recording. As anticipated, the 2D cortical neuronal network spontaneous activity is mainly composed by network bursts (green box). There are synchronized events which involve most of the recording channels interspersed by period of time in which almost no activity is recorded.

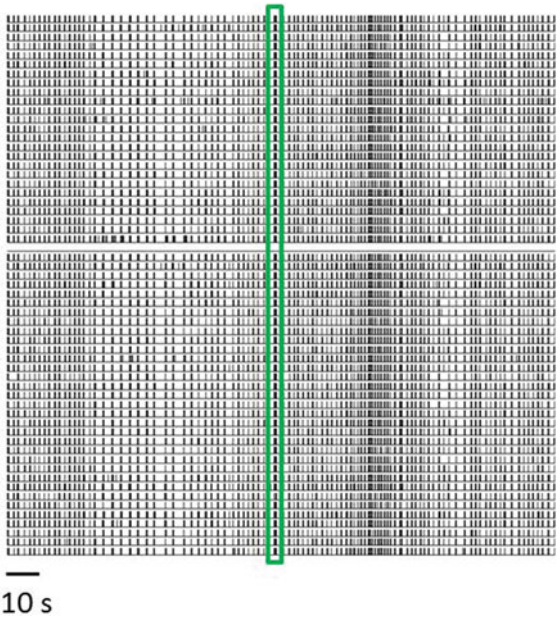

Fig. 5.59 Electrophysiological activity for a representative 2D cortical neuronal network. Raster plot showing 240 s of spontaneous activity. The highlighted area indicates a network bursting region (*green box*)

Similarly, Fig. 5.60 shows a raster plot of the spontaneous activity of a representative experiment of a sister culture (i.e., same batch) forming a 3D network at the same age of its development (i.e., fourth week). As reported for the 3D hippocampal neuronal network, also 3D cortical network exhibits a more variable activity with respect to the 2D neuronal network one. The patterns exhibited by 3D neuronal network are variable and present striking differences from the dynamics of standard high density 2D neuronal cultures. By looking at the raster plot showing 4 min of spontaneous activity, it is possible to note that the signature of the network dynamics presents a wider repertoire of activities with less global synchrony and more pronounced spiking at a single channel-neuron level. Few network burst are detectable in this type of configuration (depicted with red box). In this configuration the duration of the network burst is more variable: there is the presence of network burst with duration that seams similar to what observed in the 2D networks, but there are also network burst longer than the ones observed in 2D. As anticipated, the 3D neuronal network exhibits also a significant 'random spiking' activity (blue box).

The previous observations were further globally quantified by evaluating the percentage of random spikes in all the performed experiments. The Percentage of Random Spike values evaluated for 2D and 3D neuronal network are reported in Fig. 5.61. It is possible to observe that 2D and 3D neuronal networks random spike activity level is different. As previously reported, 2D cortical neuronal network exhibits mainly a bursting dynamic: a very low percentage of random spike is detectable (3.2 ± 0.9 %). 3D neuronal network, instead, exhibits both network bursting and random spiking activities. Accordingly with this result, the Percentage

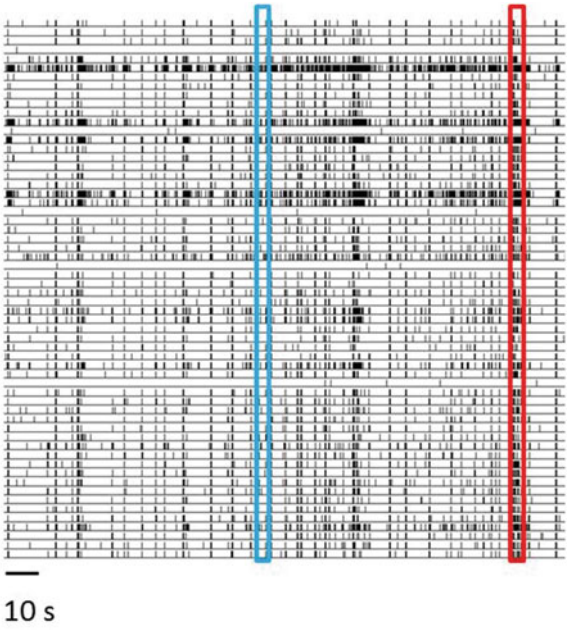

Fig. 5.60 Electrophysiological activity for a representative 3D cortical neuronal network. Raster plot showing 240 s of spontaneous activity. The highlighted areas indicate a network bursting and a random spiking activity regions (*red* and *blue boxes* respectively)

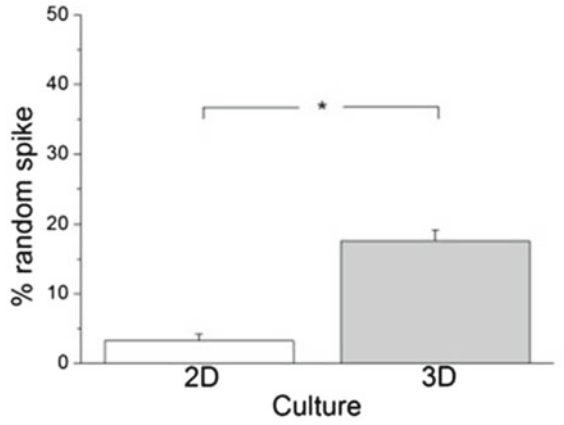

Fig. 5.61 Percentage of random spikes evaluated over the entire dataset of 2D (*white*) and 3D (*gray*) cortical networks. *Asterisk* above the plot indicates significant difference, (P-value = 10^{-3}, Mann-Whitney U-test)

of Random Spike value is higher than the one evaluated for the 2D neuronal network (17.6 ± 1.5 %).

By looking at the raster plot of a representative 2D and 3D cortical neuronal networks (Figs. 5.59 and 5.60) I observed that the burst is a common pattern of the 3D and 2D neuronal networks activities. In order to quantify the bursting activity at the single channel level, the frequency and the duration of the burst are evaluated over the entire dataset.

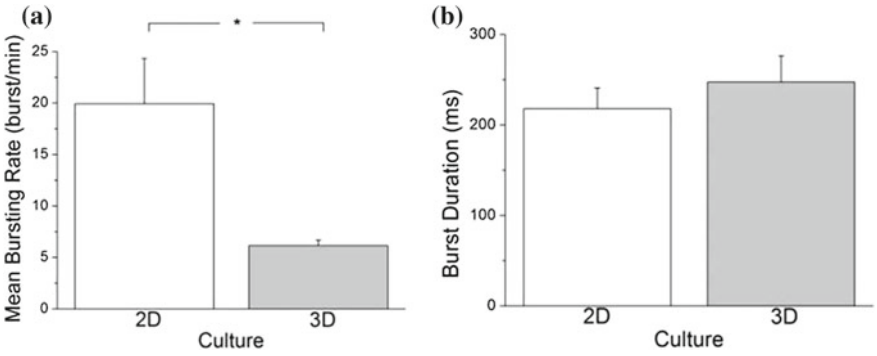

Fig. 5.62 Mean Bursting Rate and Burst Duration evaluated over the entire dataset of 2D (*white*) and 3D (*gray*) networks. *Asterisk* above the plot indicates significant difference, (P-value = 10^{-3}, Mann-Whitney U-test)

2D neuronal network exhibits a strong bursting activity: the number of network burst is very high and the percentage of random spike is low. Accordingly with these results, by looking at Fig. 5.62a, it is possible to observe an high value of Mean Bursting Rate (19.9 ± 4.4 burst/min). 3D neuronal network, instead, exhibits a low value of the parameter (6.1 ± 0.5 burst/min).

In Fig. 5.62b the Burst Duration values are reported. By looking at this graph it is clear that this parameter remains similar in all the configurations (218.2 ± 22.8 ms and 247.6 ± 28.9 ms for 2D and 3D neuronal networks respectively).

The main effects of the shift from 2D to 3D neuronal networks, are observed both in network burst frequency and duration.

As shown by the raster plot of a representative experiment of a 2D neuronal network (see Fig. 5.59), the network burst is the main pattern of activity exhibited by this network. Moreover, the level of single channel bursting rate detected is very high (see Fig. 5.62a). Accordingly with these results, number of network burst detected in 5 min of recording is very high. As reported in Fig. 5.63a, the Mean Network Bursting Rate value exhibited by 2D neuronal network is very high (20.8 ± 4.6 network burst/min). 3D neuronal network, instead, presents a more variable patterns of activities, composed by network bursting and random spiking activities. Then, the number of burst detected in 5 min of recording is very low (see Fig. 5.62a). Therefore, as reported in Fig. 5.63a, the frequency of the network burst is low (6.1 ± 0.5 network burst/min).

Regarding the burst duration, we observed that 2D neuronal network exhibited short and regular network burst, while 3D neuronal network presents network burst with more variable duration. In Fig. 5.63b the 2D and 3D neuronal Networks Burst Duration values are reported. In the case of 2D neuronal network it is possible to observe short network burst with similar duration (i.e. low standard error value). 3D neuronal network instead exhibits long and more variable network burst (i.e. high

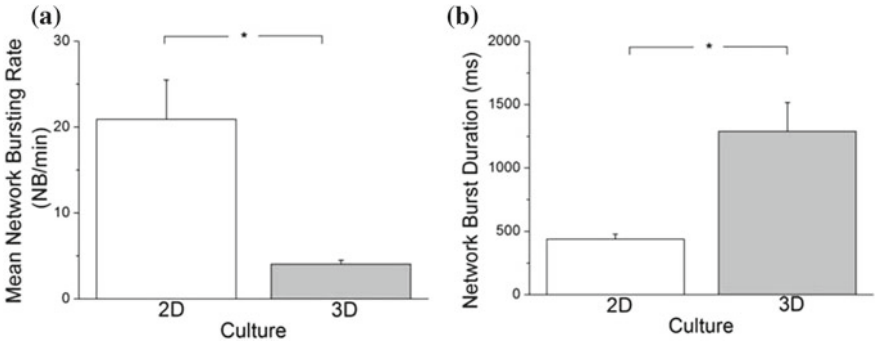

Fig. 5.63 **a** Mean Network Bursting Rate evaluated over the entire dataset of 2D (*white*) and 3D (*gray*) networks. *Asterisk* above the plot indicates significant difference, (P-value = 10^{-3}, Mann-Whitney U-test). **b** Network Burst Duration evaluated over the entire dataset of 2D (*white*) and 3D (*gray*) networks. *Asterisk* above the plot indicates significant difference, (P-value = 10^{-3}, Mann-Whitney U-test)

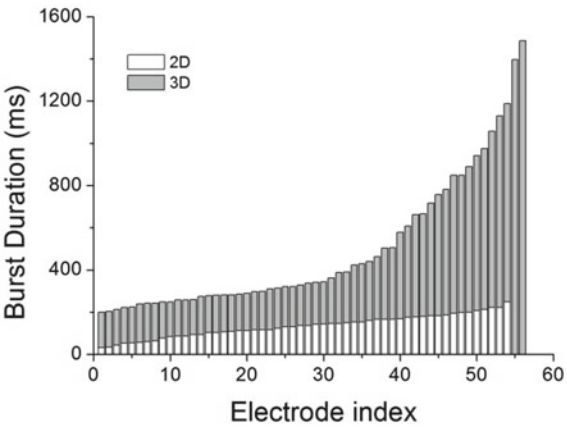

Fig. 5.64 Single channel burst duration within a network burst. 2D and 3D neuronal network burst durations are shown with *white* and *gray bars* respectively

standard error value). The values of Network Burst Duration exhibited by 2D and 3D neuronal networks are 437.8 ± 40.8 ms and 1289 ± 228.3 ms respectively.

In order to prove that the burst involved in the network burst present similar duration in the 2D neuronal network while in 3D the duration is different, in Fig. 5.64 the duration of the single channel burst that are involved in a network burst are reported. In the case of 2D neuronal network (white bars) we can observe that the duration of the burst is similar for all the channels: it spans from 50 to 248 ms. Regarding 3D neuronal network, the burst duration is more variable. The shorter burst duration are of about 200 ms and the maximum of the burst duration within a network burst is of about 1500 ms.

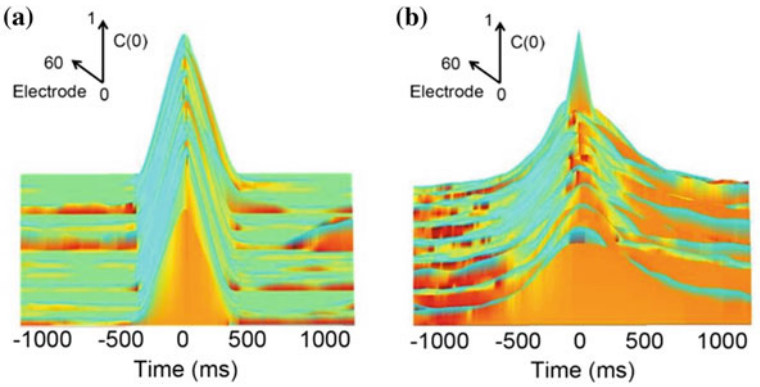

Fig. 5.65 CC function computed with a time window of 2 s and a bin size of 5 ms. **a** 2D neuronal network CC function. **b** 3D neuronal network CC function

In order to quantify the level of correlation and synchronization of the network activity, I computed the Cross-Correlation (CC) function for 2D and 3D neuronal networks with a time window of 2 s and a bin size of 5 ms.

As anticipated, 2D mature cultures exhibit a synchronized and distributed bursting network activity. During this stage of development the percentage of random spike is very low and the electrophysiological activity is dominated by bursting activity patterns. By looking at the raster plot of a representative experiment of a 2D neuronal network (see Fig. 5.59), it is possible to observe that the correlation and synchronization of the activity is very high. Figure 5.65a shows the CC function evaluated during 5 min of recording. The correlation between one channel and all the other recording electrodes for a representative experiment is reported. By looking at the CC functions reported, it is clear that an high level of correlation among all the recording channels is present. By looking at this plot, it is possible to observe that the CC functions evaluated for all the channels are similar. All the functions are centered and peaked on the central bin; also the profile of the functions seam similar.

Regarding 3D neuronal network, both network burst and random spike activity regions are present. In this case there is the presence of synchronized and distributed bursting activity mixed with spiking activity. The percentage of random spike is very high and the electrophysiological activity is various. The correlation and synchronization among all the possible pairs of channels is high when it is computed within the network burst activity region while it is low if it is computed within the random spike activity region. In Fig. 5.65b the CC functions evaluated for all the recorded channels in 5 min of both random spiking and network bursting activities are reported. 3D neuronal network exhibits a low correlation and synchronization level of the network activity. CC functions are different, only few channels are centered on the central bin and reach high maximum values.

In order to support the previous results, the C_{peak} end the C(0) values are evaluated for the entire dataset of 2D and 3D neuronal networks.

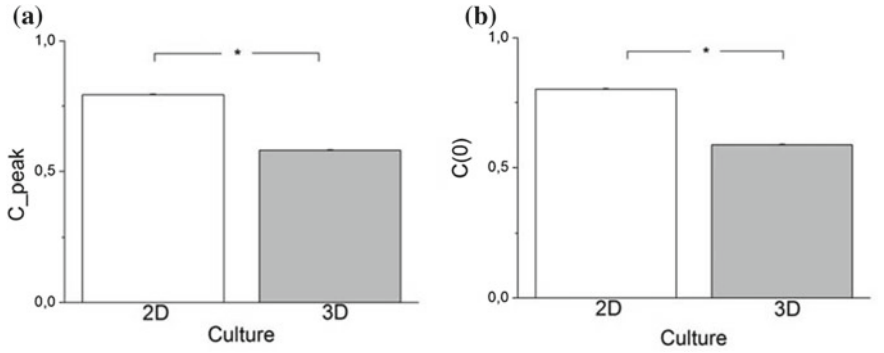

Fig. 5.66 **a** 2D and 3D networks C_{peak} values evaluated for 2D and 3D networks for all the recording channels. The parameter is computed for all the experiments of the dataset. *Asterisk* above the plot indicates significant difference, (P-value = 10^{-3}, Mann-Whitney U-test). **b** 2D and 3D networks C(0) values evaluated for all the recording channels. The parameter is computed for all the experiments of the dataset. *Asterisk* above the plot indicates significant difference, (P-value = 10^{-3}, Mann-Whitney U-test)

In Fig. 5.66a, the mean values of the CC function peaks are reported. By looking at this graph it is possible to observe that 2D neuronal network exhibits an high value of correlation between all the channels: the C_{peak} value is close to one (0.8 ± 0.002). 3D neuronal network, instead, shows a low value of this parameter, indicating a low level of correlation (0.5 ± 0.001).

In Fig. 5.66b the mean of the C(0) values is reported for 2D and 3D neuronal networks. Similarly at the results presented above, 2D neuronal network exhibits an high level of activity synchronization: the mean C(0) value is of 0.8 ± 0.002. Regarding the 3D neuronal network, instead, the value of this parameter is low (0.5 ± 0.001), indicating a low level of activity synchronization.

References

Bonifazi P, Ruaro ME et al (2005) Statistical properties of information processing in neuronal networks. Eur J Neurosci 22(11):2953–2964

Chiappalone M, Novellino A et al (2005) Burst detection algorithms for the analysis of spatio-temporal patterns in cortical networks of neurons. Neurocomputing 65–66:653–662

Chiappalone M, Massobrio P et al (2008) Network plasticity in cortical assemblies. Eur J Neurosci 28:221–237

Cullen DK, Gilroy ME et al (2010) Synapse-to-neuron ratio is inversely related to neuronal density in mature neuronal cultures. Brain Res 1359:44–55

Cullen DK, Wolf JA et al (2011) Neural tissue engineering and biohybridized microsystems for neurobiological investigation in vitro (Part 1). Crit Rev Biomed Eng 39(3):201–240

Gal A, Eytan D et al (2010) Dynamics of excitability over extended timescales in cultured cortical neurons. J Neurosci 30(48):16332–16342

Gandolfo M, Maccione A et al (2010) Tracking burst patterns in hippocampal cultures with high-density CMOS-MEAs. J Neural Eng 7(5):056001
Ichikawa M, Muramoto K et al (1993) Formation and maturation of synapses in primary cultures of rat cerebral cortical cells: an electron microscopic study. Neurosci Res 16(2):95–103
Irons HR, Cullen DK et al (2008) Three-dimensional neural constructs: a novel platform for neurophysiological investigation. J Neural Eng 5(3):333–341
Jimbo Y, Tateno Y et al (1999) Simultaneous induction of pathway-specific potentiation and depression in networks of cortical neurons. Biophys J 76:670–678
Kermany E, Gal A et al (2010) Tradeoffs and constraints on neural representation in networks of cortical neurons. J Neurosci Official J Soc Neurosci 30(28):9588–9596
Koch C (1999) Biophysics of computation-Information processing in single neurons. Oxford University Press
Kunze A, Giugliano M et al (2011) Micropatterning neural cell cultures in 3D with a multi-layered scaffold. Biomaterials 32(8):2088–2098
Lee J, Cuddihy MJ et al (2008) Three-dimensional cell culture matrices: state of the art. Tissue Eng Part B Rev 14(1):61–86
Leondopulos SS, Boehler MD et al (2013) Chronic stimulation of cultured neuronal networks boosts low-frequency oscillatory activity at theta and gamma with spikes phase-locked to gamma frequencies. J Neural Eng 9(2):026015
Marom S, Shahaf G (2002) Development, learning and memory in large random networks of cortical neurons: lessons beyond anatomy. Q Rev Biophys 35(1):63–87
Parviz M, Gross GW (2007) Quantification of zinc toxicity using neuronal networks on microelectrode arrays. Neurotoxicology 28(3):520–531
Pasquale V, Massobrio P et al (2008) Self-organization and neuronal avalanches in networks of dissociated cortical neurons. Neuroscience 153(4):1354–1369
Pautot S, Wyart C et al (2008) Colloid-guided assembly of oriented 3D neuronal networks. Nat Methods 5(8):735–740
Robinson HPC, Kawahara M et al (1993) Periodic synchronized bursting in intracellular calcium transients elicited by low magnesium in cultured cortical neurons. J Neurophysiol 70(4):1606–1616
Rowe L, Almasri M et al (2007) Active 3-D microscaffold system with fluid perfusion for culturing in vitro neuronal networks. Lab Chip 7(4):475–482
Schuz A, Palm G (1989) Density of neurons and synapses in the cerebral cortex of the mouse. J Comp Neurol 286(4):442–455
Streit J, Tscherter A et al (2001) The generation of rhythmic activity in dissociated cultures of rat spinal cord. Eur J Neurosci 14(2):191–202
Tscherter A, Heuschkel MO et al (2001) Spatiotemporal characterization of rhythmic activity in rat spinal cord slice cultures. Eur J Neurosci 14(2):179–190
Van Pelt J, Corner MA et al (2004) Longterm stability and developmental changes in spontaneous network burst firing patterns in dissociated rat cerebral cortex cell cultures on multi-electrode arrays. Neurosci Lett 361(1–3):86–89
van Pelt J, Vajda I et al (2005) Dynamics and plasticity in developing neuronal networks in vitro. Prog Brain Res 147:173–188
Wagenaar DA, Madhavan R et al (2005) Controlling bursting in cortical cultures with closed-loop multi-electrode stimulation. J Neurosci 25(3):680–688

Part III
Additional Applications with MEA Technology

Chapter 6
Neuro-Pharmacological Studies

In this Chap. 1 will present the results regarding neuro-pharmacological studies utilizing cortical and hippocampal neuronal networks coupled to MEA devices. In this Chap. 1 will show firstly the effect of ionotropic glutamate's agonists on the network activity (cf. Sect. 6.1) (Frega et al. 2012); then I will describe how the network activity is modulated by antiepileptic drugs (cf. Sect. 6.2) (Colombi et al. 2013).

6.1 Effect of Ionotropic Glutamate's Agonists

Excitatory neurotransmission in the brain is predominantly mediated by glutamate release via synaptic transmission. Glutamate activates ionotropic (ligand-gated) receptors of both NMDA and AMPA/kainite subtypes (Collingridge and Lester 1989) and metabotropic (G-protein coupled) receptors. While synaptic glutamatergic transmission onto ionotropic receptors plays a critical role during brain development and in plasticity, memory, learning processes and cognition in adult brain (Meldrum 2000; Riedel et al. 2003; Antzoulatos and Byrne 2004), stimulation of ionotropic glutamate receptors may also activate neuro-excitotoxic cascades (Rothman and Olney 1995).

In Frega et al. (2012), we used cortical cultures coupled to MEAs to investigate the short/long term effects of increasing concentrations of ionotropic glutamate's agonists, which could cause excitotoxicity. We selectively activated ligand-gated glutamatergic receptor subtypes by using glutamate agonists (NMDA, AMPA and AMPA together with cyclothiazide—CTZ) or added exogenous glutamate, at different concentrations to modulate the dynamics of cortical networks.

α-amino-3-hydroxy-5-methyl-4-isoxazolepropionic acid (AMPA) and N-methyl-D-aspartate (NMDA) are agonists of ionotropic glutamatergic receptors at the post-synaptic site. We performed experiments by adding to the culture medium

M. Frega, *Neuronal Network Dynamics in 2D and 3D in vitro Neuroengineered Systems*, Springer Theses, DOI 10.1007/978-3-319-30237-9_6

progressively increasing concentrations of each drug at intervals of 30 min. More specifically, we tested low (i.e. 0.05–0.2–1–5 μM), medium (i.e. 10–30 μM) and high (i.e. 50–100 μM) concentrations of AMPA/NMDA to different sets of cultures (N = 4 cultures for AMPA and N = 5 cultures for NMDA). At the same time, we tested the effects of increasing doses of glutamate (0.05–0.2–1–5–10–30–50–100–500 μM, N = 4 cultures). We mainly based our choices on the available literature by ours and other groups in the MEA field (Gross et al. 1992; Gramowski et al. 2000; Martinoia et al. 2005a, b; Gramowski et al. 2006).

Following activation, many ligand-gated ion channels enter in a desensitized state in which the neurotransmitter remains bound but the ion channel is closed. Both AMPA and NMDA receptors are subject to desensitization, with a different degree also related to the activating agonist. To prevent the desensitization of AMPA receptors, we used cyclothiazide (CTZ) at different concentrations (Trussell and Fischbach 1989). We treated a subset of our cultures with either low (i.e. 1–3 μM) or high (i.e. 10–30 μM) concentrations of CTZ, combined with AMPA at a fixed concentration of 0.2 μM (N = 3 cultures).

6.1.1 Effect of AMPA

To study the acute and chronic effects of an increase of glutamate and its agonists, we analyzed the changes exhibited by the electrophysiological activity of cortical networks of primary neurons prepared from E18 rat embryos and plated onto standard MEAs. After a couple of weeks in culture, cells started showing a typical electrophysiological pattern which comprised strongly synchronized bursts of action potentials, mixed with desynchronized random firing.

Low doses of the agonist (50, 200 nM and 1 μM) increase the level of activity of the network. At those concentrations, the electrophysiological activity is characterized by the presence of both spikes and bursts of action potentials. Moreover, the majority of the electrical activity takes place as part of network-wide collective events, known as ‘network bursts’ (i.e. bursts fired at the same time by most of the recording channels) (Pasquale et al. 2010). At 5 μM, only few channels are still active: they are not synchronized and network bursts are missing. At higher concentrations (above 10 μM) the electrophysiological behavior remains similar, indicating that medium and high doses of AMPA abolish most of the spontaneous electrophysiological activity of cortical networks.

To quantify our results, we derived a set of dose-response curves based on different spike/burst parameters. Low doses of AMPA induce an increase of spike and burst rates, which reach a maximum at the concentration of 200 nM–1 μM (Fig. 6.1a–b). The IC50 calculated for AMPA is equal to 2.8 ± 0.9 μM (Fig. 6.1a, inset). The bursting pattern tends to remain stable in terms of both MFB (frequency within bursts) and burst duration, apart from a drop at 1 μM for MFB (Fig. 6.1c) and a peak at 1 μM for burst duration (Fig. 6.1d). These results indicate that, for medium concentrations, the few bursting channels display longer bursts characterized by high

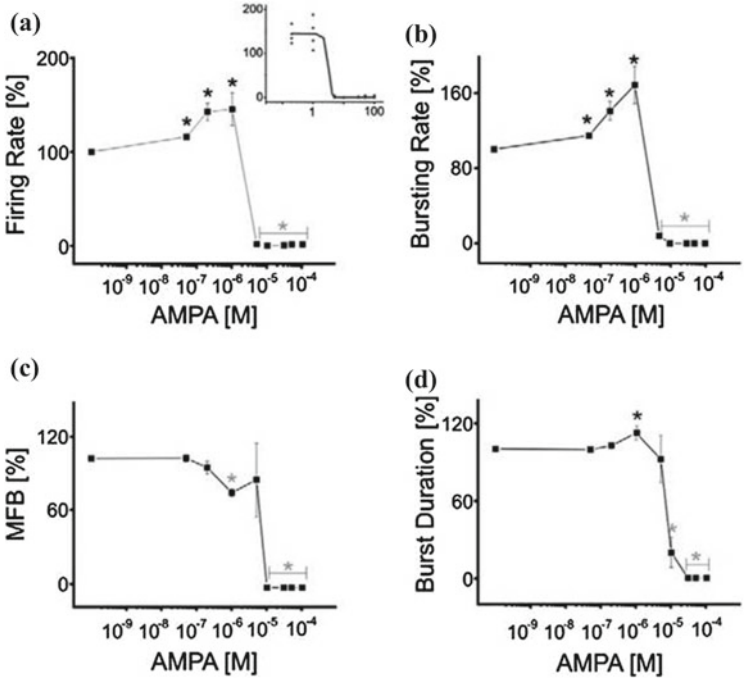

Fig. 6.1 Effects of low (0.05, 0.2, 1, 5 μM), medium (10, 30 μM) and high (50, 100 μM) doses of AMPA on the firing and bursting dynamics of cortical networks (N = 4 experiments). **a** The firing rate significantly increases for very low concentrations of AMPA (i.e. 50, 200 nM and 1 uM), while it significantly decreases starting from AMPA 5 μM till 100 μM. Inset. Fitting of the dose-response *curve* by means of the Hill equation, starting from the maximum obtained values of the firing rate (i.e. 200 nM and 1 uM). **b** The bursting rate follows a profile very similar to that observed for the firing rate, showing a significant increase for low doses of the drug (50, 200 nM and 1 uM). **c** Mean frequency of spikes within the bursts (MFB) statistically decreases at AMPA 1 μM and for concentrations higher than 10 μM. **d** Burst duration has a significant increase for 1 μM AMPA, but it drops down from 10 μM on. Statistics presented was done by using one-sample t-test, $*p < 0.05$

frequency spikes. We also quantified the changes in number of generated network bursts, whose number remains statistically stable and then drops down at AMPA 5 μM.

The correlation level does not significantly change at 50 nM, while it starts to significantly decrease at higher doses of AMPA (from 200 nM to 5 μM), falling down to zero from 10 μM on.

Upon a complete medium change, we noticed a total depression of the activity, with no recovery during an acquisition time of 60 min. After 1 day in the incubator we again measured our cultures, noting a very slow assessment of the firing rate to low levels (firing rate = 0.27 ± 0.2 spikes/s, equal to 6.27 ± 4.47 % with respect to the native state). An even slighter increase was observed 3 days after the AMPA treatment (firing rate = 1.30 ± 0.82 spikes/s, equal to 30.27 ± 17.94 % with respect

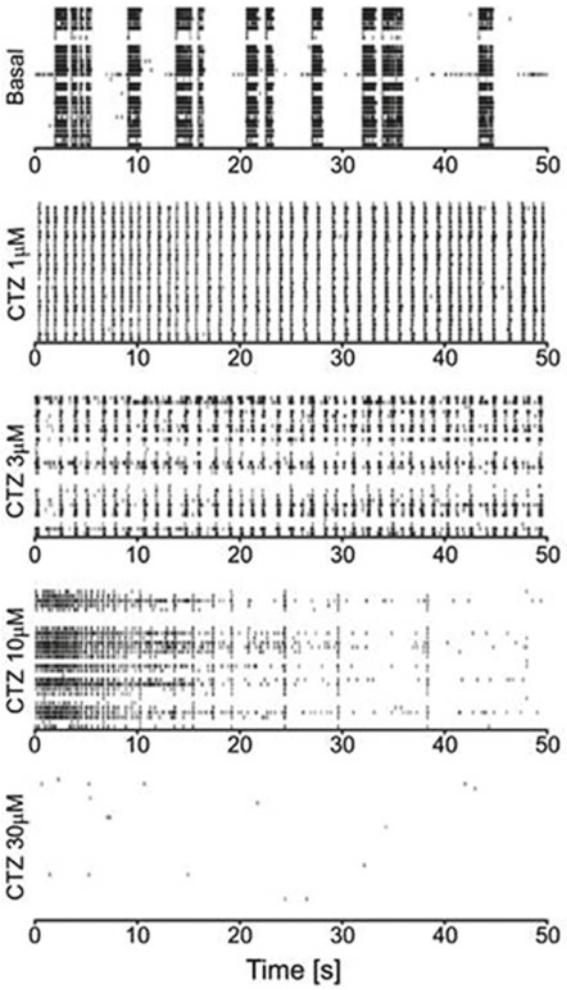

Fig. 6.2 Increasing concentrations of CTZ cause a complete abolishment of electrophysiological activity. Raster plot of 30 electrodes (out of 60) coming from a set of MEAs treated with different doses of CTZ added to a constant concentration of AMPA (0.2 μM). More specifically: basal condition, AMPA 0.2 μM + CTZ 1 μM, AMPA 0.2 μM + CTZ 3 μM, AMPA 0.2 μM + CTZ 10 μM, AMPA 0.2 μM + CTZ 30 μM

to the native state), indicating that the long term effect of the drug consists in a reduction (not a total abolishment) of the initial activity, but with a complete loss of synchronized patterns (bursts and network bursts).

To test the effect of a prolonged activation of the AMPA receptor, we decided to perform a set of experiments by employing cyclothiazide (CTZ). We combined increasing concentrations of CTZ with a constant concentration of AMPA. We used a very low dose (i.e. 200 nM) of the AMPA agonist since we knew that it caused a slight increase in the firing activity and, under this condition, the effect of CTZ administration could be better highlighted. For a qualitative judgment, let us consider the raster plots presented in Fig. 6.2. The effect of low doses of CTZ is striking: either at 1 or 3 μM, there is an evident increase in the bursting rate with respect to the basal condition. The effect drastically changes when the concentration of CTZ rises to

10 μM, during which there is a progressive loss of activity without the presence of bursting, up to 30 μM. In this last condition the network is silent, only isolated spikes can be found on few channels, completely desynchronized, indicating that the collective activity is lost.

6.1.2 Effect of NMDA

NMDA causes similar effects to those due to AMPA administration. The electrophysiological pattern does not change for very low doses of NMDA (50 and 200 nM), while it appears different at 1 and 5 μM, when the network is characterized by less bursts and an increased level of firing. The activity drops down at 10 μM NMDA, when few spiking channels are still active but the synchronized patterns totally

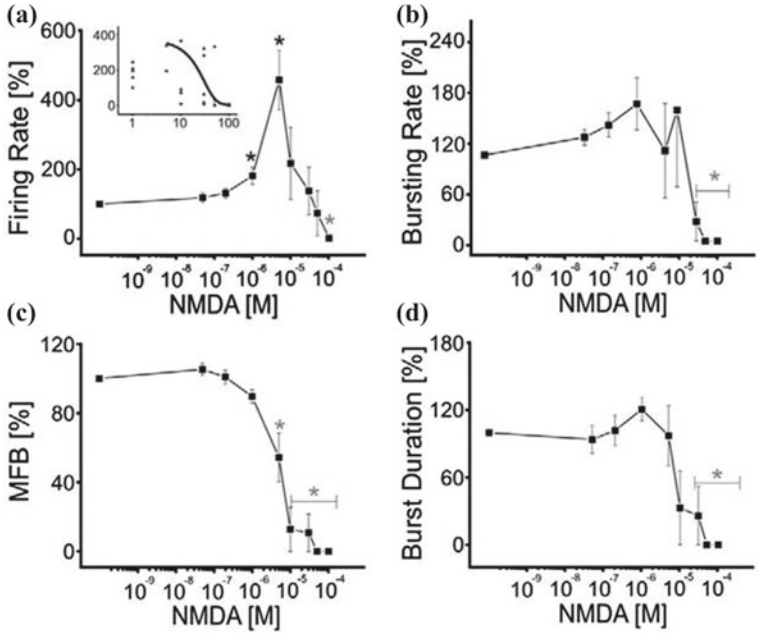

Fig. 6.3 Effects of low (0.05, 0.2, 1, 5 μM), medium (10, 30 μM) and high (50, 100 μM) doses of NMDA on the firing and bursting dynamics of cortical networks (N = 5 experiments). **a** The firing rate significantly increases for low concentrations of NMDA (i.e. 1 and 5 μM), while it does not change for lower (50 and 200 nM) and medium concentrations (10, 30, and 50 μM). A significant decrease is observed for 100 μM NMDA. Inset. Fitting of the dose-response *curve* by means of the Hill equation, starting from the maximum obtained values of the firing rate (i.e. 5 μM). **b** The bursting rate does not change till NMDA 30 μM, when it starts significantly decreasing. **c** Mean frequency of spikes within bursts starts to statistically decrease at NMDA 5 μM. **d** Burst duration has a significant decrease from NMDA 30 μM on. Statistics presented was done by using the one-sample t-test, $*p < 0.05$

disappear. The change in firing rate profile indicates a clear-cut increase of the activity at 1–5 μM NMDA and a fast decrease for higher doses of the drug (Fig. 6.3a). The obtained IC50 is equal to 33.4 ± 15.7 μM (Fig. 6.3a, inset). The bursting rate does not change statistically till NMDA 30 μM (Fig. 6.3b). MFB tends to decrease starting from 10 to 30 μM NMDA (Fig. 6.3c), while burst duration does not change significantly for low-medium doses (Fig. 6.3d), meaning that bursts have lengths similar to the native state with lower intra-burst frequency. Synchronized activity, measured in terms of change in the number of network bursts, totally disappears at 10 μM NMDA.

After a double wash-out from NMDA treatment, we completely lost the few spiking channels. No recovery, either in terms of spikes or bursts, was observed after 1 and 3 days (firing rate = 0 spikes/s).

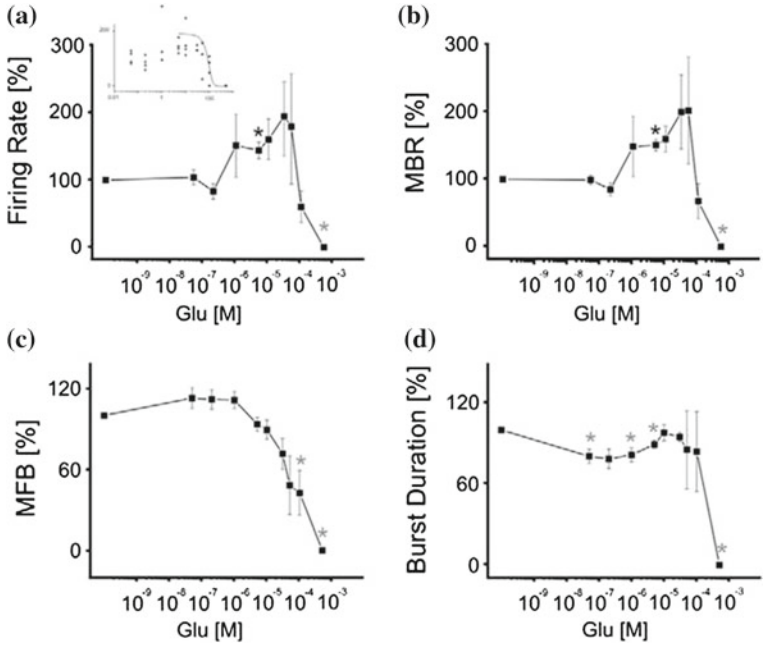

Fig. 6.4 Effects of low (0.05, 0.2, 1, 5 μM), medium (10, 30 μM) and high (50, 100, 500 μM) doses of glutamate on the firing and bursting dynamics of cortical networks (N = 4 experiments). **a** The firing rate significantly increases at glutamate 5 μM, while it does not change for the other doses. A significant decrease is observed only at 500 μM. Inset. Fitting of the dose-response *curve* by means of the Hill equation, starting from the maximum obtained values of the firing rate (i.e. 5 μM). **b** The bursting rate statistically increases only at glutamate 5 μM, dropping down at 500 μM. **c** Mean frequency of spikes intra bursts starts to statistically decrease at glutamate 100 μM. **d** Burst duration has a significant decrease for glutamate 50 nM, 1 and 5 μM, then it falls down at 500 μM. Statistics presented was done by using the one-sample t-test, $*p < 0.05$

6.1.3 *Effect of Exogenous Glutamate*

To complete our analysis on the effects of glutamate agonists on cortical cultures, we made experiments employing exogenous glutamate, to be added to the culture medium. Glutamate administration slightly changes the native electrophysiological pattern. Fluctuations in the level of the firing rate are visible (Fig. 6.4a), but the overall activity does not qualitatively change, apart from a statistical increase of the activity at glutamate 5 μM and a drop at 500 μM. The fitted dose-response curve produces an IC50 equal to 137.8 ± 40.3 μM (Fig. 6.4a, inset). A clear-cut change can be noticed at medium concentrations (from 30 to 50 μM), when 'superburst' patterns (i.e. groups of network bursts) can be observed (Wagenaar et al. 2006). Also the bursting rate presents a statistical increase at the dose of 5 μM (Fig. 6.4b). From medium doses the MFB tends to decrease, reaching the minimum (around zero) for very high concentrations (500 μM), thus indicating the total absence of bursts (Fig. 6.4c). After a slight decrease for low doses, the burst duration stays at the initial levels till 50–100 μM (Fig. 6.4d). The correlation level significantly increases with respect to the native state (i.e. from 50 nM to 10 μM) till Glu 30 μM (no statistical difference), then it significantly decreases at higher doses (50 and 100 μM), dropping to zero at 500 μM.

Also in the case of glutamate treatment, after a double wash-out of the culturing medium, we observed a complete loss of activity, which showed no recovery after either 1 or 3 days (firing rate = 0 spikes/s).

6.2 Effect of Antiepileptic Drugs

Antiepileptic drugs are the mainstay of epilepsy treatment and act to suppress seizure severity and frequency. However, such drugs can also have paradoxical effects, exacerbating seizures in some patients.

Carbamazepine (CBZ) is the drug of choice for the treatment of focal seizures; however, it commonly aggravates several generalized seizures types, including absence seizures.

Sodium valproate (VPA) is widely used as antiepileptic drug with a broad spectrum of anticonvulsant activity and particular efficacy in generalized epilepsies (Dichter and Fischbach 1977).

The mechanism of action of antiepileptic drugs, and specifically CBZ and VPA, has been investigated at the molecular and cellular levels. CBZ appears to act through the use-dependent blockade of voltage-gated sodium channels, hence inhibiting rapid burst firing neurons, while allowing normal non-bursting neuronal transmission (Kohling 2002). The anticonvulsant action of VPA is generally ascribed to an enhancement of inhibitory neurotransmission mediated by GABA receptors (Rowley et al. 1995; Loscher 1999), which increases hippocampal GABA levels (Biggs et al. 1992; Rowley et al. 1995) and inhibitory post-synaptic potentials

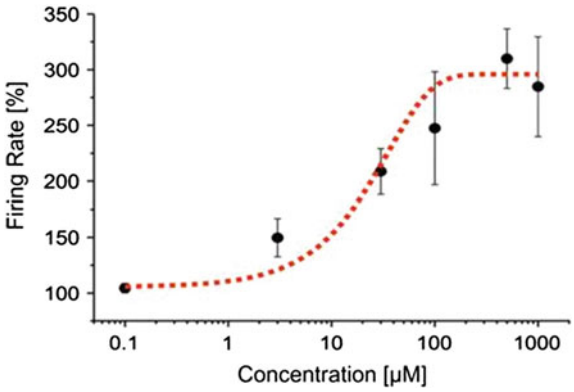

Fig. 6.5 Dose-response *curve* for increasing concentrations of BIC (100 nM, 3, 30, 100, 500 μM, 1 mM) was evaluated on a set of four experiments. The black line represents the mean response *curve* obtained by analyzing the changes in firing rate for the considered batch of experiments. The fitting of the dose-response *curve* by means of the Hill equation is the *curve*

(Preisendorfer et al. 1987). VPA also acts on excitatory neurotransmission by suppressing the responses mediated by NMDA receptors (Gean et al. 1994), blocks sodium ion channels and reduces T-type calcium currents (Kelly et al. 1990). However, how these mechanisms integrate at the neuronal network level to achieve the overall pharmacological effects remains unexplored.

In this work (Colombi et al. 2013), we used hippocampal cultures coupled to MEAs to investigate the acute effects of increasing concentrations of antiepileptic drugs (i.e., VPA and CBZ) on neuronal network activity. We also studied the changes of the electrophysiological activity when the neuronal network was previously treated with bicuculline (BIC), in order to model an epileptic phenotype (Khalilov et al. 1997).

In order to mimic ictal seizures in network of hippocampal neurons, we applied BIC at increasing concentrations to a set of four different cultures.

BIC increased the firing rate in a concentration-dependent manner, as reported in Fig. 6.5. The effective concentration yielding a 50 % response (EC50) was evaluated, according to the fitting of the concentration-response curve through the Hill equation (Frega et al. 2012). The computed EC50 was 29.75 ± 13.33 μM (mean ± SE). At 30 μM, BIC induced a significant increase in the network synchronization, firing rate, bursting rate, burst duration and frequency in bursts. In subsequent experiments, to evaluate the effects of CBZ and VPA on ictal type activity avoiding ceiling or flooring effects (cf. Sects. 6.2.1 and 6.2.2), we pretreated hippocampal cultures with 30 μM BIC.

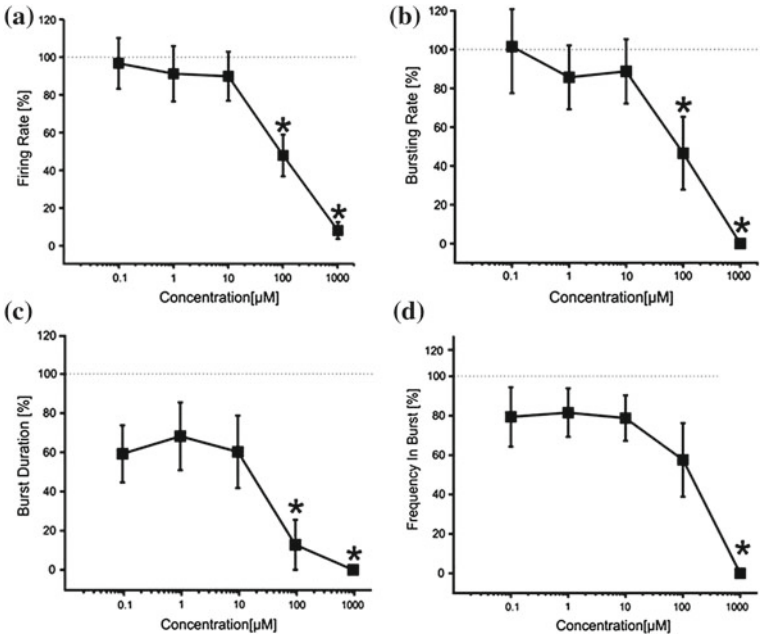

Fig. 6.6 Effects of increasing concentrations of CBZ on the firing and bursting dynamics of hippocampal networks (N = 12 experiments). **a** The firing rate upon drug administration significantly decreased compared to the control condition (dotted line at 100 %) at 100 μM–1 mM. **b** The bursting rate followed a profile very similar to that observed for the firing rate, showing a significant decrease at100 μM and1 mM. **c** Burst duration started to statistically decrease at 100 μM. **d** Mean frequency of spikes within the bursts statistically decreased at 1 mM. Statistics were performed using One-Way ANOVA followed by Bonferroni's test, $*p < 0.05$

6.2.1 Effect of CBZ

CBZ induced a decrease in the number of spikes and bursts produced by the hippocampal networks, with a statistically significant decrease in both firing and bursting rates at high concentrations of the drug (100 μM and 1 mM; Fig. 6.6a–d). At 1 mM, in particular, no burst was generated, indicating that the concentration was able to abolish the bursting activity. At lower concentrations (100 nM, 1 and 10 μM), on the contrary, bursting activity was present but the number of active channels was slightly less than in the other phases (100 % in the control and at 100 nM; 95.77 % at 1, 10, and 100 μM; 61.11 % at 1 mM).

CBZ (N = 37 cultures) reduced the BIC-induced firing rate in a significant manner at high concentrations (i.e.,100 μM and 1 mM), as shown in the drug-response curve (Fig. 6.7a). Bursting rate (Fig. 6.7b) and burst duration (Fig. 6.7c) followed a trend comparable to that of the firing rate, but the significant decrease was appreciated only at 1 mM. On the contrary, spike frequency intra burst (Fig. 6.7d) showed a significant increase for low doses of the drug, and decreased for the highest

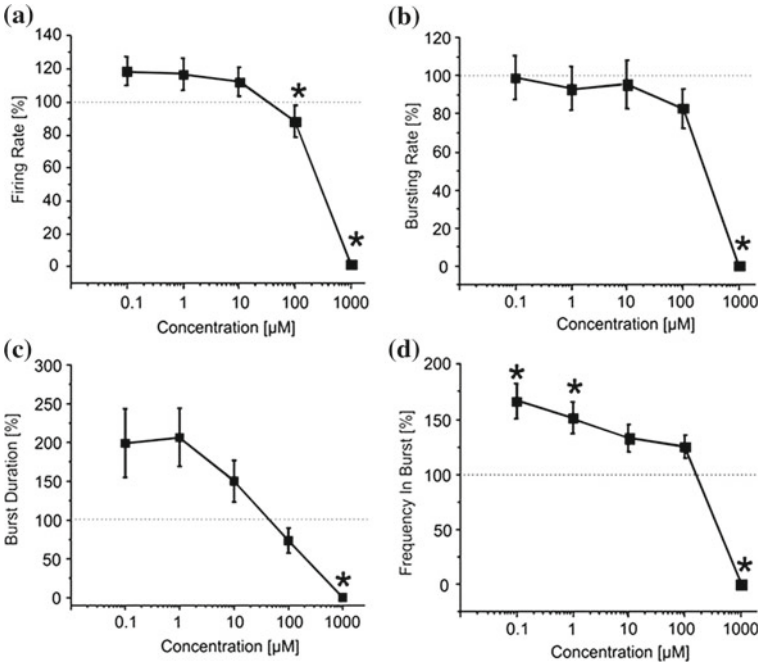

Fig. 6.7 Effects of increasing concentrations of CBZ (100 nM, 1, 10, 100 μM, 1 mM) upon BIC treatment (30 μM) on the firing and bursting dynamics of hippocampal networks. **a** The firing rate significantly decreased compared to the BIC condition for CBZ 100 μM and 1 mM. **b** The bursting rate followed a constant profile, showing no significantly change for CBZ 100 nM–100 μM. Only at 1 mM CBZ there was a significant decrease of the considered parameter. **c** Burst duration decreased in asignificant way only at CBZ 1 mM. **d** Mean frequency of spikes within the bursts (MFB) statistically increased compared to the control at CBZ 100 nM and 1 μM, while it significantly decreased at CBZ 1 mM. Statistics were performed using One-Way ANOVA followed by Bonferroni's test, $*p < 0.05$

concentration. For this experimental group, the percentage of active channels was in the range 98.11 and 97.22 % (BIC alone and plus CBZ 100 nM) till 62 % (CBZ 1 mM).

6.2.2 Effect of VPA

VPA showed a similar (but not equal) trend to that found for CBZ (Fig. 6.8). Statistical analysis performed on the drug response curves computed from different activity parameters (i.e., firing rate, bursting rate, burst duration and frequency intra burst, reported in Fig. 6.8a–d) indicated that the decrease was significant at high concentrations of the drug (i.e., 100 μM–1 mM). However, unlike CBZ, both firing and bursting were never abolished by high concentrations of VPA. For concentra-

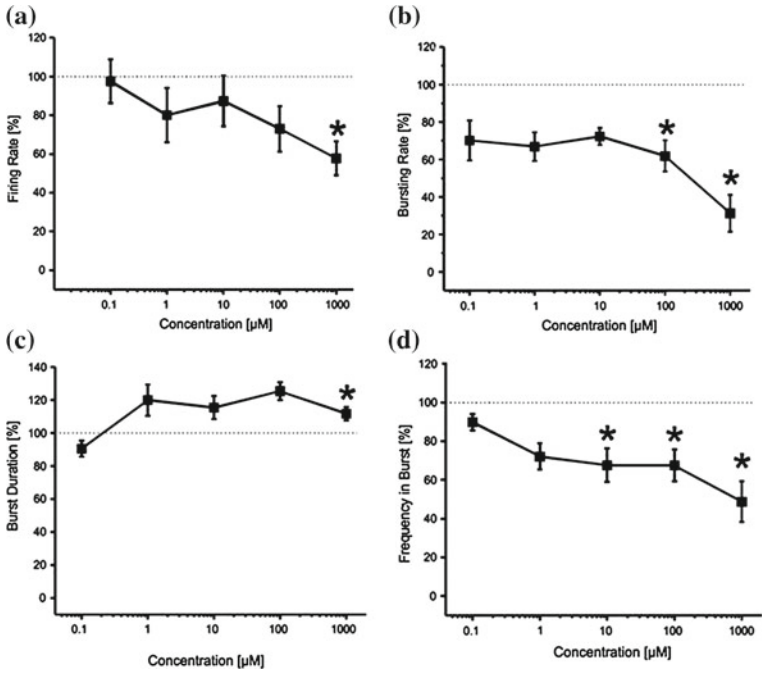

Fig. 6.8 Effects of increasing concentrations of VPA on the firing and bursting dynamics of hippocampal networks. VPA was added to the culture medium at increasing concentrations (100 nM, 1, 10, 100 μM, 1 mM). **a** The firing rate significantly decreased with respect to the "spontaneous" (control) condition (dotted line at 100 %) at VPA 1 mM. **b** The bursting rate significantly decreased at 100 μM–1 mM. **c** Burst duration showed a significant increase compared to the basal at VPA 1 mM. **d** Mean frequency of spikes within bursts statistically decreased starting from VPA 10 μM till 1 mM. Statistics were performed using One-Way ANOVA followed by Bonferroni's test, $*p < 0.05$

tions ranging from 100 nM to 1 μM changes with respect to the basal condition were overall negligible. While a decrease in the rate of the events was appreciated at 100 μM and 1 mM, an increase in the duration of the bursting patterns was observed at 1 mM, indicating that a reduced number of bursts were generated, bursts lasted longer but had fewer spikes than in the absence of VPA. The percentage of active channels was in the range 97.22 % (control) 68.44 % (1 mM).

In the presence of BIC, VPA (N = 44 cultures) triggered dual behaviors in hippocampal networks. In one group of cultures, we observed a decrease of firing at low VPA concentrations, which return to BIC-evoked levels at high concentrations of VPA. In a second group of cultures, we observed a general concentration-independent decrease of firing. We therefore, analyzed the two groups separately.

The results for the first group of experiments (N = 12 cultures) are shown in Fig. 6.9. We can observe a significant decrease in the firing rate (Fig. 6.9a) for low concentrations of VPA (i.e., 100 nM and 1 μM), accompanied by no change in the

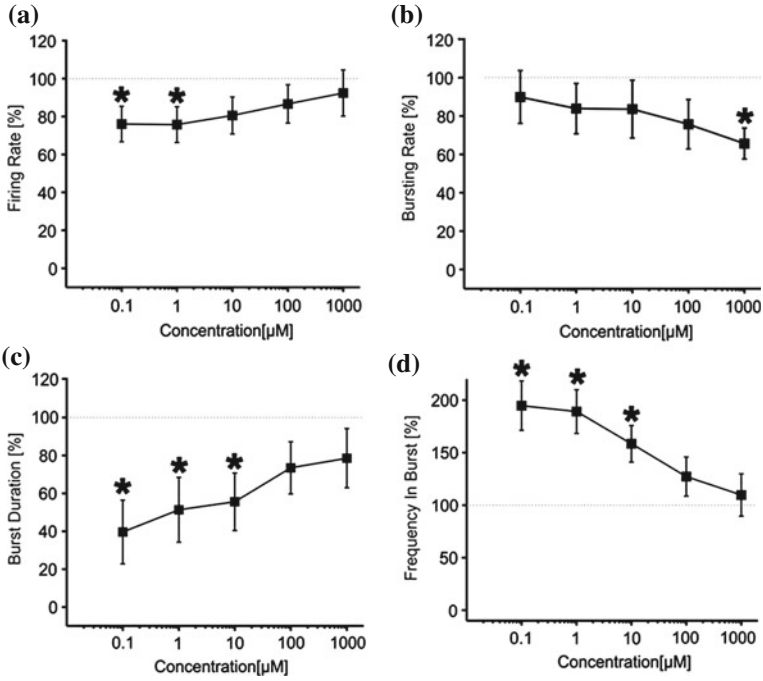

Fig. 6.9 Effects of increasing concentrations of VPA (100 nM, 1, 10, 100 μM, 1 mM) upon BIC treatment (30 μM) on the firing and bursting dynamic of hippocampal networks in a first group of experiments (N = 12). **a** The firing rate was significantly reduced at low doses of VPA (i.e., 100 nM–1 μM), while it reached values comparable with the BIC condition for higher doses (10 μM–1 mM). **b** The bursting rate significantly decreased compared to the BIC condition at 1 mM. **c** Burst duration had a significant decrease for VPA 100 nM till 10 μM, while it reached values comparable with the BIC condition for higher concentrations (100 μM–1 mM). **d** Mean frequency of spikes within the bursts statistically increased for the range of concentrations 100 nM–10 μM, while it reached values comparable to the BIC phase for higher concentrations (i.e., 100 μM–1 mM). Statistics were performed using One-Way ANOVA followed by Bonferroni's test, $*p < 0.05$

bursting rate (Fig. 6.9b) for the same doses. At concentrations of 100 nM–10 μM, burst duration was significantly reduced (Fig. 6.9c), while the frequency intra burst was almost doubled compared to culture treated with BIC alone (Fig. 6.9d). For high concentrations of the drug (100 μM and 1 mM), the firing rate (Fig. 6.9a), burst duration (Fig. 6.9c) and frequency intra burst (Fig. 6.9d) returned to values comparable to those achieved by BIC alone, while the bursting rate decreased significantly at 1 mM VPA (Fig. 6.9b). In this group of experiments, the number of active channels remained high in all experimental conditions, starting from 99.11 and 96.55 % (BIC alone and plus VPA 100 nM) to 96.55 % (VPA 1 mM).

The results for the second group of experiments (N = 32) are reported in Fig. 6.10. From the analysis of the network parameters, we can note that VPA significantly reduced firing rate (Fig. 6.10a), bursting rate (Fig. 6.10b) and burst

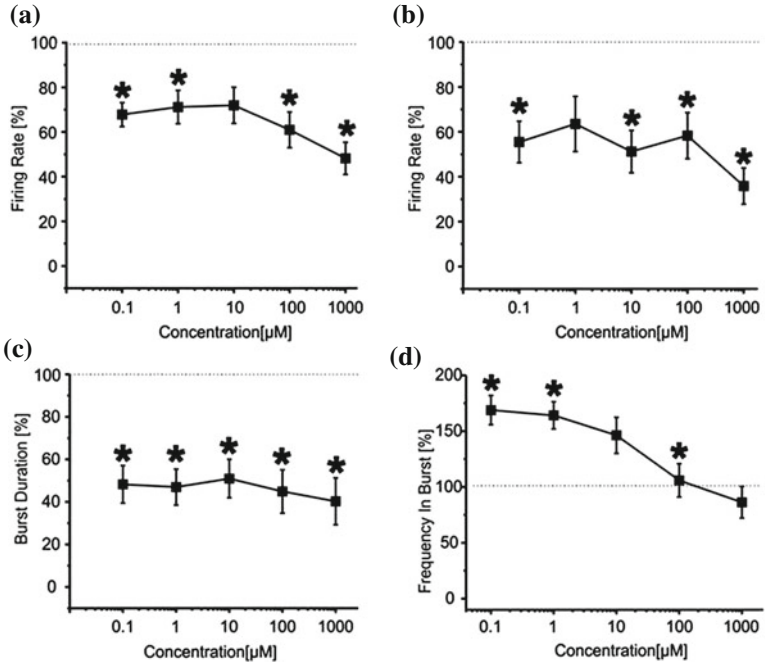

Fig. 6.10 Effects of increasing concentrations of VPA (100 nM, 1, 10, 100 μM, 1 mM) upon BIC treatment (30 μM) on the firing and bursting dynamics of hippocampal networks in a second group of experiments (N = 32). **a** The firing rate significantly decreased compared to the control at low and high concentrations (i.e., 100 nM, 100 μM, 1 mM), while it stayed the same for medium doses (1–10 μM). **b** Bursting rate significantly decreased compared to the control for all the concentrations apart 1 μM. **c** Burst duration significantly decreased for the entire range of tested concentrations. **d** Mean frequency of spikes within the bursts statistically increased for the range of concentrations 100 nM–1 μM, while it reached values comparable to the control for higher concentrations (i.e., 10 μM–1 mM). Statistics were performed using One-Way ANOVA followed by Bonferroni's test, $*p < 0.05$

duration (Fig. 6.10c) with similar effects at all concentrations tested. In fact, with respect to BIC alone, VPA decreased the firing rate by 35.9 ± 4.4 %, the bursting rate by 47.2 ± 4.7 % and the burst duration of about 53.7 ± 1.8 % and the reduction was overall constant over the concentrations evaluated. The mean frequency intra burst (Fig. 6.10d) was significantly increased at low concentrations (100 nM–1 uM) of VPA and returned to the levels of cultures treated with BIC alone at high concentrations. The percentage of active channels was 95.33 % for BIC alone, 92.55 % for VPA 100 nM and 70.33 % for VPA 1 mM.

References

Antzoulatos EG, Byrne JH (2004) Learning insights transmitted by glutamate. Trends Neurosci 27(9):555–560

Biggs CS, Pearce BR et al (1992) The effect of sodium valproate on extracellular GABA and other amino acids in the rat ventral hippocampus: an in vivo microdialysis study. Brain Res 594(1):138–142

Collingridge GL, Lester RA (1989) Excitatory amino acid receptors in the vertebrate central nervous system. Pharmacol Rev 41(2):143–210

Colombi I, Mahajani S et al (2013) Effects of antiepileptic drugs on hippocampal neurons coupled to micro-electrode arrays. Front Neuroeng 6:10

Dichter MA, Fischbach GD (1977) The action potential of chick dorsal root ganglion neurones maintained in cell culture. J Physiol 267(2):281–298

Frega M, Pasquale V et al (2012) Cortical cultures coupled to micro-electrode arrays: a novel approach to perform in vitro excitotoxicity testing. Neurotoxicol Teratol 34(1):116–127

Gean PW, Huang CC et al (1994) Valproic acid suppresses the synaptic response mediated by the NMDA receptors in rat amygdalar slices. Brain Res Bull 33(3):333–336

Gramowski A, Jugelt K et al (2006) Functional screening of traditional antidepressants with primary cortical neuronal networks grown on multielectrode neurochips. Eur J Neurosci 24(2):455–465

Gramowski A, Schiffmann D et al (2000) Quantification of acute neurotoxic effects of trimethyltin using neuronal networks cultured on microelectrode arrays. Neurotoxicology 21(3):331–342

Gross G, Rhoades B et al (1992) Neuronal networks for biochemical sensing. Sens Actuators 6:1–8

Kelly KM, Gross RA et al (1990) Valproic acid selectively reduces the low-threshold (T) calcium current in rat nodose neurons. Neurosci Lett 116(1–2):233–238

Khalilov I, Khazipov R et al (1997) Bicuculline induces ictal seizures in the intact hippocampus recorded in vitro. Eur J Pharmacol 319(2–3):R5–6

Kohling R (2002) Voltage-gated sodium channels in epilepsy. Epilepsia 43(11):1278–1295

Loscher W (1999) Valproate: a reappraisal of its pharmacodynamic properties and mechanisms of action. Prog Neurobiol 58(1):31–59

Martinoia S, Bonzano L et al (2005a) Electrophysiological activity modulation by chemical stimulation in networks of cortical neurons coupled to micro-electrode arrays: a biosensor for neuropharmacological applications. Sens Actuators B Chem 108(1–2):589–596

Martinoia S, Bonzano L et al (2005b) In-vitro cortical neuronal networks as a new high-sensitive system for biosensing applications. Biosens Bioelectron 20(10):2071–2078

Meldrum BS (2000) Glutamate as a neurotransmitter in the brain: review of physiology and pathology. J Nutr 130(4S Suppl):1007S–1015S

Pasquale V, Martinoia S et al (2010) A self-adapting approach for the detection of bursts and network bursts in neuronal cultures. J Comput Neurosci 29(1–2):213–229

Preisendorfer U, Zeise ML et al (1987) Valproate enhances inhibitory postsynaptic potentials in hippocampal neurons in vitro. Brain Res 435(1–2):213–219

Riedel G, Platt B et al (2003) Glutamate receptor function in learning and memory. Behav Brain Res 140(1–2):1–47

Rothman SM, Olney JW (1995) Excitotoxicity and the NMDA receptor–still lethal after eight years. Trends Neurosci 18(2):57–58

Rowley HL, Marsden CA et al (1995) Differential effects of phenytoin and sodium valproate on seizure-induced changes in gamma-aminobutyric acid and glutamate release in vivo. Eur J Pharmacol 294(2–3):541–546

Trussell LO, Fischbach GD (1989) Glutamate receptor desensitization and its role in synaptic transmission. Neuron 3(2):209–218

Wagenaar DA, Pine J et al (2006) An extremely rich repertoire of bursting patterns during the development of cortical cultures. BMC Neurosci 7(11)

Part IV
Discussion and Conclusion

Chapter 7
Conclusion of the Thesis and Future Perspectives

In this thesis I presented a new experimental in vitro platform: 3D neuronal cultures coupled to MEA devices.

In order to create the 3D neuronal network, I took inspiration of the method developed by Pautot and coworkers (Pautot et al. 2008). The use of micro-bead scaffolds has been specifically optimized and tailored to be integrated with planar MEA in order to investigate the functional properties (i.e. electrical activity) of 3D neuronal networks which have never been presented before. What I obtained is a high-density physically connected 3D neuronal network with an estimated final cell density of about 80,000 cells/mm^3, close to 91,000 cells/mm^3, the average neuronal density estimated in the mouse brain cortex (Schuz and Palm 1989).

7.1 Imaging Characterization

By using immunofluorescence imaging techniques, the developed 3D assemblies is characterized: it is constituted, on average, by 5–8 layers of beads and neurons. I proved in vivo like cell morphology and demonstrate that I partly controlled the development of a 3D network (cf. Sect. 5.2). Neural cells plated in 3D presented a bulbous morphology with intercellular contacts in all spatial directions. Micro-beads self-assembled in a compact hexagonal geometry and the chosen diameter provides a growth surface large enough for neuronal cell bodies and their processes. In this configuration, neuronal processes grew between the beads to form highly interconnected networks: connection among neurons belonging from different layers are shown (cf. Sect. 5.2, Fig. 5.10). The extensive encapsulation by neuritic processes around the micro-bead scaffold indicating a high-density of potential connectivity among neurons. The synaptic density evaluated in 3D neuronal network is of about 2.6×10^7 synapses/mm^3. In this type of configuration neuron health is maintained

M. Frega, *Neuronal Network Dynamics in 2D and 3D in vitro Neuroengineered Systems*, Springer Theses, DOI 10.1007/978-3-319-30237-9_7

and uniform and robust neuronal process outgrowth throughout the bead layers, including in the deep layers, is supported.

7.2 Spontaneous Activity

To characterize the electrophysiological activity of the 3D network, and to demonstrate how the 3D structure modulates the network dynamics, I compared the spontaneous electrophysiological activity of 3D cultures with the traditional network dynamics exhibited by 2D cultures (cf. Sect. 5.3.1). I observed striking differences with respect to 2D networks and I quantified evidences of a wide dynamic repertoire of activity patterns possibly recapitulating various activity dynamics of in vivo brain regions (Leinekugel et al. 2002).

2D neuronal networks exhibit stereotyped electrophysiological activity in the mature phase of their development characterized by oscillating dynamics and synchronous bursts involving most of the active channels in the MEA (Chiappalone et al. 2006; Eytan and Marom 2006; Brewer et al. 2009; Gandolfo et al. 2010). The network activity is stereotyped and the activity patterns are reliable. 2D neuronal networks exhibits a high level of bursting activity, a low level of random spike activity and a high level of synchronization and correlation (cf. Sects. 5.3.1.1 and 5.3.1.2). This type of activity represents the exploring dynamics of the close in vitro systems that, missing the natural input–output pathways of the in vivo brain, have to find a stable state with properly formed synapses. Bursting activity represents a relative simple and stable mode of activity in network of dissociated neurons essentially due to the lack of external stimuli (Wagenaar et al. 2005). The poor dynamics exhibited by such networks, often dominated by network bursting activity, is one of the major criticism raised about the validity of this model (Wagenaar et al. 2005).

On the contrary, the signature of the *3D neuronal network* dynamics presents a wider repertoire of activities with less global synchrony and more pronounced spiking at a single channel-neuron level. Quasi-synchronous network bursting activity of high density 2D neuronal networks is maintained in 3D cultures but global frequency is decreased (<1 Hz) and global synchrony is lost. 3D mature cultures exhibit an enhanced dynamic in which both network burst and random spike activity regions are present. 3D neuronal network presents a low level of network bursting activity and a high level of random spiking activity. Therefore, the level of correlation and synchronization is variable: the level of correlation and synchronization exhibited by this network is always lower than the one shown by the 2D one (cf. Sects. 5.3.1.1 and 5.3.1.2). These features suggest that there are stimuli coming from the upper layers (i.e. external stimuli) that modulate the electrophysiological activity of the network.

To prove that enhanced activity was due to the developed 3D architecture, I compared the expressed 3D dynamics with the activity of the two additional controls (cf. Sect. 5.3.1.4). The simple coupling of 3D cultured hippocampal cells with a bare MEA substrate prevents a reasonable read-out on the bottom plane and only few

spikes could be recorded in such experimental situation (Control 1). In the case of Control 2, the electrophysiological activity was, as expected, not distinguishable from the 2D neuronal network: the activity of 2D network is not affected by the presence of a micro-bead stack on top of the cell culture. Only when plating neurons directly onto the MEA substrate and at the same time assembling on such read-out layer the 3D population we could obtain a valuable 3D experimental model for network electrophysiology.

To demonstrate whether the layers are effectively connected, I studied and characterized the propagation of the signal (Streit et al. 2001; Tscherter et al. 2001) (cf. Sect. 5.3.1.3).

In *2D neuronal network*, the signal starts from one source and propagates rapidly and in a continuous way in all the network: this behavior is reliable. Few sources appear with high occurrence: the system is organized and there is reliability of the sources. The propagation of the signal is continuous and short (i.e. maximum latency of 20 ms). There is a clear (i.e. linear) correlation between latency and distance: the speed of the propagation computed for all the experiment is of 42 ± 3.5 mm/s. 2D neuronal network is a very organized system that, without external inputs, continues to repeat the same pattern of activity.

In *3D neuronal network*, instead, the signal that starts from one site propagates slowly in the network in a discontinuous way. There are several sources that appear with a low occurrence: the sources are not reliable. This is an indirect proof of the fact that there is the presence of real sources in the upper layers. The propagation of the signal is discontinuous and long: there is a random relationship between latency and distance and latency values are higher than the ones detected for the 2D neuronal network (i.e. maximum latency of 100 ms). Moreover, there is a non-linear relationship between latency and distance. It is because of the variability in the connectivity pathway that are present in the 3D structure: the signal can pass through possible paths going up and down to the 3D micro-bead layers. All these features indicate that the network activity measured at the "read-out" layer is modulated by input arriving from the upper layers of the structure. There are real sources in the upper layers, from which the signal starts and reaches the sub-networks coupled to the MEA device modulating their activity.

7.3 Stimulus-Evoked Activity

Although such enhanced spontaneous activity is a convincing hallmark of the inherent contribution of the 3D structure to the network dynamics, the ultimate evidence that we are playing with actual 3D functionally interconnected neuronal networks is given by the results obtained upon the application of an external electrical stimulation (cf. Sect. 5.3.2).

2D interconnected hippocampal networks stimulated by different electrodes, showed a relatively fast and synchronized response depending on the stimulating site. The site of stimulation causes an almost uniform response (for the high-

connectivity of the network) in all the active sites. The response time is relatively fast and confined below the first 250 ms.

3D networks stimulated from the bottom layer exhibit various types of synchronized response often generating a uniformly distributed response delay. In general, the evoked activity can be seen as the combination of two types of response. The first type is generated by subsets of neurons in the 2D layer that are connected with subgroups of neurons in the same layer. The second type of response is instead generated by subset of neurons in the 2D layer connected with sub-networks of neurons in the upper layers. The first type of response is fast, while the second type is slow: globally, the response of 3D neuronal networks stimulated by the bottom layer is slower than the 2D network response. Because of the different types of activated circuits described, the network response is not globally synchronized.

When stimulating *3D neuronal networks from the top layer*, the stimulation needs to be transmitted (possibly through neurons of different layers) to neurons of the read-out layer coupled to the MEA, thus generating time delays greater than 500 ms and a reduced number of channels recording evoked responses. The enhanced variability in the time delays of the evoked responses is the ultimate proof that we are facing a highly functionally interconnected 3D cultured network.

7.4 Chemical Modulation

Even if the recorded dynamics are very different, the proportion between GABAergic and glutammatergic populations is likely to remain similar in both 2D and 3D models (with about a 1:5 ratio) (Marom and Shahaf 2002; Bonifazi et al. 2005). In order to characterize how the excitatory and inhibitory neurons balance may affect the 2D and 3D neuronal networks driving activity, I blocked the $GABA_A$ receptors (cf. Sect. 5.3.3). When the inhibitory action of $GABA_A$ receptors is blocked, an increment of the electrophysiological activity of both 2D and 3D neuronal networks is detectable. Moreover, the level of synchronization and correlation increases in both the configurations. What I generally found is that despite the different behavior in physiological conditions, Bicuculline treatment seems to drive both 2D and 3D neuronal networks towards the same "epileptic like" and more synchronized dynamic state. This behavior could indicate that when Bicuculline is released in 3D networks, the activity of the neurons in the upper layers become much more correlated. Thus, the information that come from above have less influence on the network activity measured at the "read-out" layer. In the 3D architecture there is an enhanced dendritic development. I can speculate that the different GABAergic interneuron populations could gain a considerable increase of the functional surface compared to those grown in the 2D cultures. These possible wider and longer interactions with other neurons could contribute to desynchronize and temporally differentiate the network activity, hence producing bursting activities confined to sub-populations and global asynchronous activity patterns (Baltz et al. 2010).

7.5 Comparison with Other Studies

Primary neuronal cultures dissociated from different part of the brain have been a classical model for in vitro electrophysiological studies (Marom and Shahaf 2002; Frega et al. 2012). When neurons grows in vitro, they retain the basic processes underlying the in vivo physiological behavior. In vitro cultured neurons coupled to MEA represent a reduced neurobiological structure where, at a simplified level, the collective and functional properties of the nervous system emerge and can be experimentally investigated for basic neuroscience studies (Van Pelt et al. 2004a, b; Wagenaar et al. 2006; Rolston et al. 2007). All studies on cultured cells devoted to elucidate neurophysiological mechanisms and computational properties are based on 2D neuronal networks.

Besides clear advantages related to controllability and observability, such 2D neuronal model systems have major limitations as they might be inherently unable to exhibit characteristics of in vivo systems. For example, neurons in 2D configuration has an unrealistic morphology (i.e. flat) and yet most in vitro models utilize planar systems lacking in vivo–like extracellular matrix (Cullen et al. 2011). Regarding the electrophysiological activity, 2D neuronal network exhibits a poor dynamic dominated by network burst, indicating a lack of external inputs. The oscillating and stereotyped behavior of these models has been considered one of their major drawbacks (Wagenaar et al. 2005; Kermany et al. 2010) when interested in the study of the computational properties of neuronal networks. A possible reason is the lack of afferent and efferent signals.

The main result of this thesis is the construction of a new in vitro model capable of better emulating in vivo physiology. In recent years, 3D neuronal cultures that emulate the high cell density and connectivity seen in vivo are created (Pautot et al. 2008; Cullen et al. 2011). Even if several studies have been devoted to the introduction of in vitro 3D neuronal systems, the use of such experimental models is still limited and no paper in the literature has yet reported any kind of multi-channel electrical recording of 3D layered neuronal networks.

7.6 Applications and Further Perspectives

3D neuronal networks coupled to MEAs is a new model that permits to study in vitro neuronal systems in a more physiological condition, approaching and mimicking natural assemblies in the brain. The developed experimental paradigm constituted by functionally connected and electrophysiologically active 3D neuronal assemblies can constitute the basis for a next class of experimental model systems to study neurophysiology, computational properties of 3D networks and the relationship between structure and network dynamics. Further development of 3D patterned neuronal networks or 3D co-cultures may shed light on questions about how different neuroanatomical patterns give rise to complex dynamical state.

The model presented in this thesis allows to record the electrophysiological activity of 3D neuronal networks only from the lower layer (i.e. the one directly coupled to the MEAs). To further develop the innovative proposed 3D engineered neuronal networks and to study how the 3D neuronal network dynamic changes in different layers of the structure, different recording devices could be constructed. Finger like structure with embedded microelectrodes or sandwich-structure (i.e. standard MEA from the bottom side and a planar multi-channel recording structure on the upper side) can be developed to record the activity of the 3D neuronal network both from the bottom, middle and upper layers. 3D in vitro model with the addition of embedded functionalized scaffolds provides a biohybrid systems in which functional properties of neuronal network can be addressed in a more neurofidelic environment: cell-cell interaction is more natural and specific fundamental issues such as the interplay between structure and dynamics can be conveniently investigated.

Therefore, this new model is an appealing ideal candidate to revisit and complement in vitro neurophysiological studies.

References

Baltz T, de Lima AD et al (2010) Contribution of GABAergic interneurons to the development of spontaneous activity patterns in cultured neocortical networks. Front Cell Neurosci 4:15

Bonifazi P, Ruaro ME et al (2005) Statistical properties of information processing in neuronal networks. Eur J Neurosci 22(11):2953–2964

Brewer GJ, Boehler MD et al (2009) Neuron network activity scales exponentially with synapse density. J Neural Eng 6(1):014001

Chiappalone M, Bove M et al (2006) Dissociated cortical networks show spontaneously correlated activity patterns during in vitro development. Brain Res 1093(1):41–53

Cullen DK, Wolf JA et al (2011) Neural tissue engineering and biohybridized microsystems for neurobiological investigation in vitro (part 1). Crit Rev Biomed Eng 39(3):201–240

Eytan D, Marom S (2006) Dynamics and effective topology underlying synchronization in networks of cortical neurons. J Neurosci 26(33):8465–8476

Frega M, Pasquale V et al (2012) Cortical cultures coupled to micro-electrode arrays: a novel approach to perform in vitro excitotoxicity testing. Neurotoxicol Teratol 34(1):116–127

Gandolfo M, Maccione A et al (2010) Tracking burst patterns in hippocampal cultures with high-density CMOS-MEAs. J Neural Eng 7(5):056001

Kermany E, Gal A et al (2010) Tradeoffs and constraints on neural representation in networks of cortical neurons. J Neurosci Off J Soc Neurosci 30(28):9588–9596

Leinekugel X, Khazipov R et al (2002) Correlated bursts of activity in the neonatal hippocampus in vivo Science (New York, NY) 296(5575):2049–2052

Marom S, Shahaf G (2002) Development, learning and memory in large random networks of cortical neurons: lessons beyond anatomy. Q Rev Biophys 35(1):63–87

Pautot S, Wyart C et al (2008) Colloid-guided assembly of oriented 3D neuronal networks. Nat Methods 5(8):735–740

Rolston JD, Wagenaar DA et al (2007) Precisely timed spatiotemporal patterns of neural activity in dissociated cortical cultures. Neuroscience 148(1):294–303

Schuz A, Palm G (1989) Density of neurons and synapses in the cerebral cortex of the mouse. J Comp Neurol 286(4):442–455

Streit J, Tscherter A et al (2001) The generation of rhythmic activity in dissociated cultures of rat spinal cord. Eur J Neurosci 14(2):191–202

Tscherter A, Heuschkel MO et al (2001) Spatiotemporal characterization of rhythmic activity in rat spinal cord slice cultures. Eur J Neurosci 14(2):179–190

Van Pelt J, Corner MA et al (2004a) Longterm stability and developmental changes in spontaneous network burst firing patterns in dissociated rat cerebral cortex cell cultures on multi-electrode arrays. Neurosci Lett 361(1–3):86–89

Van Pelt J, Wolters PS et al (2004b) Long-term characterization of firing dynamics of spontaneous bursts in cultured neural networks. IEEE Trans Biomed Eng 51(11):2051–2062

Wagenaar DA, Madhavan R et al (2005) Controlling bursting in cortical cultures with closed-loop multi-electrode stimulation. J Neurosci 25(3):680–688

Wagenaar DA, Nadasdy Z et al (2006) Persistent dynamic attractors in activity patterns of cultured neuronal networks. Phys Rev E: Stat, Nonlin, Soft Matter Phys 73(5 Pt 1):051907

Appendix
Data Analysis

Data analysis was performed off-line by using a custom software package named SPYCODE (Bologna et al. 2010) developed in MATLAB (The Mathworks, Natick, MA, USA). SPYCODE provides a working environment able to perform efficient data management and processing since it incorporates a very rich repertoire of standard and advanced signal analysis tools. In this chapter the algorithms used for analyzing 2D and 3D neuronal networks activity are presented.

A.1 Spike Detection

Spike timing is the first information to extract from raw data. Since typical signal to noise ratios are much larger than one, the most used method to identify the spikes is a threshold-based algorithm (Maeda et al. 1995) resulting in a point process (e.g. spike train, ST) in which each element represents the position in time of a spike.

Equation A.1 reports the formal definition of a spike train, where t_s is the timing of a spike, N is the number of recognized spikes and t is the Kronecker delta function.

$$ST(t) = \sum_{S=1}^{N} \delta(t - t_S) \tag{A.1}$$

The two main issues related to spike detection are: the reliability of the method and the precise positioning of the detected peaks in the spike train. Extracellularly recorded spikes were detected using the PTSD (Precise Timing Spike Detection) algorithm (Maccione et al. 2009).

Precision Timing Spike Detection (PTSD), has been developed aimed at responding to both the first (i.e., reliability) and to the second (and most restrictive) issue (i.e., precision). Moreover, the PTSD provides a good trade-off between performance and computational costs and can constitute an accurate and fast tool to be applied to neural code and information transmission investigations.

M. Frega, *Neuronal Network Dynamics in 2D and 3D in vitro Neuroengineered Systems*, Springer Theses, DOI 10.1007/978-3-319-30237-9

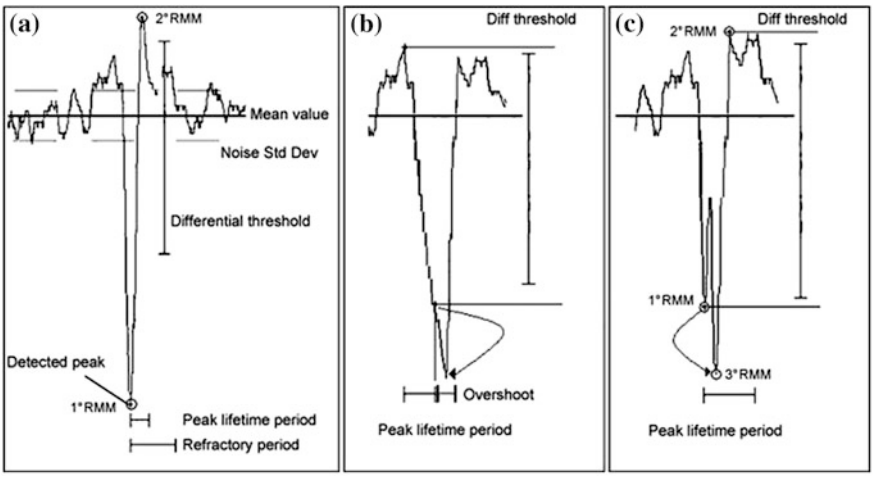

Fig. A.1 Schematic representation of the main features of the proposed PTSD. **a** Detection of two Relative Maximum/Minimum (RMM, negative and positive) closer than the peak lifetime period. A spike is detected since the voltage difference between the two RMM overcomes the differential threshold. A refractory period (starting from the temporal position of the RMM with the higher absolute value) is defined by the user and no other spikes can be detected within this temporal window. So the algorithm will look for the next spike starting from the end of the refractory period. **b** The higher absolute value corresponds to the last point of the peak lifetime period and a spike can be detected. In this case, a supplementary period (overshoot) is assigned to look for the following RMM. **c** After detecting the 1°RMM a spike can be assigned taking into account the 2° RMM. The algorithm searches for other RMM that have higher absolute voltage value within the peak lifetime period. In this case it moves the assignment of the spike time event to the 3°RMM because its absolute value overcomes the other two. From Maccione et al. (2009)

The algorithm requires three parameters: the differential threshold (DT) set to 8 times the standard deviation of the baseline noise independently for each channel, the peak lifetime period (PLP) and the refractory period (RP). The peak lifetime and the refractory period are related to the duration of a spike and the minimum interval between two consecutive events (Fig. A.1). Regarding the results shown in this thesis PLP and RP are set at 2 ms.

The algorithm computes the Relative Maximum/Minimum (RMM) of the raw data signal. When the RMM is a Minimum, the algorithm looks for the nearest Maximum within the peak lifetime (PLP) window, and vice versa. If the difference between the two found RMM (differential value) overcomes the differential threshold (DT), the spike is identified and its timestamp is stored. Whenever the user chooses to set the refractory period (RP), no other RMM within that time lag can be computed (Fig. A.1a).

In order to increase the accuracy of the temporal detection (assuming the time stamp of an event corresponding to the higher absolute value of the spike), the algorithm implements the following rules:

1. If the higher value corresponds to the last point of the peak lifetime period, a further time interval named “overshoot” is used to find the correct peak value (Fig. A.1a).
2. All the RMM inside the peak lifetime period are taken into account in detecting the precise time stamp of the event, even if they have not been used to find the spike (Fig. A.1b).

A.2 Firing Rate

Once spikes have been identified, the easiest and most direct way to characterize the level of activity of a cell is computing its Firing Rate (FR). According to Adrian's definition (Adrian 1928), the firing rate is the number of spikes in a rather large time window and it can be measured from just one representation of the neural activity, as follows:

$$FR = \frac{\int_0^T \left(\sum_{s=1}^{N} \delta(t - t_s)\right)}{T} \tag{A.2}$$

with T representing the duration of the recording and N the number of spikes occurring at time t_s.

If we count the spikes in a small window of size Δt, centered at $(t_a - t_b)/2$ and we divide by the bin width, we compute the **Instantaneous Firing Rate (IFR)**. The IFR is computed by dividing the number of spikes which falls in a small sliding window by the window length. Such a window was implemented using a Gaussian kernel (100 ms width).

Dealing with MEAs, tens of channels are likely to be involved during an experimental session. For this reason, it is useful to compute the FR of the whole culture and see how it changes given the delivered stimulation. This quantity is simply obtained by computing the FR of each single channel and then averaging among all the active electrodes of the MEA (i.e., being an active electrode defined by an activity >0.1 spike/s), obtaining the **Mean Firing Rate (MFR)**.

A.3 Burst Detection

Bursts were identified according to the method described in Chiappalone et al. (2005).

A burst consists of a fast sequence of spikes with duration equal to the sum of the inter-spike intervals (ISIs) within the burst itself and separated by an interval (inter-burst interval, IBI) relatively long compared to the burst duration. According

to this definition, a burst train of M bursts consists of a sequence of rectangular functions each of which representing a burst centered at t_m and lasting τ_m.

$$BT(t) = \sum_{m-1}^{M} \prod \left(\frac{t - t_m}{\tau_m} \right) \tag{A.3}$$

The spike train is analyzed using a shifting time window, sized as the minimum expected IBI or, equivalently, the maximum expected ISI. Two thresholds are fixed: the maximum ISI for spikes within a burst (maxISI, set at the value of 100 ms); the second one is defined as the minimum number of consecutive spikes belonging to a burst (minSpikes, set at the value of 10 spikes).

Bursts are defined as sequences of spikes with ISI smaller than the maxISI, and containing at least a number of spikes equal to minSpikes.

A similar procedure has been followed for the detection of **network bursts**, looking for sequences of closely-spaced single-channels bursts. A network burst is identified whether it involves at least the 80 % of the network active channels (Pasquale et al. 2010).

A.4 Post Stimulus Time Histogram (PSTH)

To evaluate the capability of the network to respond to the applied stimuli, the number of evoked spikes after each stimulus was computed and the histogram of their distribution was plotted.

Spike trains in response to repeated presentation of the same stimulus are not identical, so the PSTH represents the average behavior of one or more cells to a stimulation pattern. More specifically, the PSTH shows the probability of firing as a function of time after the stimulus onset. This measure is equivalent to a cross correlation between the train of stimuli and the train of spikes. The mathematical definition of the PSTH is reported below (N is the total number of stimuli delivered to the network, t_{stimi} is the timing at which each stimulus i occurs and ST is the spike train recorded at a specific channel):

$$P(t) = \frac{1}{N} \sum_{i=1}^{N} ST(t - t_{stim_i}) \tag{A.4}$$

The PSTHs were calculated by considering 2 s time windows from the recordings that follow each stimulus. The number of evoked spikes after each stimulus was computed and the histogram of their distribution was plotted for each channel. I computed the absolute maximum value of all the histograms (i.e. M). Then, I counted the number of spikes occurring in a 10 ms bin and I normalized the obtained histogram by dividing this measure by the number of stimuli and by M. In that way we obtained a probability density function.

A.5 Cross-Correlation

The level of synchronization among multi-unit recordings was estimated by the cross-correlation function (Garofalo et al. 2009).

Given two spike trains (e.g., X and Y), recorded from two electrodes of the MEA, we counted the number of events in the Y train within a time frame around the X event of ±T (set at 1000 ms), by using bins of amplitude $\Delta\tau$ = 5 ms.

The cross-correlogram coefficient, C(0), represents the area of the cross-correlogram in the central bin and it was evaluated to quantify the synchronization level among the recording channels. We defined an arbitrary threshold defined as < C(0) > + 2 std(C(0)) to detect the most synchronized electrodes.

To quantify the correlation level the C_{Peak} value was computed as the value of the cross-correlogram in an area around the maximum detected peak. C(0) and C_{peak} values are normalized with respect to the auto-correlation value.

A.6 Signal Propagation

Signal propagation is evaluated accordingly with the method described by Streit et al. (2001), Tscherter et al. (2001).

Firstly, the sites from which the network burst starts are evaluated for each network burst detected. The sites where the burst were initiated in at least 5 % of all network burst detected are indicated as signal sources.

Then, I valuated the latency of the signal. This parameter indicates the time that the signal needs to reach another electrode involved into the network burst (i.e. El_1, El_2, El_n) starting from the source (i.e. second column in Table A.1, $t_n - t_s$).

Finally, I evaluated the distance that the signal travels. The distance is computed as the physical distance from the source electrode to the other electrode involved in the network burst (i.e. distance, third column in Table A.1).

Table A.1 Signal propagation parameters

Electrode	Lactency	Distance
El_1	$t_1 - t_s$	$\sqrt{(x_1 - x_s)^2 + (y_1 - y_s)^2}$
El_2	$t_2 - t_s$	$\sqrt{(x_2 - x_s)^2 + (y_2 - y_s)^2}$
El_n	$t_n - t_s$	$\sqrt{(x_n - x_s)^2 + (y_n - y_s)^2}$

References

Adrian, E. D. (1928). The basis of sensation: the action of sense organs. New York, NJ

Bologna LL, Pasquale V et al (2010) Investigating neuronal activity by SPYCODE multi-channel data analyzer. Neural Netw 23(6):685–697

Chiappalone M, Novellino A et al (2005) Burst detection algorithms for the analysis of spatio-temporal patterns in cortical networks of neurons. Neurocomputing 65–66:653–662

Garofalo M, Nieus T et al (2009) Evaluation of the performance of information theory-based methods and cross-correlation to estimate the functional connectivity in cortical networks. PLoS One 4(8):e6482

Maccione A, Gandolfo M et al (2009) A novel algorithm for precise identification of spikes in extracellularly recorded neuronal signals. J Neurosci Methods 177(1):241–249

Maeda E, Robinson HP et al (1995) The mechanisms of generation and propagation of synchronized bursting in developing networks of cortical neurons. J Neurosci 15(10):6834–6845

Pasquale V, Martinoia S et al (2010) A self-adapting approach for the detection of bursts and network bursts in neuronal cultures. J Comput Neurosci 29(1–2):213–229

Streit J, Tscherter A et al (2001) The generation of rhythmic activity in dissociated cultures of rat spinal cord. Eur J Neurosci 14(2):191–202

Tscherter A, Heuschkel MO et al (2001) Spatiotemporal characterization of rhythmic activity in rat spinal cord slice cultures. Eur J Neurosci 14(2):179–190